Organic Solid State Lasers for Sensing Applications

Zur Erlangung des akademischen Grades eines

Doktor-Ingenieurs

von der Fakultät für
Elektrotechnik und Informationstechnik
des Karlsruher Instituts für Technologie
genehmigte

Dissertation

von
Dipl.-Phys. Thomas Woggon
geb. in Berlin

Tag der mündlichen Prüfung: 7. Juli 2011

Hauptreferent: Prof. Dr. U. Lemmer
Korreferent: Prof. Dr. V. Saile

Journal Publications

1. C. Eschenbaum, **T. Woggon** and U. Lemmer, *High speed fabrication of toroidal micro-ring resonators by two photon direct laser writing*, Nonlinear Photonics, OSA Technical Digest (CD), NThB8, (2010)

2. **T. Woggon**, S. Klinkhammer and U. Lemmer, *Compact spectroscopy system based on tunable organic semiconductor lasers*, Appl. Phys. B. **99**(1), 47–51 (2010)

3. S. Klinkhammer, **T. Woggon**, C. Vannahme, U. Geyer, S. Valouch, T. Mappes and U. Lemmer, *Optical spectroscopy with organic semiconductor lasers*, (Best Student Paper), Proc. SPIE **7722-53** (2010)

4. M. Stroisch, **T. Woggon**, C. Teiwes-Morin, S. Klinkhammer, K. Forberich, A. Gombert, M. Gerken and U. Lemmer, *Intermediate high index layer for laser mode tuning in organic semiconductor lasers*, Opt. Express **18**(6), 5890–5895 (2010)

5. S. Klinkhammer, **T. Woggon**, U. Geyer, C. Vannahme, S. Dehm, T. Mappes and U. Lemmer, *A continuously tunable low-threshold organic semiconductor distributed feedback laser fabricated by rotating shadow mask evaporation*, Appl. Phys. B. **97**(4), 787-791 (2009)

6. T. Mappes, C. Vannahme, S. Klinkhammer, **T. Woggon**, M. Schelb, S. Lenhert, J. Mohr and U. Lemmer, *Polymer biophotonic lab-on-a-chip devices with integrated organic semiconductor lasers*, Proc. SPIE **7418-9** (2009)

7. M. Stroisch, C. Teiwes-Morin, **T. Woggon**, M. Gerken, U. Lemmer, K. Forberich and A. Gombert *Photonic stopband tuning of organic semiconductor distributed feedback lasers by oblique angle deposition of an intermediate high index layer*, Appl. Phys. Lett. **92**, 021112 (2009)

8. **T. Woggon**, T. Kleiner, M. Punke and U. Lemmer, *Nanostructuring of organic-inorganic hybrid materials for distributed feedback laser resonators by two photon polymerization*, Opt. Express **17**(4), 2500–2507 (2009)

9. M. Punke, **T. Woggon**, M. Stroisch, B. Ebenhoch, U. Geyer, C. Karnutsch, M. Gerken, U. Lemmer, M. Bruendel, J. Wang and T. Weimann, *Organic semiconductor lasers as integrated light sources for optical sensor systems*, Proc. SPIE **6659-8** (2007)

10. M. Stroisch, **T. Woggon**, U. Lemmer, G. Bastian, G. Violakis and S. Pissadakis, *Organic semiconductor distributed feedback laser fabricated by direct laser interference ablation*, Opt. Express **15**, 3968, (2007)

Patent applications

1. **T. Woggon**, S. Klinkhammer, S. Valouch, J. Bach and U. Lemmer, *Tunable laser light source based on variable optical pulse excitation and method for operating same*, US2011043801 (A1), EP2287980 (A1) (2009).

Book chapters

1. **T. Woggon**, M. Punke, M. Stroisch, M. Bruendel, M. Schelb, C. Vannahme, T. Mappes, J. Mohr and U. Lemmer, *Organic Semiconductor Lasers as Integrated Light Sources for Optical Sensors* in: Organic Electronics in Sensors and Biotechnology, 265-298, Mcgraw-Hill, ISBN-10: 0071596755, (2009)

Awards

1. *VISOLAS: the tunable organic laser*, 1st Prize, "Best Innovation by an Individual Researcher", European Photonics Innovation Village, SPIE Photonics Europe, Brussels, Belgium, April 12-16, (2010)

Conferences

1. S. Klinkhammer, **T. Woggon**, X. Liu, C. Vannahme, T. Mappes and U. Lemmer, *Plastic Lasers for Optical Spectroscopy*, 1st Winter School of Organic Electronics, Heidelberg, Germany, December 9-12, (2010)

2. S. Klinkhammer, C. Vannahme, **T. Woggon**, T. Mappes and U. Lemmer, *Organic semiconductor lasers for sensing applications*, Polydays, Berlin-Dahlem, Germany, October 3-5, (2010)

3. S. Klinkhammer, **T. Woggon**, C. Vannahme, T. Mappes and U. Lemmer, *Optical spectroscopy with organic semiconductor lasers*, SPIE Photonics Europe 7722: Organic Photonics, Brussels, Belgium, April 12-16, (2010)

4. C. Eschenbaum, **T. Woggon** and U. Lemmer, *High speed fabrication of toroidal micro-ring resonators by two photon direct laser writing*, OSA Topical Meeting: Nonlinear Photonics, Karlsruhe, Germany, June 21-24, (2010)

5. C. Vannahme, S. Klinkhammer, A. Kolew, **T. Woggon**, T. Mappes, U. Lemmer and J. Mohr, *Hot embossing of micro- and nanostructures for the integration of organic semiconductor lasers and deep UV induced waveguides towards a lab-on-chip system*, 35th International Conference on Micro Nano Engineering (MNE), Ghent, Belgium, September 28 - Oktober 1, (2009)

6. S. Klinkhammer, **T. Woggon**, U. Geyer, C. Vannahme, T. Mappes and U. Lemmer, *Rotating shadow mask evaporation and its use for continuously tunable low-threshold organic semiconductor distributed feedback lasers*, 10th European Conference on Molecular Electronics (ECME), Copenhagen, Denmark, September 9-12, (2009)

7. S. Klinkhammer, **T. Woggon**, U. Geyer, C. Vannahme, T. Mappes, S. Dehm and U. Lemmer, *A Continuously Tunable Low-threshold Organic Semiconductor Distributed Feedback Laser*, Mini-Symposium on Organic Lasers and Hybrid Optical Structures, Grasmere, June 22-25, (2009)

8. **T. Woggon**, *Organic Lasers for Laser Induced Fluorescence Measurements for Life Sciences*, Seminar Course: Research Topics in Optics and Photonics, Karlsruhe School of Optics and Photonics, November 5, (2008) **Invited talk**

9. **T. Woggon**, *Potential Usage of Organic Electro-Optic Components in Bio-molecular Analysis*, Agilent Technologies University Relations Research Fair, Waldbronn, Germany, September 19, (2007) **Invited talk**

10. C. Gärtner, C. Karnutsch, J. Brückner, **T. Woggon**, S. Uebe, N. Christ and U. Lemmer, *Numerical study of annihilation processes, excited state absorption and field quenching for various organic laser diode design concepts*, 9th European Conference on Molecular Electronics (ECME), Metz, France, September 5-8, (2007) (Poster presentation)

11. M. Punke, **T. Woggon**, M. Stroisch, C. Karnutsch, S. Mozer, U. Lemmer, M. Bruendel, D.G. Rabus and T. Weimann, *All-organic waveguide coupled solid-state distributed feedback laser*, CLEO/Europe-IQEC 2007, CH-2-4, Munich, Germany, June, 17-22, (2007)

12. **T. Woggon**, M. Punke, M. Stroisch, B. Ebenhoch, U. Geyer, C. Karnutsch, M. Gerken, U. Lemmer, M. Bruendel, J. Wang and T. Weimann, *Organic semiconductor lasers as integrated light sources for optical sensor systems*, SPIE Optics+Photonics 6659, San Diego, CA, USA, August 26-30, (2007)

13. M. Punke, M. Stroisch, **T. Woggon**, A. Pütz, M.P. Heinrich, M. Gerken, U. Lemmer, M. Bruendel, D.G. Rabus, J. Wang and T. Weimann, *Fabrication and characterization of organic solid-state lasers using imprint technologies*, IEEE / LEOS Summer Topicals 2007, Portland, OR, USA, July 23-25, (2007)

14. **T. Woggon**, M. Punke, M. Stroisch, M. Gerken, U. Lemmer, M. Bruendel, D.G. Rabus, J. Wang and T. Weimann, *Integrated organic semiconductor lasers for lab-on-a-chip applications*, NanoBio-Europe 2007, Münster, Germany, June 13-15, (2007) (Poster presentation)

Supervised work

1. Karl Lüll, *Modifikation eines Blu-ray Pickups zum Anregen eines organischen Halbleiterlasers*, Bachelor thesis, 2010

2. Carsten Eschenbaum, *Herstellung mikrooptischer Bauelemente mittels 3D-Laserlithographie*, Master thesis, 2009

3. Tobias Kappler, *Ankopplung einer organischen Photodiode an ein mikrooptisches System*, Studienarbeit, 2009

4. Thomas Kleiner, *Einsatz der direkten Laserlithographie zur Realisierung optischer Mikro- und Nanostrukturen für die Biosensorik*, Diplomarbeit, 2007

Contents

Zusammenfassung

Das Forschungsgebiet der organischen Halbleitermaterialien erfreut sich stetig zunehmender Beliebtheit. Organische Leuchtdioden werden bereits vielfältig in kommerziellen Anwendungen wie z.B. in Informationsanzeigen von Unterhaltungselektronik eingesetzt. Erste kommerzielle organische Solarmodule wurden bereits angekündigt. Eine weitere Klasse organischer Bauelemente sind organische Halbleiterlaser. Diese zeichnen sich gegenüber herkömmlichen Festkörperlasern insbesondere durch die Möglichkeit aus, die Wellenlänge im gesamten sichtbaren Spektralbereich frei einstellen zu können. Darüber hinaus lassen sich organische Laser kostengünstig auf vielen Trägermaterialien herstellen und einfach in mikrooptische Systeme integrieren. Diese Eigenschaften prädestinieren diese Laser für den Einsatz in optischen Spektroskopieanwendungen, insbesondere in Lab-on-a-chip Anwendungen. Doch obwohl bisher vielfältige Forschungserfolge bei der Entwicklung von effizienten, niedrigschwelligen organischen Lasern publiziert wurden, blieb ein kommerzieller Einsatz dieser bisher aus. Ein Grund hierfür sind fehlende Möglichkeiten für eine effiziente Entwicklung von Analyseanwendungen. Für einen kommerziellen Erfolg einer solchen Analyse sollte diese im Idealfall den entscheidenden Vorteil von organischen Lasern ausnutzen: die freie Wahl der Wellenlänge.

Diese Arbeit befasst sich mit zwei Kernpunkten die für eine solche effiziente Anwendungsentwicklung notwendig sind: Effiziente Prototypenfertigung von organischen Lasern mit den nötigen sub-Mikrometer Strukturgrößen und Entwicklung eines organischen Lasersystems zur Bereitstellung beliebiger Laserwellenlängen in einer Entwicklungsumgebung.

Hierzu wurde die Verwendbarkeit eines Verfahrens zum dreidimensionalen direkten Laserschreiben für die schnelle und kostengünstige Prototypenfertigung von Laserresonatoren und mikrooptischen Systemen untersucht. Durch die Optimierung verschiedener Prozessparameter konnten Strukturen mit sub-Mikrometer Abmessungen bis hin zu mehreren hundert Mikrometern mit der gleichen Technologie hergestellt werden. Die Wahl geeigneter Schreibstrategien führte zu einer deutlichen Verkürzung der Prozesszeiten auf praxistaugliche Werte. Die Optimierung des Verfahrens für die Verwendung eines Fotolackes mit glasähnlichen optischen und weitgehend physikalischen Eigenschaften unterstützt die Tauglichkeit für die Prototypenfertigung.

Als weiterer Punkt wurde die Tauglichkeit organischer Laser für Spektroskopieanwendungen in dieser Arbeit untersucht. Dazu wurden Aspekte wie die Optimierung der operativen Lebensdauer und das Verhalten bei Temperaturänderungen sowie Konzepte zum Anregen und Durchstimmen von organischen Festkörperlasern betrachtet. Im speziellen wurde die erste Anwendung eines durch mechanisches Verschieben durchstimmbaren organischen Lasers für Transmission- und Fluoreszenzspektroskopie gezeigt. Weiterhin wurde ein Verfahren entwickelt, mit dem die für einen Wechsel der Wellenlängen eines durchstimmbaren organischen Lasers benötigte Zeit um Größenordungen auf wenige Millisekunden reduziert werden konnte.

Zur Einordung des Potentials eines solchen durchstimmbaren organischen Lasers für eine kommerzielle Anwendung wurde ein solcher in Form einer Technologiedemon-

stration entwickelt und aufgebaut. Dieser wurde mit etablierten Spektroskopielicht-quellen hinsichtlich der reinen Leistungsdaten und der Anwendungstauglichkeit verglichen. Das Ergebnis lässt die Schlussfolgerung zu, dass organische Laser das Potential einer wirtschaftlichen Lösung für Anwendungen besitzen, für welche Monochromatorlichtquellen untauglich sind, die jedoch nicht das Leistungsspektrum ausschöpfen, welches optisch parametrische Oszillatoren und Flüssigfarbstofflaser bieten.

Chapter 1

Introduction

Abstract

The field of organic optoelectronic devices continues to enjoy steady growth rates. Organic light-emitting diodes (OLEDs) are already used in small displays and OLED based general lighting devices are on the verge of entering the markets. Organic devices, including organic solar cells and photodetectors, can be fabricated on a wide range of different substrates at relatively low-cost. A special type of organic light-emitting devices, organic solid state lasers, garnered a lot of attention from the research community in the recent years. Organic lasers can be tailored to emit any wavelength in the visible spectrum with low cost fabrication methods. Also integrating multiple of these laser sources with different wavelengths on a chip based microoptical system is much simpler than with inorganic semiconductor laser sources. Possible applications are integrated analytical systems for use in medicine, drug discovery or environmental monitoring which move the analysis closer to the point of care without the need of a centralized full scale laboratory.

The field of solid state lasers based on organic semiconductor gain materials gathered great interest in research during the last decade. This is attributed to numerous appealing properties these devices exhibit [1, 2]. The most intriguing feature of organic lasers is the possibility to tailor their emission wavelength on demand [3, 4]. Optically pumped organic lasers have been demonstrated for the full visible range [5–9], the near UV [10] and also for the near-infrared [11]. Even continuously tunable devices have been demonstrated [12–14].

Organic materials can be processed easily at low temperatures on a wide range of organic and inorganic substrates which allows to use low-cost fabrication methods [15, 16]. There has also been progress made on the monolithic integration of organic lasers on polymer substrates [17–19]. Such integrated waveguide coupled lasers would enable advanced on-chip sensing schemes beyond absorbance or laser induced fluorescence [20]. Pumped with a low-cost laser diode [21, 22] or even a light emitting diode [23] such compact integrated analysis systems may be able to revolutionize medical diagnostics [24].

However, despite these clear advantages of organic lasers over their inorganic counterparts, there is still a lack of applications. The commercial breakthrough of organic lasers is, hence, still holding back. Degradation issues due to photo-oxidation or low output powers are often presented arguments for this situation. Interestingly, these two arguments fail for the most promising application scheme for organic lasers: the integrated sensor systems. These devices can be used as disposables so degradation can be neglected. The reported microwatt peak powers for the first integrated waveguide coupled organic lasers [17, 18] should also be sufficient regarding the progresses made on integrated single photon detectors [25]. Accordingly, there have to be other reasons.

Organic lasers can be realized with many different resonator geometries [26]. DFB resonators with mixed periods [27], two-dimensional photonic crystals [21, 28] or circular Bragg gratings [29, 30] are just a few examples. Exploring different resonator geometries and optimizing the parameters for a specific application requires the ability to rapidly transfer a new design into a working device. Traditional photolithographic methods or imprinting techniques and elaborate electron beam lithography are not economically applicable for this. A deficit in fabrication technology is even more evident for developing the integrated systems as this requires to pattern sub-micron features and several tens of microns extending microoptics on the same substrate. With conventional lithographic methods, this requires multiple processing steps which slows down development and drives costs.

The great freedom in design application developers gain with organic lasers is another problem. The major benefit of organic solid state lasers, the ability to tailor their emission wavelength, is also the major obstacle for developing applications. To exploit the wavelength design freedom, application developers require tunable laser sources which allow them to identify promising wavelengths for advanced detection schemes. Adequate tunable lasers sources like liquid dye lasers or optical parametric oscillators are expensive and require specially trained personnel as well as a specialized infrastructure.

In summary, it is therefore assumed that two issues are currently hampering the commercial breakthrough of organic laser based sensing applications:

- Optimization of organic laser resonator geometries requires the ability for low-cost and rapid prototyping.

- Developing applications that benefit from the unique properties of organic lasers requires organic lasers applicable for development.

This doctoral thesis addresses these two aspects and is structured as follows: Chapter 2 lists, as a brief reference, general principles of optics and photonics responsible for the effects observed in the later studies. The materials and processing technologies which were used during this work will be introduced in chapter 3. It focuses on alternative fabrication methods to costly electron-beam lithography.

Chapter 4 explores the applicability of a three dimensional direct laser writing technology for rapidly prototyping DFB laser resonators as well as microoptical systems with extents of multiple millimeters. A major part of the chapter describes optimization strategies for shortening the processing times and for patterning multiple feature scales in a single automated process run. To satisfy the prototyping aspect, the process is based on a novel hybrid inorganic-organic polymer. Due to its high chemical and thermal resistance this material can be used directly after development.

Chapter 5 investigates the applicability of organic lasers for spectroscopy applications. It deals with improving the operational life time obtainable from organic lasers and their sensitivity to temperature changes which are key questions for any sensing application scenario. In particular, a spectrophotometer based on a through physical displacement tunable organic laser is developed. It is applied for absorption spectroscopy and fluorescence excitation of dyes which marks the first usage of organic lasers for sensing applications.

A novel nonlinear tuning approach for position-dependent distributed feedback lasers is proposed in Chapter 6 which allows to accurately change the emission wavelength over a broad spectral range in a couple of milliseconds with low-cost mechanics. This enables to use organic lasers for high throughput screening at multiple laser lines.

Chapter 7 discusses the commercial potential of tunable organic semiconductor lasers for sensing applications. This includes a review of current competing technologies and the technology demonstration of a benchtop tunable organic laser.

Chapter 2

Fundamentals

Abstract[1]

This chapter lists fundamental principles of optics and photonics applied during the work on this thesis as a brief reference. Particular attention is paid to organic semiconductor lasers which, due to their unique features, will play a prominent role in this work.

---

[1]Parts of this chapter have already been published in:

T. Woggon, M. Punke *et al.*, *Organic Semiconductor Lasers as Integrated Light Sources for Optical Sensors* in: Organic Electronics in Sensors and Biotechnology, 265-298, Mcgraw-Hill, ISBN-10: 0071596755, (2009)

2.1 Optics

The field of optics usually describes the behavior of visible, ultraviolet and infrared light but is not limited to these. In general, optics is defined as the branch of physics which studies the behavior and properties of electromagnetic waves. These studies also include the interaction of electromagnetic waves with matter. Due to the nature of light, optics provide the ability to conduct measurements without the need for a mechanical interface and thus to measure at atomic scales as well as over astronomical distances. Optical science is therefore relevant in many disciplines including natural sciences, engineering, photography and medicine. Practical applications of optics can be found in a variety of technologies and everyday objects.

2.1.1 Snell's law and total internal reflection

Light travels in a vacuum at a fixed speed of $c_0 = 2.997\,924\,58 \times 10^8\,\mathrm{m\,s^{-1}}$. In any other medium the speed of light c is directly proportional to c_0 with the proportionality constant n called index of refraction:

$$n = \frac{c_0}{c} \tag{2.1}$$

It has to be noted that albeit this definition for n suffices for the considerations in this section it is not complete. The refractive index depends in general on the frequency ω of the light. To also include additional optical effects like extinction due to absorption and scattering the refractive index can be defined as a complex number:

$$N(\omega) = n(\omega) + i\kappa(\omega) \tag{2.2}$$

With the imaginary part $\Im(N) = \kappa(\omega)$ being the wavelength dependent extinction coefficient.

The relation 2.1 implies a change of c when light passes an interface between two different media. As the angular frequency ω of the light is constant the wavelength λ_0 of the light in a vacuum has to change with n:

$$\lambda_0 = 2\pi \frac{c_0}{\omega} \tag{2.3}$$

$$\Rightarrow \lambda = 2\pi \frac{c_0}{n\omega} \tag{2.4}$$

This change of c is responsible for the refraction of light depicted in figure 2.1 that can be observed at an interface when light passes from one medium to another. The relation of the transmission angle θ_2 of the light into the second medium is related to the incidence angle θ_1 by Snell's law[2]:

$$\frac{\sin \theta_1}{\sin \theta_2} = \frac{c_1}{c_2} = \frac{n_2}{n_1}$$

$$\Leftrightarrow n_1 \sin \theta_1 = n_2 \sin \theta_2 \tag{2.5}$$

---

[2]named after Willebrord Snell Van Royen, Leiden, Netherlands, ⋆1581 †1626
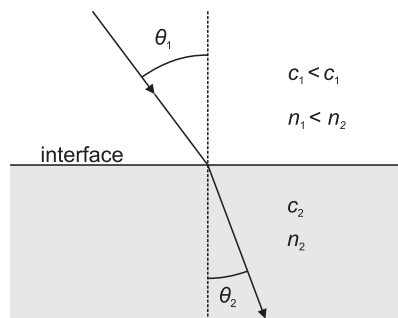
Figure 2.1: Refraction of light at an interface between two materials with different refractive indexes.

Total internal reflection

Snell's law (2.5) states that light crossing an interface into a medium with a higher index of refraction is bend towards the normal. Vice versa, light propagating from a higher refractive index region to a lower one will be bend away from the normal. This implies that under a specific critical incident angle θ_c, light traveling from a medium with higher n_1 to a medium with $n_2 < n_1$ will be refracted along the interface, i.e. $\theta_2 = 90°$. Inserting $\theta_2 = 90°$ in Eq. (2.5) yields:

$$\theta_C = \arcsin\left(\frac{n_2}{n_1}\right) \tag{2.6}$$

For any incident angle $\theta > \theta_c$ Snell's law lacks a solution for the refraction angle. In these cases the incident light is totally reflected off the interface, obeying the law of reflection as depicted in figure 2.2.
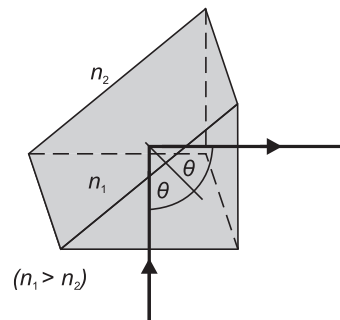
Figure 2.2: For angles above θ_c the incident light is totally reflected at the interface to the lower refractive index medium. According to the law of reflection the incident angle is equal to the reflected beam angle.

Fresnel equations

The Fresnel equations[3] extend Snell's law with a formalism which describes the degree of reflection and transmission of electromagnetic waves at a dielectric interface. The equations can be derived from the Maxwell equations by applying

---

[3]named after Augustin Jean Fresnel ⋆May 10th, 1788, †July 14th, 1827

boundary conditions for electromagnetic waves at an interface with no free charges or currents. In the special case of the two media having the same permeability and with the use of Snell's law (2.5) the reflection and transmission coefficients can be calculated according to:

$$\left(\frac{E_t}{E_i}\right)_{TE} = t_{TE} = \frac{2N_1 \cos\theta_1}{N_1 \cos\theta_1 + N_2 \cos\theta_2} \tag{2.7}$$

$$\left(\frac{E_r}{E_i}\right)_{TE} = r_{TE} = \frac{N_1 \cos\theta_1 - N_2 \cos\theta_2}{N_1 \cos\theta_1 + N_2 \cos\theta_2} \tag{2.8}$$

For transversal electrical or s-polarized light and transversal magnetic or p-polarized light respectively:

$$t_{TM} = \frac{2N_1 \cos\theta_1}{N_2 \cos\theta_1 + N_1 \cos\theta_2} \tag{2.9}$$

$$r_{TM} = \frac{N_2 \cos\theta_1 - N_1 \cos\theta_2}{N_2 \cos\theta_1 + N_1 \cos\theta_2} \tag{2.10}$$

2.1.2 Optical waveguides

Optical waveguides are structures which are able to guide light in a defined direction. The effect of wave guiding in optical thin films plays an important role for the practical realization of organic distributed feedback lasers. The following elucidates the theoretical concept for the understanding of light guiding in thin films. The considerations will be briefly extended to the special case of an square shaped rip waveguide. The argumentation is a brief summary derived from the book *Integrated Optics: Theory and Technology* by R.G. Hunsperger [31].

Planar waveguides

The three layer system as depicted in figure 2.3 represents the simplest case of a planar waveguide. In this case the waveguide is the middle layer with the refractive index n_2. It is limited by two parallel interfaces to the layers n_1 and n_3. For the theoretical discussion it is convenient to assume an infinite thickness and lateral extension of these outer layers.
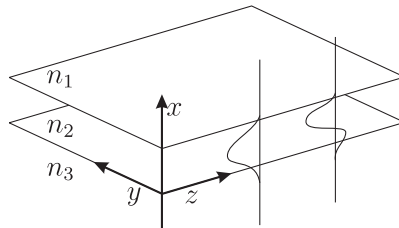

Figure 2.3: Schematic drawing of a three layer planar waveguide. The two depicted curves represent the electrical field distribution along the x-axis for different waveguide modes

For a closer view on the waveguide properties it is assumed that an electromagnetic wave propagates along the z-axis. The spatial distribution of the electrical

field $\mathbf{E}(\mathbf{r}, t)$ is a solution of Maxwell's equations and called a waveguide mode:

$$\nabla^2 \mathbf{E}(\mathbf{r}, t) = \left(\frac{n^2(\mathbf{r})}{c_0^2}\right) \frac{\partial^2 \mathbf{E}(\mathbf{r}, t)}{\partial t^2} \tag{2.11}$$

with the position vector $\mathbf{r}$ and the refractive index $n(\mathbf{r})$. For monochromatic waves the solutions of this Helmholtz-type equation (2.11) have the form of:

$$\mathbf{E}(\mathbf{r}, t) = \mathbf{E}(\mathbf{r})e^{i\omega t}, \tag{2.12}$$

By substituting (2.12) in (2.11) one derives

$$\nabla^2 \mathbf{E}(\mathbf{r}) + k^2 n^2(\mathbf{r})\, \mathbf{E}(\mathbf{r}) = 0 \tag{2.13}$$

with $k \equiv \omega/c$. For simplification the propagating wave is assumed to be homogeneous and planar:

$$\mathbf{E}(\mathbf{r}) = \mathbf{E}(x, y)\, e^{-i\beta z},$$

with the propagational constant β. Equation (2.13) can thus be transformed to

$$\frac{\partial^2 \mathbf{E}(x, y)}{\partial x^2} + \frac{\partial^2 \mathbf{E}(x, y)}{\partial y^2} + \left(k^2 n^2(\mathbf{r}) - \beta^2\right)\, \mathbf{E}(x, y) = 0. \tag{2.14}$$

Because of assuming the waveguide being of infinite extent along the y-axis equation (2.14) can be separated to different forms for each regions n_1, n_2 and n_3:

$$
\begin{aligned}
n_1: \quad & \frac{\partial^2 E(x, y)}{\partial x^2} + \left(k^2 n_1^2 - \beta^2\right) E(x, y) = 0 \\
n_2: \quad & \frac{\partial^2 E(x, y)}{\partial x^2} + \left(k^2 n_2^2 - \beta^2\right) E(x, y) = 0 \\
n_3: \quad & \frac{\partial^2 E(x, y)}{\partial x^2} + \left(k^2 n_3^2 - \beta^2\right) E(x, y) = 0.
\end{aligned}
\tag{2.15}
$$

Possible solutions for the terms in equation (2.15) are either sinusoidal oder exponential functions of x, depending on the sign of the term

$$k^2 n_i^2 - \beta^2, \quad i = 1, 2, 3.$$

Due to the continuity conditions at the interfaces for $E(x, y)$ and $\partial E(x, y)/\partial x$ the possible waveguide modes are restricted to the ones depicted in figure 2.4.

The shown variants of waveguide modes depend on the propagation-constant and can be categorized accordingly:

$\underline{\beta > k n_2:}$
$E(x)$ is of exponential type in all three refractive index regions. The continuity conditions at the interfaces can be only fulfilled with an electrical field distribution like it is displayed at the outer right side in figure 2.4. Such a distribution of the electrical field is, however, not physically possible as the electrical field in the layers n_1 and n_3 is not limited. This would require an infinite amount of energy.
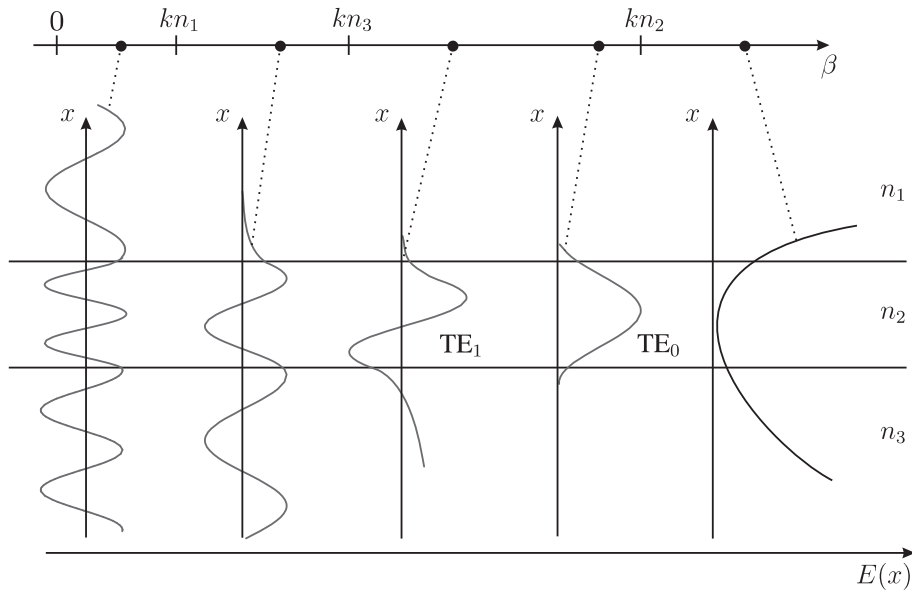
Figure 2.4: Schematic drawing of the possible modes for a planar waveguide structure. The frequency ω of the wave is constant. (adapted from *Integrated Optics: Theory and Technology* by R. G. Hunsperger [31])

$kn_1 < kn_3 < \beta < kn_2$:
Modes with this propagation-constant β are guided inside the waveguide layer n_2. The two modes shown in figure 2.4 are referred to as transversal electrical modes of zero (TE_0) and first order (TE_1). Waveguide modes of higher order are respectively possible.

$kn_1 < \beta < kn_3 < kn_2$:
This type of modes is restricted in their propagation at the interface to the lowest refractive index region (typically air). On the substrate side, however, they are sinusoidally shaped. These modes are guided inside the waveguide but they continuously loose energy through radiating into the substrate. Therefore these modes are also referred to as *substrate radiation* modes.

$\beta < kn_1$:
The solutions of $E(x)$ are sinusoidal in all three refractive index regions. The modes are not guided by the waveguide.

Mostly guided modes are relevant for organic distributed feedback lasers. A formal calculation of the solutions of (2.11) results, due to the boundary conditions, in discrete values for β_m. These represent the different modes TE_j ($j = 1, 2, 3, \ldots$). The number of guided modes in such asymmetrical waveguides is linked to the thickness d of the wave-guiding layer. For fixed values d, n_1, n_2 and n_3 there is a minimal frequency ω_c, the so called cut-off frequency. No guided modes exist below this frequency.

For the magnetic field distribution $\mathbf{H}(\mathbf{r}, t)$ the discussion can be conducted in the same way as for the electrical field. The resulting modes are called transversal magnetic modes (TM). This indicates, that the electrical field of a TM-mode is polarized perpendicular to the waveguide plane.

The propagation of a guided mode inside the waveguide can be described by introducing an effective refractive index n_{eff}. It accounts for the distribution of the mode over the regions with different refractive indexes:

$$n_{\text{eff}} = \frac{\beta_m}{k} \qquad \text{with} \qquad n_1, n_3 < n_{\text{eff}} < n_2 \qquad (2.16)$$

Rip waveguides

A rip waveguide is defined over a refractive index profile as it is shown in figure 2.5. An analytical deviation of the possible modes in such a profile is not trivial. An approximation which works for most applications, however, can be done by assuming two different sets of guided modes. The first one can be calculated the same way as a planar waveguide with the refractive indexes n_1, n_2 and n_4. The second one can be calculated accordingly but with the refractive indexes n_1, n_3 and n_5. A much more detailed discussion of the optical properties of rectangular shaped waveguides can be found in [31] and [32].
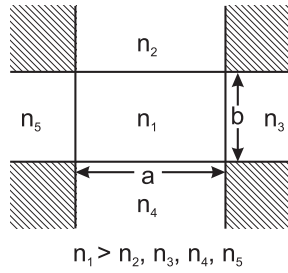
Figure 2.5: Refractive index profile of a rectangular rip waveguide which is surrounded by lower refractive index regions

2.1.3   Geometric etendue and resolution limits

The french word etendue translates literally to *extend* or *space*. In radiometry the geometric etendue, G, specifies the ability of an optical system to accept light. It is a function of the area S of the emitting source and the solid angle Q it emits into.

$$\mathrm{d}^2 G = \mathrm{d}S \mathrm{d}Q \, G = \iint \mathrm{d}S \mathrm{d}Q \qquad (2.17)$$

The numeric value of G is a constant of an optical system and is determined by the least optimized segment. The relevance of the geometric etendue for designing an optical system can be clarified by considering the simple setup shown in figure 2.6. The setup comprises a spherical lens which creates an image of a light emitting diode (LED).

By approximating a conical beam and integrating, the etendue for this setup results in:

$$G = \pi S \sin^2 \mathrm{d}\Omega \qquad (2.18)$$

The geometric etendue can thus be considered as the maximum beam size an optical system is able to accept. Therefore, when designing an illumination system it is

Figure 2.6: Example optical system for the geometric etendue. The light emitted by an LED with the active area S_1 is imaged by a spherical lens with the image spanning the area S_2

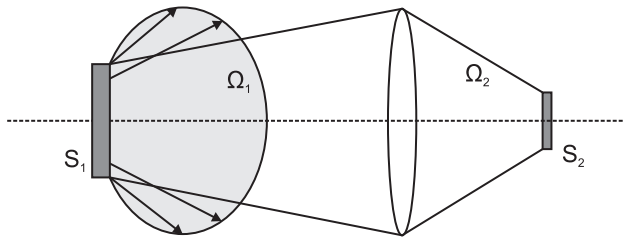necessary to start at the light source and ensure that the optical system including ancillary optics collects and propagates the maximum amount of light.

According to equation (2.18) G is minimized by minimizing S and Ω. Reducing the light emitting area requires a higher radiation energy density for the same performance. The use of a parabolic reflector can reduce Ω but will increase S.

Another important implication of Eq. (2.18) is that focusing a light source below the initial area S without losses can only be achieved if it matches the etendue of the focusing system. As the size of lenses in an optical system is limited, typically low diverging light sources like lasers are preferred as they simplify the optical design significantly.

2.1.4   Optical resolution limits

The fabrication of microoptical devices often relies on optical lithography (see Sec. 3.2.1, p. 42). With the steady downsizing of pattern features this technology is constantly pushed towards the physical limits [33]. Modern lithography systems use the optical system of a microscope (inverse telescope) to project a reduced image of a mask onto the photoresist. The achievable feature size is therefore determined by the microscope resolving power. It is typically determined by the quality of the lenses used. But, apart from such fabrication-induced limitations the resolving power is ultimately limited by diffraction.

To illustrate this limitation of the resolving power it is expedient to take a closer look on the diffraction pattern generated by a circular aperture which is illuminated with parallel light. The resulting circular intensity pattern shown in figure 2.7 is known as an Airy pattern with the central bright lobe being called called an Airy disk. Both were named after George Biddell Airy[4] who gave the first first full theoretical explanation of the phenomenon in 1835 [34].

The diffraction pattern generated by light which passes through a circular aperture is rotationally symmetric. The intensity distribution can be expressed in terms of the Bessel function of the first kind $J_1(\theta)$:

$$I(\theta) = I_0 \cdot \left(\frac{2J_1(r)}{r} \right)^2 \qquad \text{with} \qquad r = ka \sin\theta, \qquad (2.19)$$

where k is the wave number of the light and a the radius of the aperture.

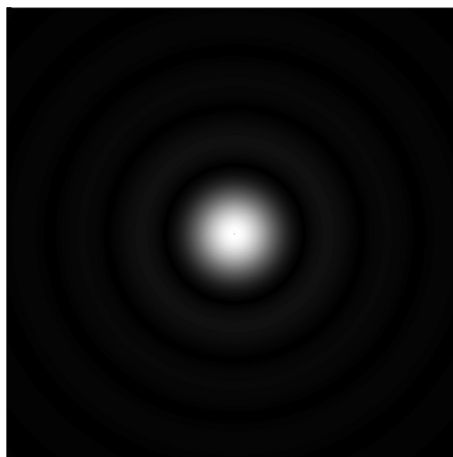[4] $\star$July 27th, 1801, †January, 2nd 1892

Figure 2.7: Calculated square root of the Airy intensity pattern generated by diffraction at a circular aperture which is illuminated with parallel light. The pattern would be hardly visible at a linear scale.

A generally accepted criterion for the minimum resolvable distance d_0 between two adjacent points in the object was defined by Lord Rayleigh[5]. The Rayleigh criterion says that two point sources are regarded as just resolved when the principal diffraction maximum of one image coincides with the first minimum of the other as it is illustrated in figure 2.8a. If the distance is greater than d_0, the two points are well resolved (Fig. 2.8b) while they are regarded as not resolved if it is smaller (Fig. 2.8c).

With Eq. (2.19) for a circular aperture this translates into the minimum angular resolution:

$$\sin\theta = 1.220\frac{\lambda}{D} \qquad \text{with the wavelength } \lambda = \frac{2\pi}{k} \qquad (2.20)$$

The factor of 1.220 originates from the first null of the Bessel function. Assuming a small θ and hence the object distance being equal to the focal length f of the lens, the spatial resolution, i.e. the size d_0 of the smallest object that the lens can resolve, can be approximated to

$$d_0 = 1.220\frac{f}{D}\lambda \qquad (2.21)$$

The ratio f/D, the so called f-number is a characteristic value of a lens. Optical systems, however, are often characterized by the numerical aperture (NA). It is defined over the half-angle θ of the maximum cone of light that can enter or exit the system:

$$\text{NA} = n \cdot \sin\theta \overset{(2.20)}{=} n\sin\arctan\left(\frac{D}{2f}\right) \qquad (2.22)$$

The coefficient n represents the refractive index of the medium from which the light enters the optical system. With Eq. (2.21) the smallest resolvable distance between two objects can then be expressed in terms of the NA with:

$$d_0 = 1.220\frac{\lambda}{2n\sin\theta} = 0.61\frac{\lambda}{\text{NA}} \qquad (2.23)$$

---

[5] ⋆November 12th, 1842, †June 30th, 1919
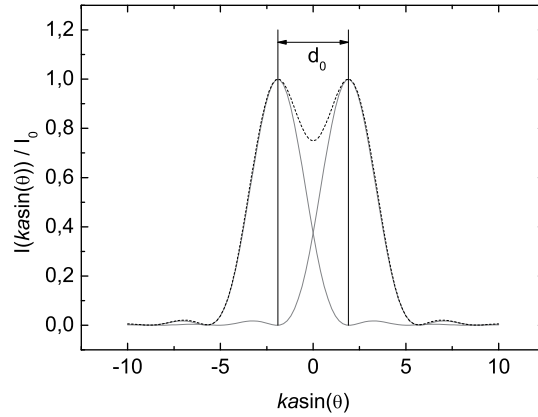
(a) Rayleigh criterion
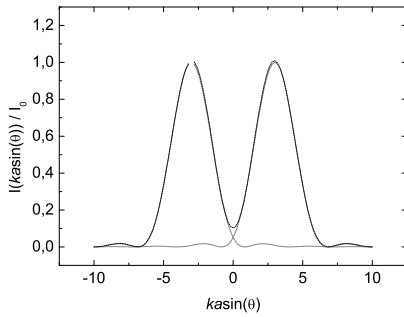
(b) resolved
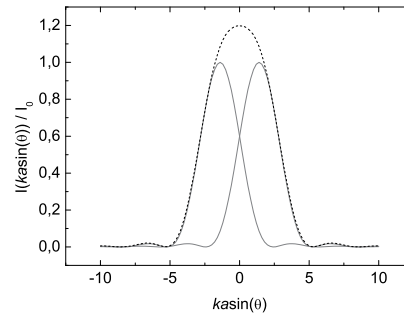
(c) unresolved

Figure 2.8: Diffraction patterns of two adjacent points in the object. According to Rayleigh, the two points can be resolved in the image if the angular separation of the two points is greater than d_0.

When the system is operated in air the highest obtainable numerical aperture is $\mathrm{NA} = 1$. Immersing it in a liquid with a higher refractive index increases the NA. Typical immersion oils have refractive indexes around 1.5 thus roughly speaking the smallest resolvable distance is limited to half of the wavelength.

It has, however, to be noted that equation 2.23 has to be regarded as a rule of thumb as the underlying Rayleigh criterion is somewhat arbitrarily. Also it fails in predicting the three dimensional resolving power which is especially important for two-photon absorption direct laser lithography (see Sec. 3.2.2, p. 42). A more detailed theoretical discussion on the three dimensional focusing of electromagnetic waves can be found in the studies of Richard and Wolf [35, 36].

2.2 Organic semiconductor lasers

This section introduces basic principles for lasers as well as terms and definitions connected with them. Unless otherwise noted, the given explanations orient themselves on the extensive book *Lasers* by Anthony E. Siegman [37]. Building on this knowledge and after a brief look on organic gain materials the organic distributed feedback semiconductor laser is introduced. This section ends with elucidating different concepts for the emission wavelength tuning of organic semiconductor lasers.

2.2.1 Stimulated emission and the LASER principle

The term LASER is an acronym for "light amplification by stimulated emission of radiation". The LASER principle is based on interactions between light and matter which induce transitions of electrons between different energy states. Figure 2.9a shows a fundamental model for these interactions. It includes only two energy states: a ground state and an excited state. The energy E_0 equates to the ground state energy eigen-value of the electron. In case of the excited state the electron energy is increased from E_0 by the value ΔE to E_1. The possible electron energy transitions between these two states can be divided into three cases:

- *Absorption*, a photon with the energy $\hbar\omega = E_1 - E_0 = \Delta E$ is absorbed by lifting an electron into the excited state E_1 (Fig. 2.9a).

- *Spontaneous emission*, an electron drops from the excited state E_1 to the ground state E_0 and emits a photon with the energy $\hbar\omega = \Delta E$ (Fig. 2.9b).

- *Stimulated emission*, a photon with the energy $\hbar\omega = \Delta E$ induces the transition of an electron from the excited state E_1 to the ground state. A photon is emitted which is coherent with the incident photon (Fig. 2.9c).
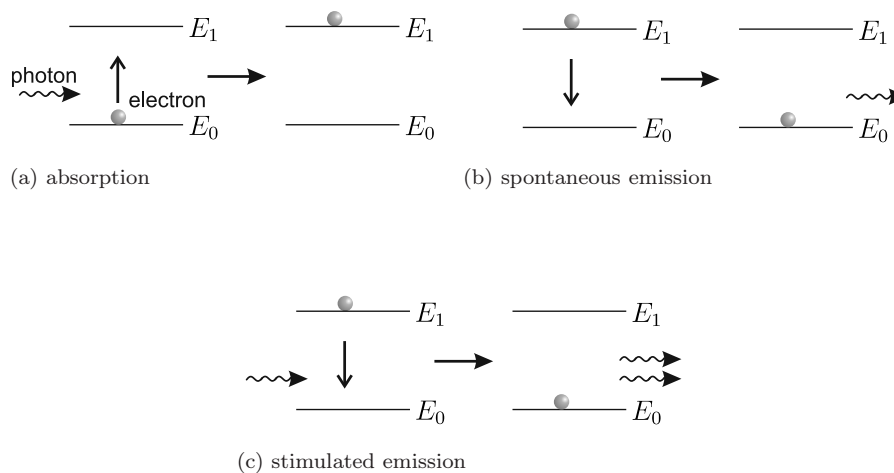

(a) absorption   (b) spontaneous emission

(c) stimulated emission

Figure 2.9: Interaction processes of light and matter based on electron energy transitions

Population inversion and four level systems

In an infinitely extended medium with unlimited excited electron states a sponta-
neously emitted photon can thus be amplified by repeated stimulated emissions. In
general, however, only a limited number of excited states is occupied. This results
in absorption losses due to the excitation of ground states. This in turn prevents
LASER operation in a two level system. Efficient amplification of photons thus re-
quires a system were the number of excited states constantly exceeds the number of
ground states. This condition is called population inversion and requires a system
with a minimum of three energy levels. A three level system, however, requires to
lift at least half of the ground state electrons into an excited state within a single
pump instance. A four level system as it is depicted in figure 2.10 represents the
ideal case due to lower requirements on the pump source.
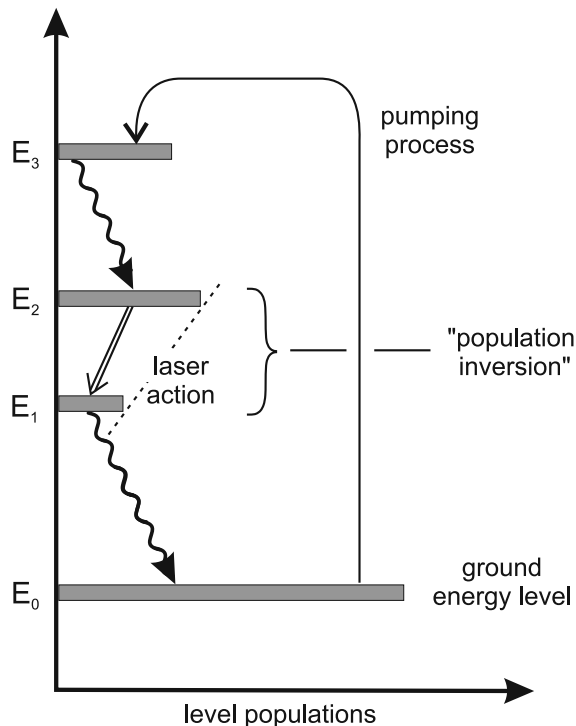
Figure 2.10: Four level laser energy diagram. Electrons are lifted into an excited state E_3
by an external energy pump. Successively, they relax into the upper laser state
E_2. From there a transition to the E_1 energy band takes place either due to
stimulated emission or spontaneously after the average lifetime expired. After
a dwell time in the E_1 state the electron finally drops into the ground-state.

Electrons are lifted into an excited state E_3 by feeding energy from an external
source. This pumping process can be done with electro-magnetic radiation, direct
electrical injection of electrons, chemical reactions or even the kinetic energy of
nuclear fission fragments [38]. The excited electrons then relax with the average
lifetime τ_1 into the upper state E_2 of the laser transition. From there transitions
to the E_1 energy band take place either due to stimulated emission or after the
average lifetime τ_2 expired. After the dwell time τ_3 the electrons finally drop into
the ground-state. Hence, for actually generating a population inversion the excited

states life times have to fulfill the condition:

$$\tau_2 \gg \tau_1, \ \tau_3 \tag{2.24}$$

The majority of the known laser materials can be described as a four level system. The main difference is, that generally more than a single discrete laser transition exist. Additionally these materials exhibit optical gain over a more or less extended wavelength region due to the broadening of the energy bands.

Optical feedback with resonators

The probability for a photon of inducing a stimulated emission is proportional to the excited state population number and the photon dwell time in the active region. Providing an optical feedback by a resonant optical cavity as shown in figure 2.11a can, hence, increase the efficiency significantly. Due to the highly directional
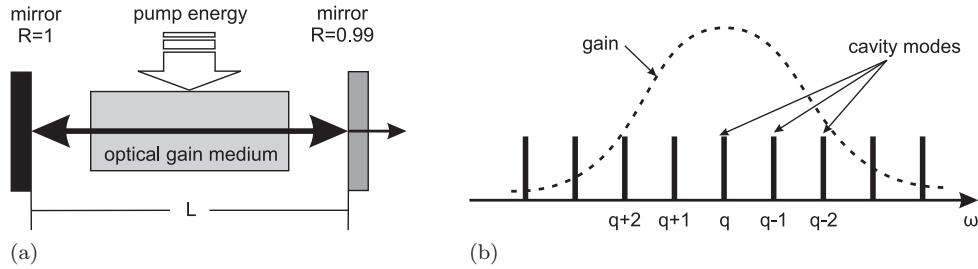
Figure 2.11: (a) Resonant cavity for optical feedback. The active gain medium is enclosed by a highly reflecting mirror and an out coupling mirror with a low transmittance. (b) The possible laser modes are determined by the spectral gain and the resonator length L.

feedback mechanism of such a resonant cavity it gives also the benefit of a very low emission divergence. This is advantageous especially for the design of optical systems (see section 2.1.3). In general, for the desired efficient amplification of a discrete (vacuum-)wavelength λ_L an oscillation build-up of additional laser modes has to be suppressed. A straightforward approach for this is to shorten the resonator length L to such an extent, that only the fundamental mode is located inside the gain region of the laser material:

$$L = \frac{\lambda_L}{2n_{\mathrm{medium}}}; \qquad n_{\mathrm{medium}} = \text{gain medium refractive index} \tag{2.25}$$

It has to be noted, that these contemplations provide only a basic view on the topic of resonant cavities. A much more detailed essay on *Laser Beams and Resonators* was published by Kogelnik and Li in 1966 [39].

Mirrorless lasing

The laser principle does not imply the need for a resonator. Increasing the excitation energy and/or the excited volume increases also the probability of a spontaneously emitted photon to induce a radiating transition before it is absorbed or scattered out

of the optical gain region. Similarly to lasing with optical feedback this phenomenon exhibits also a threshold characteristic and a spectral narrowing of the emission. The latter originates from the fact, that modes with the highest spectral gain will induce the majority of the radiating transitions. In return, this leaves only a small probability for excited states to spontaneously emit into other modes. The spectral narrowing of the emission bandwidth depends on the width of the spectral gain. Materials with a broad gain spectrum exhibit a lower narrowing than materials with a narrow gain spectrum.

Although this phenomenon is consistent with the LASER definition, it is commonly labeled separately as super luminescence or amplified spontaneous emission (ASE). ASE requires high excitation energies and a large excited volume in the gain material due to high radiation losses. Emitting a spectrally narrow laser line also requires gain materials with discrete spectral lines. Despite the inefficiency, the mirrorless nitrogen laser [40] shows that ASE allows to produce laser radiation with simple means. A directed output is achieved with such lasers by introducing a preferred direction in the distribution of the optical gain. For an isotropic spatial distribution of the optical gain the ASE emits equally into all directions as depicted in figure 2.12a. Photons emitted spontaneously along the preferred direction have a higher probability of stimulating an emission than photons traveling in another direction as shown in figure 2.12b.

(a) homogeneous optical
gain distribution

(b) inhomogeneous optical gain distribution
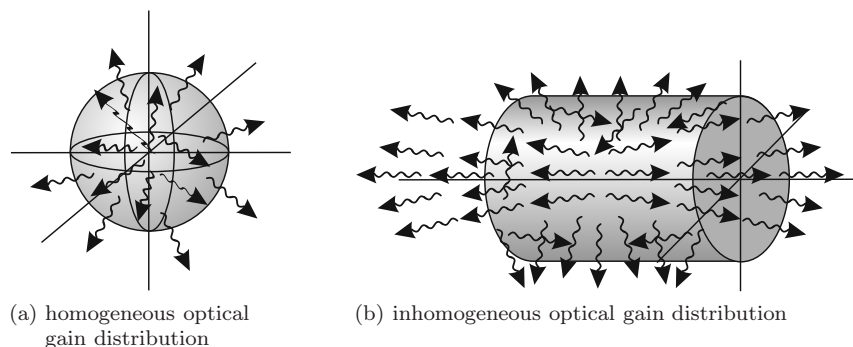
Figure 2.12: Directed emission from ASE induced by a inhomogeneous optical gain distribution

2.2.2   Distributed feedback resonators for organic lasers

Among different approaches for the resonator design for organic lasers [26] the distributed feedback (DFB) resonator scheme is one of the most popular realizations due to its rather simple and efficient design which provides a high degree of spectral selection. Typically, an organic distributed feedback laser consists of a thin film active material that is deposited on top of a periodically corrugated substrate. Common film thicknesses range from (100 to 400) nm. The active material is optically pumped, for example by an external pulsed ultra violet (UV) laser. The layer sequence forms a slab waveguide confining the optical wave in the substrate plane. Instead of using mirrors, the optical feedback is provided by the so called distributed feedback mechanism. This mechanism relies on backward Bragg scat-

tering at a wavelength scale periodic perturbation of the refractive index and/or the gain of the laser medium [41]. The first DFB lasers employed a holographic pump scheme to induce such perturbations [42, 43]. Most modern devices employ surface corrugations (gratings) of the substrate or the active waveguide. Organic DFB laser devices can be realized by patterning either the active layer at the air interface or the substrate or both as illustrated in figure 2.13. Patterning of the active layer (Fig. 2.13a) can be achieved with photoisomerization [44], direct embossing [3, 45] or laser interference ablation [4, 46]. The process parameters for patterning the active layer have to be optimized specifically for each applied gain material. From the processing point of view it is therefore advantageous to pattern the substrate material. Thus, this is the most common choice taken for fabricating organic DFB lasers. For patterning the substrate a large variety of well established processes can be employed. For a brief overview the reader is kindly referred to T. Woggon et al., *Organic Semiconductor Lasers as Integrated Light Sources for Optical Sensors* [47].
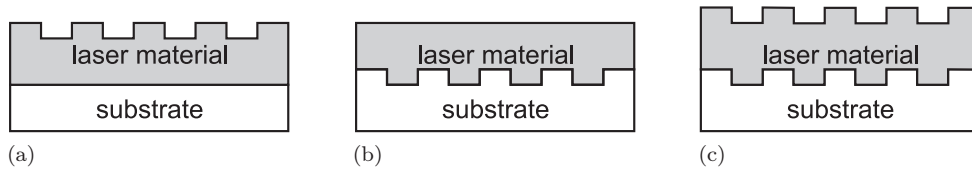
Figure 2.13: (a) Direct patterning of the organic laser (b) Patterning of the substrate (c) Pattering of both interfaces with vapor deposition or subsequent patterning (T. Woggon et al. [47])

The complete modeling for slab waveguide DFB lasers is very complex. Their emission wavelength and direction can, however, be estimated well by a separate view on the waveguide and the Bragg scattering process. Figure 2.14 illustrates the distributed feedback mechanism in a slab waveguide structure with a one-dimensional, periodic variation of the refractive index.
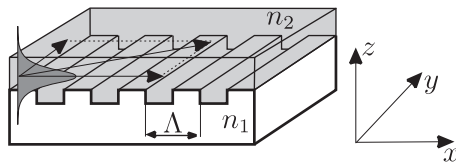
Figure 2.14: One dimensional slab waveguide structure with a periodic variation of the refractive index (T. Woggon et al. [47])

The lattice constant Λ of the grating transforms to the reciprocal lattice constant $\mathbf{G}$ in the momentum space (k-space):

$$\mathbf{G} = \begin{pmatrix} 0 \\ \frac{2\pi}{\Lambda} \\ 0 \end{pmatrix}$$

Lasing operation occurs in plane and can be discussed by starting with a plane wave

propagating in the slab with wave vector $\mathbf{k}$:

$$\mathbf{k} = \begin{pmatrix} k_x \\ k_y \\ 0 \end{pmatrix} \text{ with } |\mathbf{k}| = n_{eff} \cdot \frac{2\pi}{\lambda}$$

The scalar n_{eff} represents the effective refractive index of the propagating guided wave. For efficient feedback, which is essential for laser operation, constructive interference of a scattered wave is required. This is the case if $\mathbf{k}$ fulfills the Bragg equation.

$$k_{x,m} = \frac{m}{2}|\mathbf{G}| \qquad m \in \mathbb{N} \tag{2.26}$$

The positive integer factor m determines the scattering order. The scalar $k_{x,m} = 1$ gives the smallest possible value of the wave vector component (corresponding to the largest wavelength) in the direction of the refractive index modulation for which constructive interference is possible. In the special case of a wave traveling parallel to the reciprocal lattice vector $\mathbf{G}$ one gets the well known equation:

$$\Lambda = \frac{m}{2} \frac{\lambda}{n_{eff}}$$

In general the constructive scattering of an incident wave with the vector $\mathbf{k}_i$ occurs if the Laue condition is fulfilled:

$$2\mathbf{k}_i \cdot \mathbf{G} = |\mathbf{G}|^2 \qquad \text{with } \mathbf{k}_i = \begin{pmatrix} k_{x,m} \\ k_y \\ 0 \end{pmatrix} \tag{2.27}$$

This formulation of the feedback condition states that Bragg scattering can occur if the incident photon $\mathbf{k}_i$ vector is located on a Bragg plane, being the perpendicular bisector of a line connecting the origin with the reciprocal lattice point $\mathbf{G}$. A wave vector $\mathbf{k}_i$ which is located on a Bragg plane is scattered to $\mathbf{k}_d$ and vice versa. The wave vector $\mathbf{k}_i$ of the incident and $\mathbf{k}_d$ of the scattered wave correlate in the form:

$$\mathbf{k}_d = \mathbf{k}_i + \mathbf{G} \tag{2.28}$$

Energy conservation results in the additional relation:

$$|\mathbf{k}_i| = |\mathbf{k}_d| = \text{const} \tag{2.29}$$

Figure 2.15a shows first order scattering ($m = 1$) of a wave vector. If the incident wave vector $\mathbf{k}_i$ complies with the condition in Eq. (2.27) it is scattered as stated in Eq. (2.29). Second order scattering ($m = 2$) is depicted in figure 2.15b. In this case the vector component k_x of the incident wave vector $\mathbf{k}_i$ equals to the reciprocal lattice vector. The component $k_{d,x}$ of the scattered wave vector can take the values of either $k_{d,x} = -k_{i,x}$ for the second order Bragg feedback or $k_{d,x} = 0$ in case of first Bragg order scattering. The latter implies that the light can be scattered perpendicularly in two opposite directions of the waveguide plane.

The scattering condition Eq. (2.26) determines only the component k_x of the wave vector. This results in a nonzero z-component of the wave vector since the energy

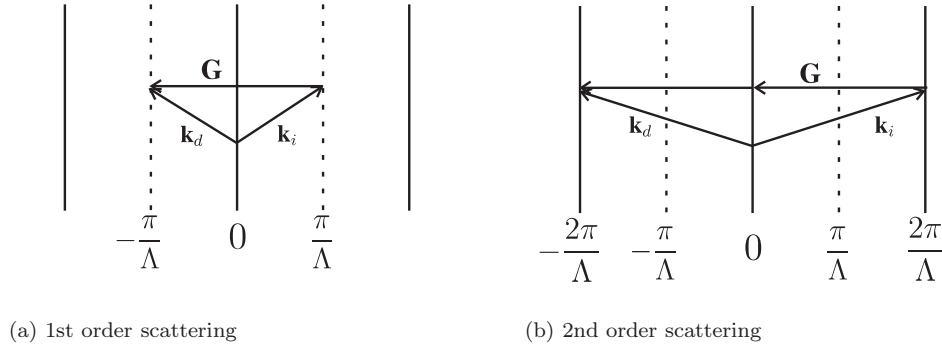(a) 1st order scattering   (b) 2nd order scattering

Figure 2.15: (a) Feedback due to 1st order scattering:
The vector component $k_{i,x}$ of the incident wave vector $\mathbf{k}_i$ equals to half of
the reciprocal lattice vector. The scattered wave vector thus has to fulfill the
condition $\mathbf{k}_d = -\mathbf{k}_i$.
(b) Feedback due to 2nd order scattering:
The vector component k_x of the incident wave vector $\mathbf{k}_i$ equals to the recip-
rocal lattice vector. The component $k_{d,x}$ of the scattered wave vector can
take the values of either $k_{d,x} = -k_{i,x}$ for the second order Bragg feedback or
$k_{d,x} = 0$ in case of first Bragg order scattering. (T. Woggon et al. [47])
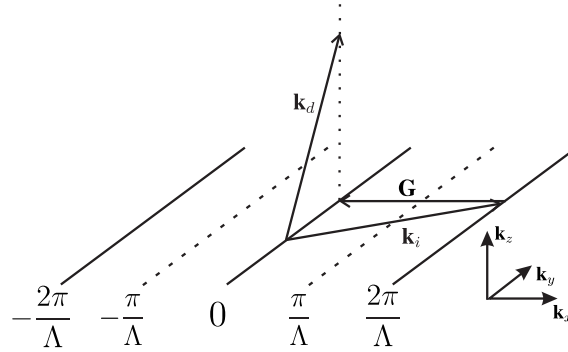
Figure 2.16: Out-of-plane coupling due to 2nd order scattering:
For a zero vector component of the scattered wave ($k_{d,x} = 0$) a nonzero com-
ponent $k_{d,z} \neq 0$ is required to comply with the principle of the conservation
of momentum $|\mathbf{k}_i| = |\mathbf{k}_d|$.

conservation law has to be met. This means the incident wave is scattered out of
the waveguide. First order resonators are of special interest for on-chip integration
and enable lower laser thresholds. Second order laser resonators are advantageous
for applications with free space optics due to their good light extraction efficiencies.

It must be pointed out, that in contrast to k_z the vector k_y is not defined by
the Laue condition Eq. (2.27). The thus allowed arbitrary values for k_y for a one
dimensional DFB resonator result in an oscillation build-up of multiple laser modes.
Due to this disadvantage the concept of distributed feedback has been extended
early to two dimensions using square lattices [48].

One major advantage of the DFB resonator concept is a good thermal stability
as the wavelength determining scales are in the region of the emission wavelength.

According to the definition of the CTE in Eq. (2.30) a polymer DFB laser with $\alpha = 1 \times 10^{-6}\,\mathrm{K}^{-1}$, a grating periodicity of $400\,\mathrm{nm}$ and an excited region width of $500\,\mathrm{\mu m}$ for example has only an elongation factor of $4\,\mathrm{pm\,K^{-1}}$ for the grating period. This is three orders of magnitude lower compared to the elongation factor of $5\,\mathrm{nm\,K^{-1}}$ which a fabry perot laser cavity with a length of $500\,\mathrm{\mu m}$ and the same CTE has.

$$\alpha = \frac{1}{L_0} \cdot \frac{\Delta L}{\Delta T} \tag{2.30}$$

2.2.3 Absorption and emission of light in organic materials

In chemistry, the term organics includes all compounds that contain both hydrogen and carbon. These hydrocarbons can be subdivided into saturated and unsaturated hydrocarbons. The latter comprise at least one double or triple bond of a carbon atom. These double bonds are mainly responsible for the optical properties of organic materials. A specific configuration of this double bond, the so called π-conjugated bond forms a system of delocalized electrons. These electrons can move freely along the molecule backbone.

This explanation is a very simplified view on the physical background of delocalized electron systems in hydrocarbons. A detailed treatise of this topic can be found e.g. in the book *Molecular Physics and Elements of Quantum Chemistry* by H. Haken and H. C. Wolf [49]. For the understanding of the processes relevant for this thesis it suffices, however, to acknowledge the existence of delocalized electrons in organic materials with unsaturated hydrocarbons. A step further in simplifying is treating this system as a free electron gas in a potential well. The π-conjugated system of organic molecules condensed at room temperature typically extends over several bonds. This behavior can be reflected in the width of the potential well. With each bond contributing a delocalized electron the available states can, bearing the Pauli exclusion principle in mind, be occupied with two electrons. This leads to singlet and triplet electronic states. These states form further various vibrational levels yielding an Jablonski[6] energy diagram as depicted in figure 2.17. Between these electron energy states transitions can take place via different processes which are also denoted in figure 2.17.

Absorbing a UV-VIS photon promotes π-electrons into one of the upper singlet states S_i. The process happens very fast with a time span in the range of $10^{-14}\,\mathrm{s}$. Absorption of light excites molecules to different vibrational levels of the excited singlet state. Successively, over vibrational relaxation (VR) the molecule returns to the lowest level of the excited state. From there, the molecule can return to the ground state with emitting a photon. With $(10^{-6}$ to $10^{-12})\,\mathrm{s}$, the fluorescence process occurs on a much longer timescale than the absorption process. This return to the ground state can also happen due to radiation less processes called internal or external conversion.

Internal conversion is regarded as being the most efficient deactivation process especially for molecules with electronic energy levels spaced so close, that their vibra-

---

[6]named after Alexander Jablonski ⋆February 26th, 1898 in Voskresenovka, Ukraine, †September 9th, 1980 in Skierniewice, Poland
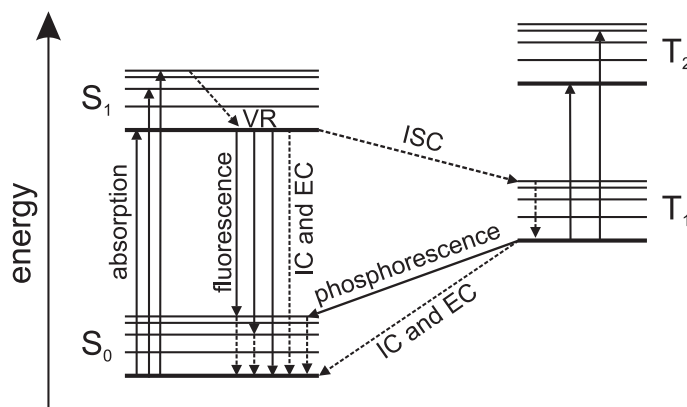
Figure 2.17: Jablonski energy diagram presenting the various energy levels and processes involved in the absorption and emission of light by a organic compound: The electronic levels of the singlet ground (S_0) and first excited state (S_1) as well as the excited triplet states T_1 and T_2 are drawn as thicker lines. The thinner lines indicate different vibrational energy states. Transitions between the states associated with absorption or emission of a photon are denoted as straight arrows. Dashed arrows mark the non-radiative processes as internal and external conversion (IC and EC), vibrational relaxation (VR) and intersystem crossing (ISC). The rotational substrates are not resolved.

tional energy levels of ground and excited state overlap. External conversion denotes the process of excited molecules losing their energy by colliding with and/or transferring energy to neighbor molecules. This process is thus an important loss process when exciting molecules in a solid matrix or in a highly concentrated solution.

A third process which can take place for the transition of a molecule present at the first excited singlet state is the intersystem crossing (ISC). This process involves a transfer of the molecule from an excited singlet to a triplet state. This process is possible since the vibrational levels in the singlet and triplet states overlap in energy. To satisfy the conservation law of the total angular momentum, however, crossing of the singlet state to the triplet state requires a flip in electron spin which basically forbids this process. Nevertheless, intersystem crossing can be facilitated by internal and external perturbations, e.g. the presence of non-bonding electrons as well as heavy or paramagnetic atoms. Intersystem crossing can also take place backwards from the triplet to the singlet state and thus result in a delayed fluorescence emission with the same properties of fluorescence but with a much longer lifetime.

The first excited triplet state exhibits with $(10^{-3}$ to $10^{-3})\,$s a very long lifetime. This state can be also excited to higher triplet states with energies comparable to the fluorescence emission. This triplet–triplet absorption is therefore a strong loss process in laser media. Besides relaxing to the ground state by internal and/or external conversion, electrons in the first triplet state can also loose their energy by emitting a photon in a process called phosphorescence. Again, all three processes require a flip in spin to satisfy the singlet ground state. The phosphorescence process is the summation of an intersystem crossing and two flips in spin. Hence, the phosphorescence lifetime is much longer than the fluorescence lifetime. Regarding the high possibility of radiationless deactivation, phosphorescence plays only a minor

role in the absorption and emission of light in most organic materials. An exemption are OLEDs were electrophosphorescence enables very high internal quantum efficiencies [50].

The previous contemplation of the processes involved in the absorption and emission of light in organic materials does not account for any changes of the distances between the atomic nuclei of the molecule. The distance between two atomic nuclei is, however, larger in the excited molecule than in the ground state. The resulting effects on the absorption and emission energy spectrum can be elucidated by applying the Born-Oppenheimer approximation. It assumes, that due to the short timespan of an electron transition and its low mass the position of the atomic nuclei can be seen as fixed during a transition. Transferred to a potential energy curve picture this results in the transitions being reflected as vertical arrows as depicted in figure 2.18a. The probability of a molecule transition from the ground state to a vibra-
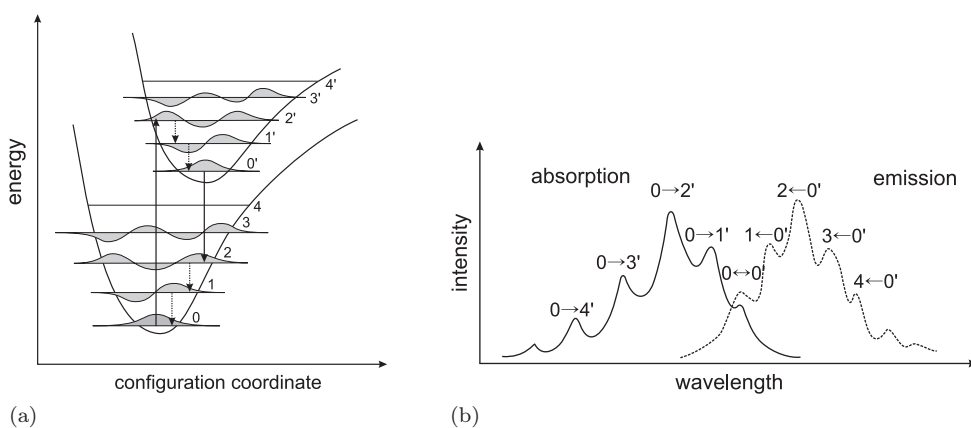

Figure 2.18: (a) Transitions involved in the absorption and fluorescence emission of light by a fluorophore described with the Franck-Condon principle. Since nuclear motion can be neglected during electronic transitions, vibrational states are favored where the initial and the excited vibrational wave function overlap, i.e. correspond to a minimal change in the nuclear coordinates. (b) The absorption spectrum reflects the vibrational structure of the excited state. The fluorescence spectrum represents the vibrational structure of the ground state respectively. The fluorescence is shifted towards lower energies with respect to the absorption spectrum. Both spectra are in general symmetrically whereas the $0 \leftrightarrow 0'$ transitions can be identical for small spectral shifts.

tional level of the excited state has its maximum when the excited state vibrational wave function has a maximum overlap with the ground state wave function. This semi-classical interpretation for explaining the intensity of vibrational transitions is called the Franck-Condon principle[7]. Applying the Franck-Condon principle as depicted in figure 2.18a results in absorption and emission spectra shown in figure 2.18b. The absorption spectrum reflects the vibrational structure of the excited state. The fluorescence spectrum represents the vibrational structure of the ground state respectively. The fluorescence is shifted towards lower energies with respect

---

[7]named after James Franck ⋆August, 26th, 1882 in Hamburg, †May, 21th, 1964 in Göttingen and Edward Uhler Condon ⋆March 2nd, 1902 in Alamogordo, New Mexico, †March 26th, 1974 in Boulder, Colorado

to the absorption spectrum. The absorption and fluorescence spectra are symmetrically to each other whereas the $0 \leftrightarrow 0'$ transition can be identically for small spectral shifts, called the Stokes-shift[8].

Organic laser materials

The photophysical processes discussed previously can be generally applied for organic materials. A suitable organic laser material has, however, to meet specific requirements. Organic materials are natural four level systems due to the vibrational sidebands of the electronic states. A requirement for achieving a population inversion which supports lasing is therefore a long lifetime of the excited singlet state and fast vibrational relaxation processes according to Eq. (2.24). The internal and external conversion efficiency should be as low as possible. Additionally, to efficiently prevent a build-up of triplet states, the probability for a intersystem crossing should be low or at least, the triplet lifetime should be short. A good laser material should exhibit a large Stokes-shift with, at best, no overlap of the emission spectrum with the absorption spectra to prevent self-absorption. Due to intrinsic properties which are elucidated in detail in the book *Dye lasers* by F.P. Schäfer [51] the absorption spectrum of stable organic laser materials is also limited to the range from (220 to 1000) nm.

2.2.4   Energy transfer systems

Material systems with a large spectral gap between the absorption of the excitation light and the laser emission are of particular interest for organic semiconductor lasers. This reduces the self-absorption of the emission resulting in a more efficient lasing operation. Such a system can be created by doping the active material into an active matrix thus forming a so called guest-host material. The exciting radiation is absorbed in the host material. The absorbed energy is then transferred by a radiationless process to the guest material lifting it into an electronically excited state (see Fig. 2.19). The predominantly utilized energy transfer mechanism for organic semiconductor lasers is the so called Förster resonance energy transfer [5]. This process, first formalized by T. Förster in 1948 [52], is based on a dipole–dipole interaction and therefore requires a spectral overlap of the donor's emission with the acceptor's absorption. Förster found that the transfer rate between two molecules spaced at a distance r is given by

$$F(r) = \frac{1}{\tau_{\text{guest}}} \left(\frac{R_0}{r} \right)^6 \qquad \text{with} \quad R_0 \propto \int\limits_0^\infty \left(\frac{c}{n\omega} \right)^4 f_{\text{guest}}(\omega)\sigma_{\text{host}}(\omega)\mathrm{d}\omega \qquad (2.31)$$

with the normalized donor fluorescence spectrum $f_{\text{guest}}(\omega)$ and acceptor absorption spectrum $\sigma_{\text{host}}(\omega)$ and the rate of spontaneous emission $1/\tau_{\text{guest}}$ for the guest molecules. According to Eq. (2.31), the rate of dipole–dipole transfer will exceed $1/\tau_{\text{guest}}$ if the distance r is less than the effective Förster radius R_0 defined by the the

---

[8]named after Sir George Gabriel Stokes ⋆August 13th, 1819 in Skreen, County Sligo, †February 1st, 1903 in Cambridge

overlap between fluorescence and emission spectrum [52, 53]. This effective radius R_0 can be up to 10 nm. The second important energy transfer process is the Dexter transfer. Here, an excited electron is transferred from the donor to the acceptor. In return, an electron in the ground state is moved from the acceptor to the donor. This particle exchange needs the atomic orbitals of acceptor and donor to overlap. Therefore, this process is typically only effective at distances of less than 1 nm.
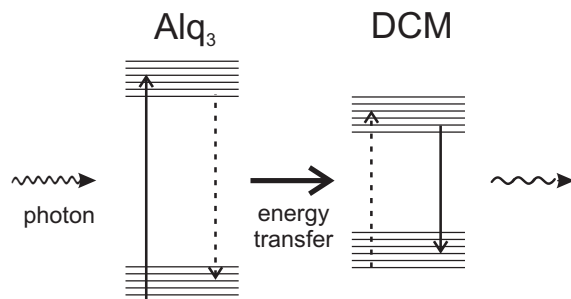

Figure 2.19: Energy transfer in dye doped organic semiconductors: The exciting radiation is absorbed in the host material. The absorbed energy is then transferred by a radiationless process to the guest material lifting it into an electronically excited state. (T. Woggon et al. [47])

2.2.5 Optical excitation of organic semiconductor lasers

Optical vs. electrical excitation

Comparing the structure of an organic DFB laser with an organic light emitting diode, one would expect that adding injection and hole transport layers and electrical contacts would suffice to create an electrically driven organic laser diode. Thus, starting with the first published organic DFB lasers in 1996 [1,54,55] research groups enthusiastically aimed for the first organic laser diode. But, despite huge efforts being made in the recent years, optical gain under electrical excitation is, apart from two questionable reports, still unaccomplished [56,57].

The necessity of an excitation light source for organic lasers is commonly seen as a handicap. For certain applications, however, optical excitation can be quite advantageous. Especially for integrating lasers on disposable lab-on-chip devices the contactless excitation may bear advantages compared to injection lasers [18]. Optical pumping also allows a fast and low cost mechanical tuning of organic lasers (see Ch. 6). There are several ways to optically pump an organic laser. The basic requirement of a high absorbance of the pump light in the laser material applies to all of them. Additionally, short pulses and the ability to focus the radiation onto a small spot with minimized losses are advantageous.

Pulse duration and polarization

Pulse length is important as organic dye molecules tend to be trapped in triplet states, in which they cannot participate in the stimulated emission process. Continuous wave excitation therefore requires additional provisions for steadily replacing

the dye molecules. Depending on the material the pulse duration has a critical influence on the threshold where lasing can be observed. The ideal case would be an instantaneous population inversion, i.e. at the end of the pump pulse as many electrons as possible have been lifted into an upper state. The capability of the material system for this depends strongly on the ratio of the fluorescence lifetime to the pulse duration. For the special case with a ratio of one only 63 % are still in an upper state when the pump pulse ends [58]. Higher energy densities can compensate this, but besides the decreased efficiency the risk of thermally destroying the organic material increases.

Lasers are a good choice for optical pumping due to the low divergence yielding a high focusability (see Sec. 2.1.3, p. 13). Attention should be paid to the highly polarized emission typical for lasers. Wright et al. could show a polarization dependence of the laser threshold with a ratio of 1:3 for dye molecules embedded in a polymer matrix [59]. This phenomenon is due to the polymer chains aligning themselves parallel to the substrate plane during the spin coating process. In a guest-host system this in turn may force also the dye molecules to be in plane due to guest-host molecular interactions. Perpendicular to the feedback grating polarized pump radiation preferably excites the dye molecules dipoles which are also aligned perpendicular to the grating. This leads to most of the dye radiation being emitted perpendicular to the feedback direction and thus a decreased efficiency. Vapor deposited small molecule material systems should in general not be affected by this effect as the molecules have no preferred alignment due to the thin film deposition. Accordingly, pump radiation polarization dependency of the lasing threshold could not be observed for thermally vapor deposited Alq_3:DCM DFB lasers [12].

Diode pumped solid state laser (DPSS)

Q-switched (laser-)diode pumped solid state (DPSS) lasers are able to create sub-nanosecond laser pulses with high energy densities, hence, they were the first compact laser sources used for pumping organic solid state lasers [60, 61]. For this the most common laser type is the neodymium-doped yttrium aluminum garnet laser (Nd:YAG) with an emission wavelength of 1064 nm which is frequency doubled or tripled to 532 nm or 355 nm respectively. Besides the YAG also yttrium-vanadate (YVO_4) or yttrium lithium fluoride (YLF) crystals are used as a guest system due to their better pump light absorption.

Laser diodes and LEDs

Until recently directly pumping organic lasers using inorganic laser diodes stood in conflict with the low pulse power available from UV or green laser diodes. With steady advances in developing low threshold organic lasers and UV laser diodes being made, a gallium nitride (GaN) laser diode-pumped organic laser was presented in 2006 [22,62,63]. GaN laser diodes feature a very compact design and low fabrication costs as they benefit from the scaling effects of the large volume home entertainment sector (Blu-ray Disc™). The huge demand for laser diodes which are powerful enough for laser projection also pushes the development of powerful green GaN laser diodes

[64]. The drawback of these laser diodes is the still limited availability of high power laser diodes and the restriction to only a small set of emission wavelengths available.

Light emitting diodes (LED) are also an alternative for pumping organic lasers at even less cost. They cover the whole visible spectral range down to ultraviolet wavelengths yielding in a perfect adaptability to the absorption peak wavelength of the organic laser material. The major setback for the use of LEDs as pump source is their, compared to a laser, high divergence and low radiant exitance. The limited focusability hence results in a considerable worse efficiency. To achieve the pulse energy densities necessary for a laser operation todays LEDs have to be operated with currents far beyond the manufacturers specifications. Thus, so far only one LED pumped organic laser could be demonstrated by Yang et al. in 2008 [23]. They operated a commercially available LED with 47 ns long current pulses of 160 A.

2.2.6 Identifying laser operation

A laser is traditionally attributed with exhibiting a coherent, low divergence beam with a narrow spectral bandwidth. The small geometric dimensions of organic lasers, however, are able to produce light featuring some of theses criteria which can lead to misinterpretation [57]. For certain identification if laser operation takes place it is expedient to take a look on the typical characteristic of an organic laser under excitation.

The idealized considerations in section 2.2.1 assumed a gain material without optical losses due to radiation less transitions or scattering. Also resonator losses are not taken into account. Transferred to real laser devices these factors negatively affect the device efficiency. This results in a nonlinear dependency between the excitation energy and the optical amplification as depicted in figure 2.20a. With increasing the excitation energy the slope changes at a distinct threshold energy E_{th}. At this excitation energy level the optical gain equals the cavity losses. This results in a considerably steeper slope above E_{th}. The slope can not exceed a value of one due to the conservation of energy. This threshold characteristic is a key indicator for optical amplification but can also be a result of a nonlinearity of the pump source, for example a pump laser diode being operated at its threshold current.

It is therefore mandatory to also observe the evolution of the emission spectrum of the laser device at different excitation energies which is exemplified in figure 2.20b to 2.20d. At excitation energies below the threshold energy E_{th} a photoluminescence (PL) spectrum can be observed which is specific to the gain material. For organic materials this is typically a broad spectral distribution as displayed in figure 2.20b. Slightly above the threshold energy the resonator mode with the largest gain is amplified more efficiently than the remaining emission modes. This results in the formation of a narrow peak out of the PL spectrum as depicted in figure 2.20c. At excitation energies considerably above E_{th} almost all radiating transitions are induced by the disproportionately high number of photons of the laser mode due to the optical feedback. Spontaneous emission of photons is drastically reduced due to the shorter lifetime of spontaneous emission due to the high number of laser mode photons inside the cavity. This causes the spectrum to narrow down to the laser line as shown in figure 2.20d. For an idealized resonator which supports only a
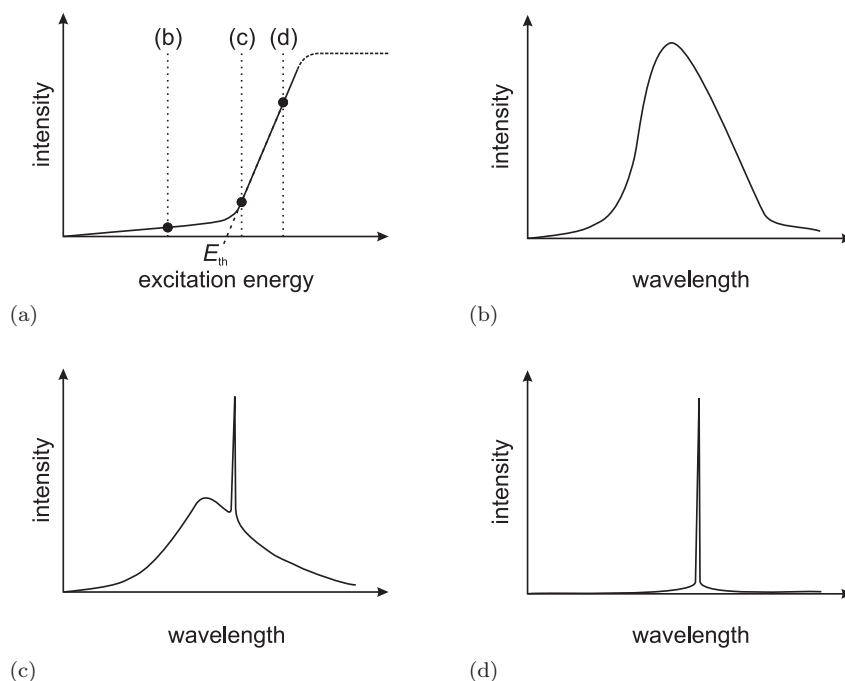
Figure 2.20: Characteristics of a laser: (a) The input-output characteristic shows a nonlinear behavior with a sharp bend at the threshold excitation energy E_{th} (b) At excitation energies below the threshold energy $(E < E_{\text{th}})$ a broad photoluminescence (PL) spectrum is observed. (c) With exceeding the threshold energy $(E > E_{\text{th}})$ a distinct narrow laser peak rises from the PL spectrum. (d) At excitation energies considerably above the threshold energy $(E \gg E_{\text{th}})$ the spectrum narrows to the laser line.

single laser mode the excitation can be increased until all available energy states are saturated. In organic DFB lasers the resonator allows typically the lasing of multiple TE and TM modes due to the broad gain spectrum of the gain material. Instead of a saturation it is more likely to observe the evolution of additional laser lines in the spectrum.

The evolution of the laser emission spectrum from the broad PL distribution to the narrow laser line has to be evaluated in its entity as e.g. a narrow spectral bandwidth can also be a result of optical filtering. Together with the nonlinear behavior and a distinct emission beam as e.g. shown in figure 2.21 these criteria are a valid proof of laser operation.

2.2.7   Wavelength-tuning of organic DFB lasers

The major advantage of organic DFB lasers over their inorganic counterparts is the ease of tuning the emission wavelength due to their broad spectral emission range in the visible. While a lot of research has been done on demonstrating discrete tuning of organic semiconductor lasers, only few reports on continuous and easily controllable wavelength tuning of such lasers exist.

Figure 2.21: Photograph of an organic laser based on a two dimensional DFB resonator on a flexible polymer substrate and its output beam. The laser is on the foreground of the photograph. The beam can be seen as a red cross on the paper screen. The bright blue spots originate from scattered UV pump light which causes the paper to luminesce. (T. Woggon [65])

Discrete tuning

As elucidated in 2.2.2, the lasing emission wavelength $\lambda_{l,j}$ of a DFB laser with a grating period Λ can be derived in a simplified manner from the Bragg condition Eq. (2.26):

$$\lambda_{l,j} \approx \frac{2n_{\text{eff},j}\Lambda}{m} \tag{2.32}$$

The subscripted index i emphasizes the possibility for different guided electromagnetic modes. According to this dependency an increase of either $n_{\text{eff},j}$, Λ or both increases the lasing wavelength $\lambda_{l,j}$. This of course implies, that the design wavelength lies within the spectral gain region of the active material. The effective refractive index $n_{\text{eff},i}$ can be modified by altering the film thickness of the active material [60] or by changing the waveguide index profile with high index intermediate layers [14]. Discrete tuning by grating period variations [18,66] typically yields in a larger achievable tuning range compared to a film thickness variation. The reason for this is that the slab waveguide allows more guided modes with increased film thickness hence reducing the overall tunability.

Seamless tuning

Being able to set the emission wavelength of an organic DFB laser online is not only of interest for spectroscopical methods but also a convenient way to compensate fabrication tolerances and environmental influences. Researchers approached this problem with quite different solutions. These can be categorized into pump position dependent and independent solutions. The latter category comprises pumping with variable interference patterns [67], the use of nematic liquid crystals [68,69] or

mechanical strain [70]. The pump position dependent approach uses a gradient of
one ore more wavelength determining parameters on a single substrate. This can be
done with a wedge-shaped fabry perot microcavity [71], a spatially and continuously
changing DFB grating period [72] or by using a waveguide structure with a thickness
gradient of the active material [13] or an intermediate high index layer [14].

Chapter 3

Materials and processing technologies

Abstract

This chapter introduces the materials and processing technologies used for fabricating the organic lasers in this work. It will present a set of polymer materials which are promising candidates for the use as substrate for organic distributed feedback lasers. The fabrication of organic lasers involves to pattern the substrate with sub-micron optical gratings. The focus for the selection of processing technologies is therefore set on alternative fabrication methods to costly electron-beam lithography.

3.1 Materials

Due to the simple processing, polymers can be a low cost alternative to glass. For integrated microoptics the suitability of a specific polymer is mainly determined by its optical characteristics. For the use as substrate for organic lasers, the temperature stability and the chemical resistance additionally gain importance depending on the method used for depositing the organic active material. Table 3.1 gives an overview on the characteristics of the polymeric materials used in this thesis.

	BK-7 glass	PMMA	COC (Topas®)	SU-8	ORMOCER® (Ormocomp)
refractive index (633 nm)	1.52	1.49	1.53	1.596	1.53
attenuation (dB cm^{-1}) (633 nm)	0.09	0.65	0.5	>1.4	0.06
CTE (1×10^{-5} K^{-1})	0.83	7.5	6.0	5.2	6.0
heat resistance	>400 °C	80 °C	125 °C	315 °C	270 °C
water absorption	0 %	0.3 %	<0.01 %	0.6 %	<0.5 %
chemical resistance					
acid and bases	good	poor	fair	good	good
polar solvents	good	poor	good	good	good
non polar solvents	good	good	poor	good	good

Table 3.1: Properties of selected optical materials [73–79].

Thermoplastic polymers like poly(methyl methacrylate) (PMMA) and cyclic olefin copolymer (COC) can be easily processed with molding processes at low costs. They are used for optical waveguides, integrated optics and DFB resonators because of their high transmittance in the visible. The application range of these thermoplastics is, however, limited by their temperature stability and chemical resistance.

Photolithography resins like SU-8 or ORMOCER® can also be used for microoptical devices. Both materials can be cured by UV radiation exposure. The ORMOCER® variant Ormocomp has been developed especially for this application field. This allows to fabricate microstructures with photolithography or direct laser writing as well as replicating them with UV nanoimprint lithography. After curing both photoresists exhibit a glass-like high chemical and heat resistance. The modern organic-inorganic hybrid ORMOCER® polymer class additionally offers the ability to widely tune the mechanical as well as optical characteristics during the resin synthesis. Adjusting the refractive index, e.g., allows the fabrication of optical waveguides [80].

3.1.1 Poly(methyl methacrylate) (PMMA)

Poly(methyl methacrylate) (PMMA) is the one of the oldest transparent thermoplastic materials. It was developed in 1928 independently in Germany, Great Britain and Spain. Up to today, PMMA was used for a large spectra of applications from contact lenses and commodity products to bone cement for affixing implants [81]. PMMA is polymerized mainly from the colorless liquid monomer MMA which can be synthesized by esterifying methyacrylic acid. PMMA has only a low chemical resistance against acids, bases and polar solvents like alcohols, acetone or benzole.

brand	company
Perspex, Diakon	ICI
Plexiglas, Plexidur, Altuglas, Vedril	Ato Haas
Acrifix	Rohm
Vestiform	Hüls
Paraglas, Degalan	Degussa
Lucryl	BASF
Sumipex	Sumitomo

Table 3.2: Selection of major brand names and manufacturers of PMMA

Compared to common thermoplastics PMMA distinguishes itself with the highest light transmission of 93 % in the wavelength range between (380 to 780) nm. A unique feature of PMMA is the possibility to locally modify the refractive index by deep ultra-violet (DUV) radiation exposure. This allows for conveniently defining waveguides with DUV lithography [47]. This process was used in the fabrication of the first waveguide coupled integrated organic semiconductor laser [18]. Treating the material with DUV also enhances its already high bio-compatibility [82,83]. PMMA is available from various companies each offering a specific formulation. A selection of the major PMMA manufacturers is listed in table 3.2.

3.1.2   Cyclic olefin copolymer Topas®

Olefines are unsaturated hydrocarbons with one or more double carbon-carbon bonds existent in their molecule structure. In systematic chemical nomenclature these molecules are grouped under the collective name alkenes with the suffix *-ene*. The lower alkenes ethylene, propylene and butylene represent the most important base material for the petrochemicals industry. Alkenes can be polymerized in three different ways whereas each route ends with its own polymer type. Each of these differs in structure and properties from the other two [84].

COCs are polyolefines which were polymerized without ring opening reactions by using a metallocene catalyst [85–88]. In contrast to the semi-crystalline polyolefines polyethylene and polypropylene, COCs are of amorphous structure. They exhibit unique optical properties, excellent moisture resistance, high glass transition temperature, toughness and a low dielectric constant.

The first commercially available COC products were Apel and Zeonex produced by Mitsui Petrochemical in limited amounts. The most popular COC variant today has the trade name Topas®, a copolymer of ethylene and norbornadiene developed 1997 by Hoechst and Mitsui. With respect to Apel and Zeonex, Topas features lower production costs [89].

The glass transition temperature of Topas can be adjusted between (60 to 226) °C [90] whereas, due to the amorphous character of the material, a melting point is not observable. Topas also stands out with high chemical resistance against acids, bases and polar solvents. As it is also highly transmissive for UV light Topas is well suited for fabricating mold inserts in UV nanoimprint lithography [91]. With additionally being certified biocompatible and absorbing extremely low amounts of water [92], Topas is an ideal candidate for analytical systems. The compared to other thermoplastics low CTE, suggests Topas also as wrought material for high
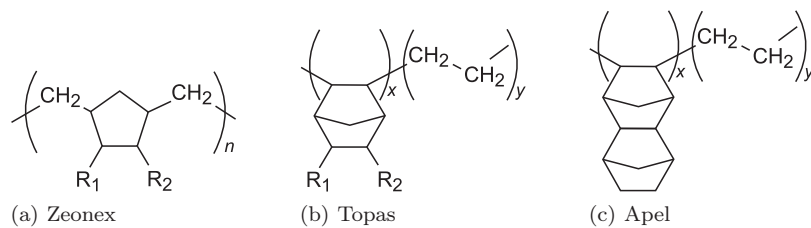
Figure 3.1: Chemical structure of different cyclic olefin copolymers

quality thermal molding processes.

3.1.3 Permanent epoxy negative photoresist SU-8 2000

The negative resist SU-8, originally developed and patented by IBM-Watson Research Center [93], can be processed to millimeter thick layers while allowing for aspect ratios larger than 20 with contact lithography systems. The main ingredients of SU-8 are an epoxy resin (bisphenol-a-diglycidyl-ether), an UV-sensitive photoacid generator from the family of the triarylium-sulfonium salts and the solvent γ-butyrolacton. SU-8 2000 is a modern variant of SU-8 being merchandised by *MicroChem Corp.* which uses cyclopentanon as solvent. The resist is cured with a light induced cationic polymerization. The polymerization kinetics are temperature dependent whereas heating causes an increase in speed. A detailed description of the chemical composition and the polymerization mechanism is given in the work of Deubel [94].

With SU-8, feature sizes in the sub-30 nm regime have been demonstrated with 100 kV electron beam lithography [95]. The large aspect ratios combined with an excellent chemical resistance and mechanical strength made *SU-8* to a popular resist for MEMS applications [96, 97].

In this work *SU-8 2000* was employed for the fabrication of microoptical devices with 3D direct laser writing (see chapter 4.3). This choice was made based on the good results already reported in literature [94, 98, 99].

3.1.4 Organically modified ceramic Ormocomp

Ormocomp is a UV curable organic-inorganic hybrid polymer. It belongs to the family of organically modified ceramics first developed by Fraunhofer Institute in the 1980s [100] and better known under the acronym ORMOCER®. These hybrid polymers are synthesized in a condensation polymerization of different organoalkoxysilanes, the so called sol-gel process, forming an inorganic Si-O-Si backbone with organic side chains and functional groups as illustratively shown in figure 3.2a [80]. Physical properties, e.g. the refractive index, of ORMOCER® can be widely tailored in the synthesis process by varying the amount of inorganic and organic elements [101]. The sol-gel synthesis can be controlled accurately yielding a deviation of the refractive index of less than 5×10^{-4} and a deviation of less 0.2 Pa s for the dynamic viscosity [102]. Because of its organic-inorganic hybrid nature, ORMOCER® combines the properties of polymers (functionalization, processing

temperature, toughness) with the hardness, transparency, chemical- and thermal stability of glasses and silicones.

As it can be seen in the plot of the wavelength dependent optical transmission in figure 3.2b ORMOCER®s are highly transparent with losses of less than $0.1\,\text{dB}\,\text{cm}^{-1}$ in the visible. These unique properties of ORMOCER®s led to using them for a wide range of applications from anti-static and anti-adhesive coatings [101] to devices for life sciences [103] and integrated photonic circuits [104, 105].

(a)   (b)
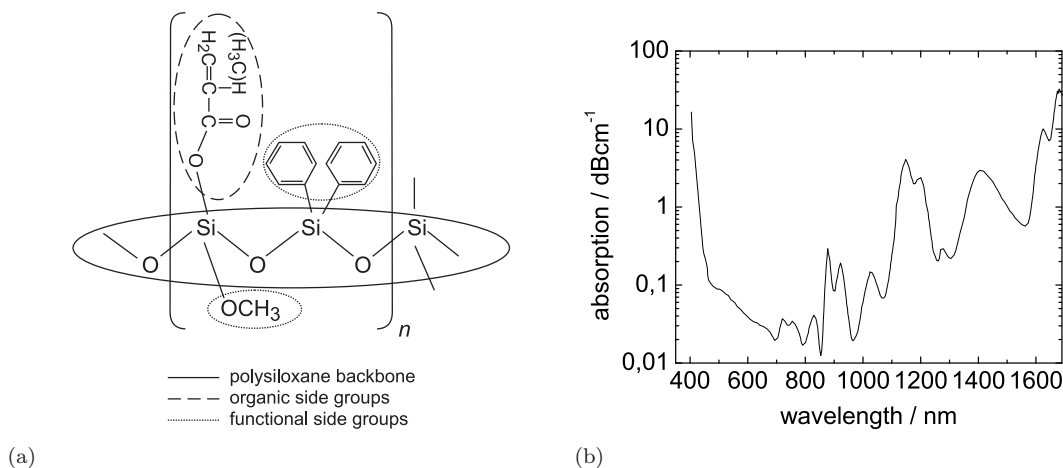
Figure 3.2: (a) Exemplary chemical structure of ORMOCER®. The molecule is composed of an inorganic Si-O-Si backbone with organic side chains and functional groups. (b) Absorption spectrum of an ORMOCER® resin including an UV initiator (data taken from R. Houbertz et al. [106])

Ormocomp was designed for molding microoptics using UV nanoimprint lithography (UV NIL, see 3.2.5). Compared to other polymers it exhibits a high optical transparency in the near UV region. This enables the use of an Ormocomp nanostructure as a master for UV NIL itself. The Ormocomp oligomeres exhibit methacrylate side groups which crosslink the polymer in a photoinitiated free radical polymerization to a duroplastic polymer. Ormocomp can be processed to (30 to 200) µm thick films with a single coating. Film thickness below 30 µm can be fabricated by using a specific thinner (Ormothin).

3.1.5   The composite molecular system Alq$_3$:DCM

The organic gain material Alq$_3$:DCM comprises the metal-organic semiconductor material Alq$_3$[1] (Fig. (a)) doped with small amount, typically (2 to 3) mol %, of the laser dye DCM[2] (Fig. (b)). Both materials belong to the small molecules material class. This allows to process them to composite thin films with vapor deposition methods.

Alq$_3$:DCM was chosen as the gain material for all devices fabricated in this thesis as the physical and optical properties and doping concentration effects have been

---

[1]tris-(8-hydroxyquinoline) aluminum
[2]4-dicyanomethylene-2-methyl-6-(p-dimethylaminostyryl)-4H-pyran

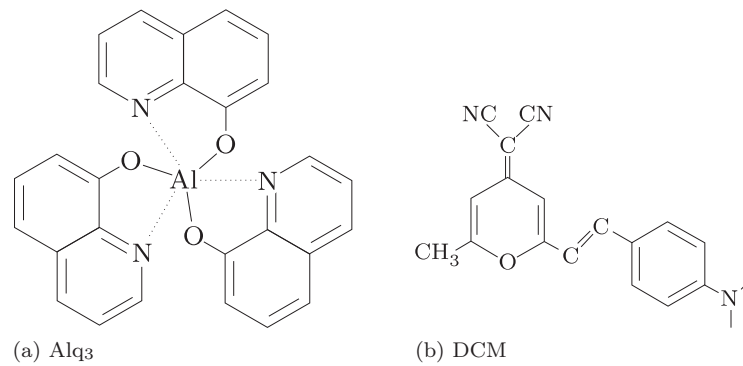(a) Alq₃   (b) DCM

Figure 3.3: Chemical Structure of the metal-organic semiconductor material Alq$_3$ and the laser dye molecule DCM

studied in detail by Kozlov et al. and Riechel [5, 53]. Alq$_3$ is a popular charge carrier transport material used in OLEDs. DCM is a laser dye which, when in solution, forms a four-level system. It distinguishes itself with a high photostability and broad gain spectrum [107]. Both materials are commercially available and a highly reproducible vapor deposition process which has been established during the doctoral thesis of Marc Stroisch [12] could be employed for this thesis.

The optical properties of Alq$_3$ and DCM are plotted in figure 3.4. They originate from delocalized π-bonding electrons in the molecules. When exposed to light, Alq$_3$ efficiently absorbs photons with a wavelength around 400 nm and emits photoluminescence with peak wavelengths around 470 nm. The absorbance curve of DCM peaks around 550 nm with a large spectral overlap with the Alq$_3$ emission spectrum.

The composite molecular system Alq$_3$:DCM forms a so called Förster energy transfer system (see 2.2.4) with the Alq$_3$ acting as host for the DCM guest material. This results in the optical characteristics depicted in figure 3.4b with an absorption peak at 400 nm and an emission peak around 625 nm. Compared to other organic laser materials it exhibits a good chemical stability and a approximately 100 nm broad spectral gain with its maximum located at 614 nm.
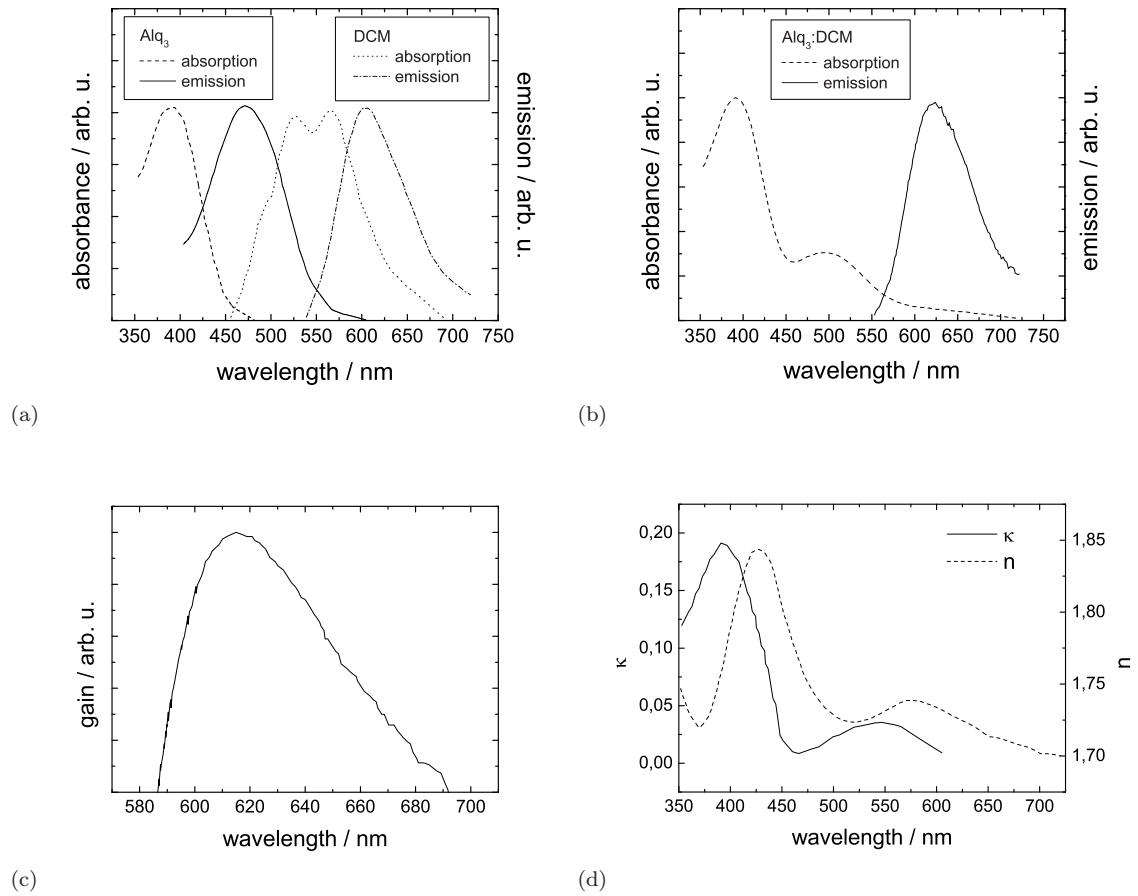
Figure 3.4: Optical properties of the laser gain material Alq$_3$:DCM (data taken from S. Riechel [53])

3.2   Processing technologies

3.2.1   Photolithography

The term photolithography denominates a series of process steps to transfer a geometric pattern from a photomask to a photosensitive thin film. The underlying process steps are depicted in Fig. 3.5. The photosensitive film, the so-called photoresist, is normally spin-coated onto a substrate [108]. The pattern from the photomask is then transfered by casting shadows with a light source. The light induces a photoreaction in the exposed areas of the resist which affects the solubility in a specific developer solution. In case of a positive resist the solubility is increased thus the exposed areas will be removed in a subsequent developer bath. Accordingly, when using a negative resist the unexposed areas will be removed [109]. Depending on the
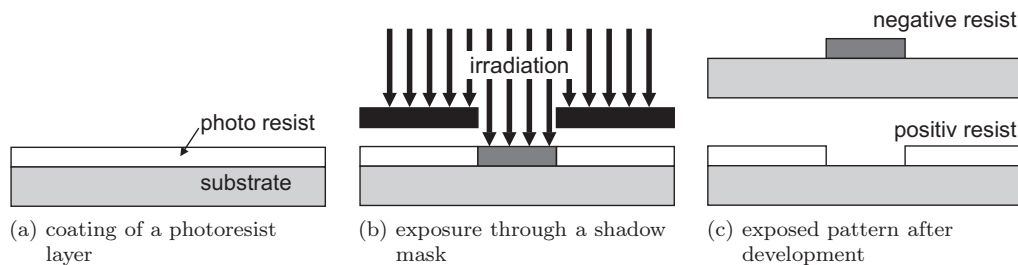

Figure 3.5: Basic process steps of photolithography

photoresist and target applications patterns can be directly used after developing. Alternatively a variety of processes can be applied to the now unprotected areas of the substrate. Depositing additional materials onto, introducing dopants into or etching the substrate are just a few examples. After these processes the resist is stripped, leaving the patterned substrate.

3.2.2   Laser interference lithography

Laser interference lithography (LIL) is one of the most important techniques for the fabrication of periodic structures. In contrast to electron beam lithography this technique offers to quickly pattern large areas with periodic structures. Although the basic principle behind the LIL is quite simple, the actual realization of large area, high quality structures can be an elaborate task [110]. A simplified scheme of an LIL setup is shown in Fig. 3.6. A laser beam is split up into two single beams which are directed onto a photosensitive resist. Typically the setup is symmetrical, causing both beams to interfere with each other and thus to form a linear light-dark intensity pattern. The locally varying exposure dosage hence inscribes a periodic structure into the resist. The periodicity Λ of the interference pattern can be calculated with the equation $\Lambda = \lambda/(2\sin\alpha)$, where α is the angle between the substrate normal and the laser beam. The grating constant is therefore limited to half of the laser wavelength λ. For the commonly used argon ion laser which emits at 364 nm this means a minimal theoretical obtainable lattice period of 182 nm. Additionally to the mandatory mechanically stable optical setup also a long coherence length of the
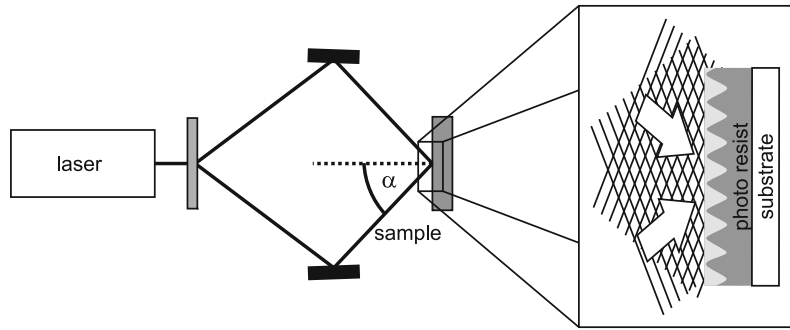
Figure 3.6: Schematic experimental setup for laser interference lithography. A laser beam is split up into two single beams which are directed onto a photosensitive resist. The inset shows the intensity modulated pattern created by the interfering beams (M. Punke, T. Woggon et al. [18])

laser is needed in order to realize substrate sized interference pattern. As a rough estimation the displacement of the interference pattern should be lower than 1/10 of the period during exposure.

After developing the structure, it can be used either directly, for example as a DFB laser resonator or transferred into other materials. Rotating the substrate by 90° or 60° also allows to pattern square and triangular lattices with multiple LIL exposures. Another extension to LIL is the laser interference ablation (LIA) where the interference pattern is transferred directly into the active material layer with short high energy laser pulses [4]. LIL allows to pattern very large surfaces. The achievable modulation depth is, however very limited and decreases with reducing the period of the interference pattern. LIL is not applicable for the patterning of small areas using masks due to diffraction [111].

3.2.3 3D direct laser writing

Conventional, two-dimensional direct laser writing is used as a cost saving alternative to electron beam lithography. Commercially available systems are able to pattern substrates as large as $(400 \times 400) \, mm^2$ with feature sizes down to 0.6 µm. In the direct laser writing process a photoresist is patterned by locally exposing it with a focused laser beam. Common systems use a helium-cadmium gas laser source with an emission wavelength of 442 nm [112–114].

An extension to these systems came up when Maruo et al. proposed the use of two photon absorption (TPA) induced polymerization. Since then, TPA based 3D laser writing has become an established processing technique for the fabrication of 3D structures in the micro- and nanometer scale [115–117] by using a femtosecond laser as light source [118–121]. Recently also the first commercial solutions reached the market [122, 123].

The TPA process entitles the simultaneous absorption of two low energy photons which induces a reaction in the material normally requiring twice as much of the excitation energy in a single photon process. This nonlinear phenomenon needs very high irradiation densities. This heats up the photoresist when using continuous-wave lasers. Preventing thermal destruction of the resist hence requires

short, highly intense laser pulses [94]. Typically employed sources fulfilling this criteria are titanium-sapphire based femtosecond lasers. They emit near infrared radiation (NIR) at around 800 nm. The pattern is scribed into a photoresist which is only sensitive in the near UV spectral range and transparent in the NIR.

The TPA process features a distinct threshold characteristic for the curing of the photoresists. The curing process is initiated only when the particle density of radicals reaches a critical value. This corresponds to a threshold radiation dosage [124]. This threshold behavior can not only be used to get below the resolution limit of traditional optical systems (see Fig. 3.7a), it can be also exploited for three dimensional writing. The chemical reaction to the irradiation only occurs in the focal volume, the so called volume pixel or voxel, of the femtosecond laser beam. Moving the sample (or the laser beam) as depicted in Fig. 3.7b enables to pattern arbitrary three-dimensional structures. Depending on the numerical aperture of the focusing optics and the chemical properties of the photoresist, it is possible to write voxels with axial dimensions down to 500 nm and lateral dimensions down to 100 nm [125].
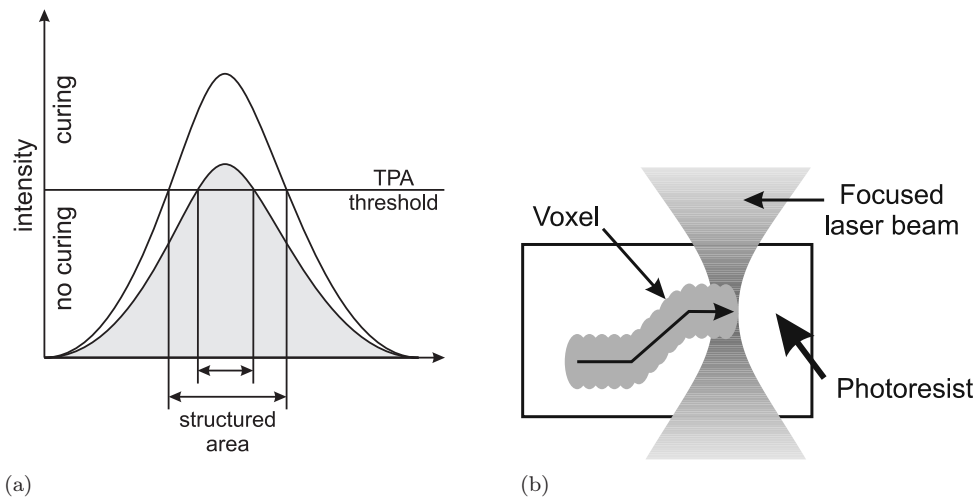

Figure 3.7: (a) Intensity profiles of two Gaussian beams. Depending on the pulse energy different sized areas can be patterned. (b) By moving the beam focus relative to the sample, arbitrary structures can be written. (T. Woggon et al. [47])

There are two approaches mainly used for the relative movement of the focal volume. Either moving the substrate with a piezo-actuated nanometer positioning stage [126, 127] or moving the focal volume by deflecting the laser beam with a galvanometric scanner [124]. The latter approach yields a significantly faster writing speed but the high resolution of a piezo-stage system is not achievable.

3.2.4   Thin film deposition

The deposition of thin films of organic materials is an important task in the processing of organic electrooptical components. For organic lasers for example, the active material waveguide layers have typical layer thicknesses of (130 to 400) nm while exhibiting low optical losses. Such thin films can be either obtained by spin-coating conjugated polymers [23, 55, 128] or evaporating small molecules [7, 129] on top of a substrate.

Every thin film deposition requires to have a clean substrate to begin with. Hereby, the possible cleaning techniques are often limited by the substrate's resistance against treating it with chemicals. If there are no limitations, a cleaning cycle with acetone, isopropanol and deionized water rinsing will remove most residues. Treating the substrate subsequently with a plasma cleaning step (e.g. argon/oxygen plasma) removes remaining organic compounds on the surface and additionally enhances the wettability.

Dissolving the active material in a suitable solvent permits to spin-coat it. The solution is applied to the substrate which rotates at up to $4000 \, \mathrm{r/min}$ causing any superfluous liquid to be spun out. A thin solid film remains after the solvent evaporated. Although being of impressive simplicity, this technique becomes problematic when the layer should be processed further using photolithographic methods. Due to the good solubility of organic materials traditional concepts used for inorganic materials as masking and etching cannot be applied.

A convenient solution which allows to additionally pattern an organic thin film is the vapor deposition of the material. Due to the typically low boiling temperatures of organic compounds the vapor deposition of organic materials does not require chemical vapor deposition or electron beam sputtering. A controlled thermal evaporation source inside a vacuum chamber is sufficient. Typically the source consists of a crucible equipped with a heating wire holding the organic material. The temperature of the crucible is measured with a thermocouple element. The current through the heating wire is regulated according to the measured temperature. To have a measure of the deposited film thickness, usually the deposition rate is determined with an oscillating crystal detector placed above the evaporation source and close to the substrate. If multiple materials should be co-evaporated at different rates additional crystal detectors have to be placed in the vicinity of the crucibles. Also baffles are used to prevent any cross talking.

Such a co-evaporation creates often high demands on the stability of the deposition rates. For example, when depositing the popular laser gain material Alq_3:DCM laser with a typical doping concentration of around 3% DCM, the deposition rates for the two materials are on the order of $0.3 \, \mathrm{nm \, s^{-1}}$ and $0.01 \, \mathrm{nm \, s^{-1}}$, respectively. This ratio has to be held constant for more than 15 minutes when a target layer thickness of about 300 nm is assumed. Hence, the process control is typically automated to ensure reproducible evaporation conditions and deposition results.

Patterning of the organic layer can be achieved with metal foils comprising cut-outs which are fixed as a mask close to the substrate. This allows for example the coating of specific single laser fields. Wafer scale shadow mask fabrication of integrated organic lasers whose active layer had areal dimensions down to $(500 \times 500) \, \mathrm{\mu m^2}$ has been demonstrated [18, 91]. Depositing different materials on

different areas is also possible by the subsequent use of different masks. This is of particular interest for devices, where several laser materials on one substrate with a wide range of different emission wavelengths is needed.

With rotating shadow masks it is also possible to deposit active layers with a seamless thickness gradient in a controllable manner [13, 130]. This is especially required for wavelength tunable organic semiconductor lasers.

3.2.5   Hot embossing and UV nanoimprint lithography

As cleaning and sterilization would be quite inconsistent with the Lab-on-chip concept, the design of such devices should preferably allow to use them as disposables. Key technologies for the thus needed low-cost mass production are microreplication procedures like hot embossing and UV nanoimprint lithography.

Hot embossing

The first microstructures molded into polymer materials were fabricated with hot embossing. The basic steps of this process are depicted in Fig. 3.8. In principle, a microstructured mold is pressed onto a substrate at temperatures above the substrate materials glass transition temperature T_{g}. This creates a negative copy of the mold pattern [131]. Uniformly imprinting of large areas requires an additionally applied vacuum to avoid air cushions between stamp and sample [132]. To prevent the master from being damaged or worn during the embossing step the so called LIGA process can be applied to replicate the master structure into a durable metal imprinting tool.
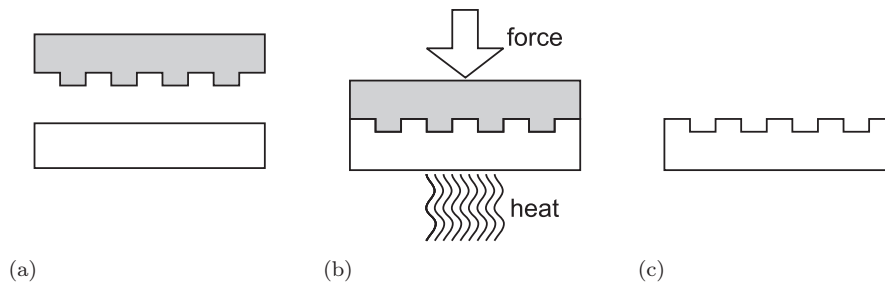

Figure 3.8: Processing steps for hot embossing: (a) A thermoplastic substrate is aligned to a mold. (b) The mold is imprinted with force into the substrate which is heated above the glass transition temperature T_{g}. (c) After cooling the substrate below T_{g} the mold is separated and can be used for the next replication. (T. Woggon et al. [47])

LIGA is a German acronym for *Lithographie, Galvanik und Abformung* [133, 134] denominating the individual process steps lithography, electroforming, and plastic molding. For low aspect ratio nanostructures, the metal imprinting tool can be produced with electroforming using the process steps outlined in Fig. 3.9. A conductive material, typically gold, is evaporated upon the insulating master structure to act as a starting layer. The actual metal tool is then electroformed as a secondary metallic structure. Commonly used metals for plastic molding tools are nickel alloys, such

as nickel-cobalt and nickel-iron where the composition is optimized for the thermal expansion coefficient of the stamp being as close as possible to the coefficient of the plastic. The tool, a so called shim [135, 136] is typically plated to a thickness of about (200 to 300) µm. Basically an unlimited number of replicas can be fabricated as the master tool is not worn out during this process. The LIGA process is hence applicable for high volume production of nano- and microcomponents at low-cost.
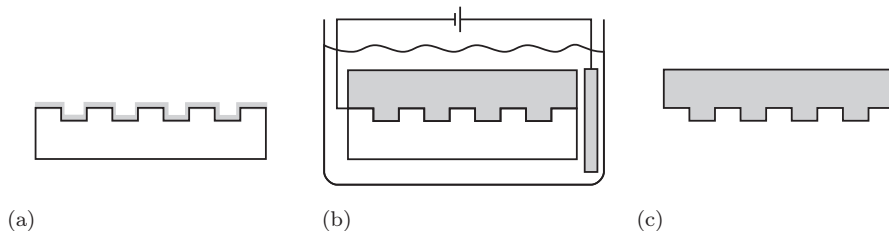

(a)   (b)   (c)

Figure 3.9: Fabrication scheme of a Ni-shim for following the LIGA process: (a) A thin conducting starting layer is deposited onto the nanostructure. (b) In an electroplating process the thin starting layer is reinforced to thicknesses of several hundred microns. (c) The final nanostructured metal foil can be glued to a bulk backplane and used a durable replicating tool. (T. Woggon et al. [47])

Nanoimprint lithography and microcontact printing

Nanoimprint lithography (NIL) is one approach towards decreased process times by eliminating the heat-up and cool-down phases necessary with hot embossing (Fig. 3.10). Instead, an optically transparent imprinting tool is pressed into a photosensitive liquid prepolymer or sol-gel material. The material is then cured by exposing it to radiation [28, 137]. This not only speeds up the imprinting process, it also avoids introducing strain into the material due to different thermal expansion coefficients of stamp and substrate. With its high-throughput capability, NIL clearly stands out as a promising technology for reel-to-reel processing [138]. NIL allows the use of metal tools which where originally designed for hot embossing if the substrate material is transparent in the UV. Transparent tools can be fabricated via hot embossing into transparent polymers or by casting a transparent resin like polydimethylsiloxane (PDMS).

Another replication method usable for nanoscale fabrication is the microcontact printing (µCP) process [139, 140]. Here, an etch mask is transfered on the substrate using an inked stamp which makes this method inapplicable for multi-scaled structures.
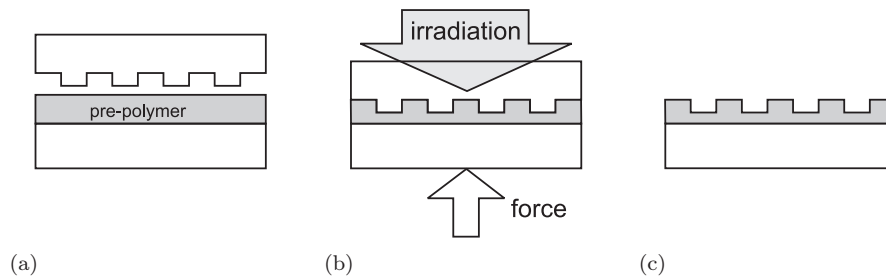
Figure 3.10: Process steps for the NIL process: (a) A substrate which is coated with a photocurable material is aligned to a transparent mold. (b) The mold is imprinted with force into the substrate while UV radiation cures the material. (c) After curing the mold is separated and can be used for the next replication.

Chapter 4

Rapid prototyping of laser resonators and microoptical systems

Abstract [1]

Organic lasers can be realized with many different resonator geometries. DFB resonators with mixed periodicities, two-dimensional photonic crystals or circular Bragg gratings are just a few examples. Exploring different resonator geometries and optimizing the parameters for existing solutions requires the ability to rapidly transfer a new design into a working device. The development of low-threshold organic lasers, hence, requires elaborate electron beam lithography for the fabrication of advanced resonator schemes. This lack in fabrication technology is even more critical when organic lasers should be integrated into microoptical systems as this requires to pattern sub-micron features together with structures with extents of several tens of microns. Prototyping fabrication schemes therefore ideally employ a direct fabrication process which allows to pattern structures from the sub-millimeter and micron regime down to sub-micron scale. This chapter describes how two photon absorption induced polymerization in combination with a photocurable organic-inorganic hybrid polymer can be used as a fast and powerful prototyping tool for DFB laser resonators as well as microoptical systems that extend multiple millimeters.

4.1　Rapid prototyping of sub-micron structures

Up to the early 1990s the electron beam (e-beam) lithography was the only applicable direct fabrication method available for structuring in the sub-micron regime. Albeit the very high resolution provided by e-beam lithography, its use as a prototyping tool for integrated microoptical systems is limited as it is restricted to two dimensional designs. Design visions for integrated lab-on-chip devices feature micro- as well as nano-scaled structures which are situated at different levels paired with extended fluidic channels and optical waveguides. Fabricating these complex devices would require multiple e-beam exposure steps. Each step of course involves an obligatory developing/etching process and a new resist coating.

The two photon absorption (TPA) induced polymerization process allows to pattern arbitrary three dimensional micro- and nanostructures in a single process (see 3.2.3, p. 43). Although the achievable resolution of this three dimensional direct laser writing (3D-DLW) cannot yet compete with e-beam lithography, the large variety of optical components fabricated with 3D-DLW [141–144] clearly shows its potential for using it as a rapid prototyping tool.

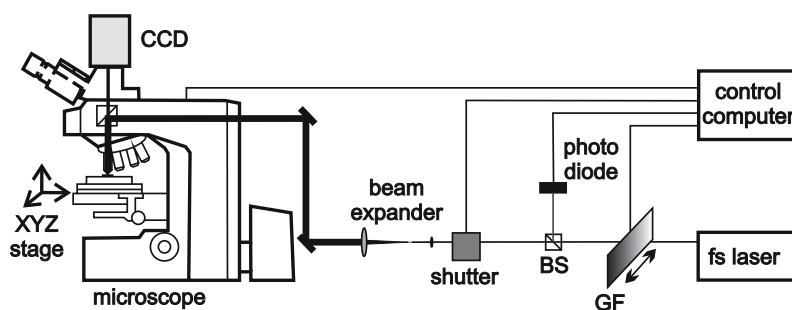## 4.1.1　Basic optical setup of a 3D-DLW system

Figure 4.1: Schematic representation of the basic components in the employed 3D laser writing setup. (T. Woggon et al. [144])

The structures in this work have been written with a custom setup based on a *Coherent Mira 900D* titanium:sapphire laser and a *Zeiss Axioplan* upright optical microscope. Figure 4.1 schematically represents the key components of the opto-mechanical setup. The laser is configured to deliver 150 fs long pulses with a repetition rate of 76 MHz. The central wavelength of the output pulses is set to 800 nm. As elucidated in chapter 3.2.3 (p. 43) the voxel size depends strongly on the pulse energy. In the used setup a motorized gradient neutral density filter (GF) and a photodiode (*Thorlabs DET 110*) were installed to monitor and control the laser power in a closed loop manner. This measure ensures reproducible results. To minimize the temporal broading of the laser pulse the beam is coupled into the optical microscope with free space optics. The laser beam is expanded with a 7× beam expander from *Linos* to ensure to completely illuminate the microscope objective pupil. This is essential to minimize the focal area. The microscope focuses the beam onto the sample surface through a *Zeiss Apochromat* 100× oil immersion

objective with a numerical aperture of NA = 1.4. To write patterns, the sample is translated relatively to the focused laser beam with a three axis nanometer positioning table (*PI P-563.3CD*). The nano positioning table provides a translation range of 300 μm in all directions when operated with a closed loop control setup and 340 μm in open loop control. An additional XY-scanning stage with a maximum displacement of 100 mm and 120 mm (*Märzhäuser Scan 120x100*) mounted underneath the nanometer positioning table extends the systems patterning abilities to larger extended structures with a stitching accuracy of 3 μm. The exposure of the sample with the laser radiation can be turned on and off with a mechanical shutter (*Thorlabs SH05*).

4.1.2   Fabrication speed considerations

Apart from the different approaches mentioned in chapter 3.2.3 for displacing the focal volume the applied writing strategy plays a critical role for the performance of a TPA lithography system. The straight forward method of raster scanning writes the pattern voxel-by-voxel. This method provides the highest degree of freedom combined with little programming effort. A major downside of this approach is the need for fast optical switches, e.g. acusto-optic modulators for keeping process durations at acceptable values. A more critical point is, however, the surface quality which, due to the direct dependence on the voxel spacing (see Fig. 4.2a-b), will always be a trade-off between writing speed and surface roughness.

A more advanced writing strategy which combines a high surface quality with low process times is the vector scanning method. Here, a computer model of the target structure is fragmented into exposure paths which can be written with a continuous line (Fig. 4.2c). This also speeds up the writing process especially when using a low-cost mechanical beam shutter instead of an acoustic optical one for controlling the exposure dose.

(a) Voxel-by-voxel raster scanning

(b) Improved surface quality with reduced scanning step size

(c) High quality surface with continuously writing along a vector path
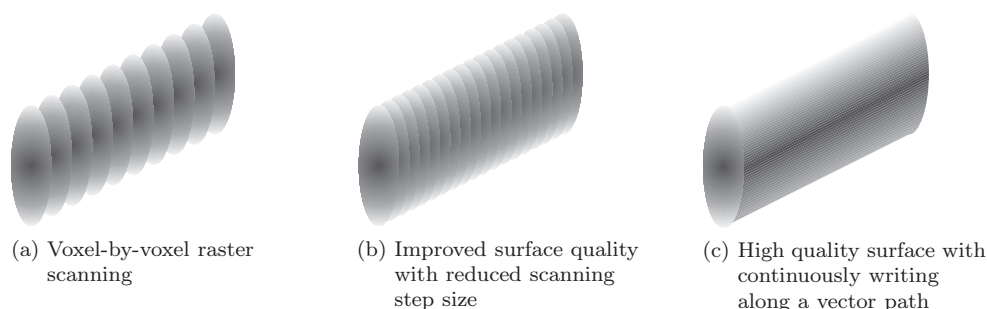
Figure 4.2: Writing strategies for 3D direct laser writing: (a) Voxel-by-voxel scanning with a large step size results in a rough surface. (b) Reducing the step size improves the surface quality but prolongs the process duration. (c) Writing lines on vector path combines a high surface quality with low process times.

On the system programming side, however, the vector scan method requires far more elaborate algorithms as electronic delays and motion dynamics of the positioning stage have to be taken into account. Especially the inertia of the positioning

publication year	writing speed / $\mu m\,s^{-1}$	reference
1999	10	Sun, Matsuo et al. [127]
1999	50	Cumpston, Ananthavel et al. [145]
2001	50	Miwa, Juodkazis et al. [146]
2002	200	Yin, Fang et al. [147]
2004	70	Teh, Dürig et al. [148]
2007	60	Haske, Chen et al. [149]
2009	1000	Woggon, Kleiner et al. [144] (see sec. 4.2)
2010	1500	Eschenbaum, Woggon et al. [150] (see sec. 4.4)

Table 4.1: Comparison of the line writing speed for different laser lithography systems. Employing an optimized vector scan approach yields a significant gain in writing speed.

stage can cause unwanted results. The employed piezo controller (*PI E710.2*) allows to define waveform functions as exemplified in figure 4.3 for driving a piezo and triggering external events. For this the controller features a set of frequency filters to prevent resonances and PID parameter set for the closed loop control. To fully exploit the high speed processing capabilities with vector scanning these controller settings were optimized with respect to the positioning stage load. Additionally the trigger line delays for the mechanical shutter have been compensated in the system control software. The comparison with other published results in table 4.1 shows that the writing speed which was achieved in this work with the aforementioned optimizations shows the huge potential of the vector scanning approach.
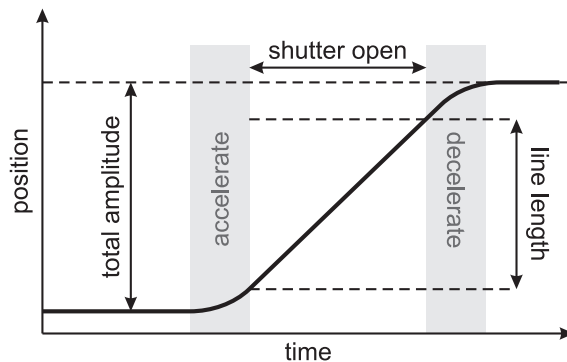

Figure 4.3: Schematically representation of waveforms used for pattering voxel-lines: The minimal acceleration and deceleration times are determined by the mechanical system. The trigger events for the shutter have to be optimized with respect to electronical and mechanical delays.

4.1.3 Measuring the position of the resin-glass interface

The position of the interface between the microscopy cover slip and the photoresist is a key parameter for 3D direct laser writing. The special attention for this parameter originates in the fact, that adhesion of a structure to the cover slip requires to partially write the voxels inside the glass. Mainly driven by the requirements in the evolving field of confocal microscopy, microscope manufacturers and aftermarket

suppliers provide a variety of hardware and software solutions addressing this issue. Early hardware solutions relied on measuring the distance between the objective front lens and the cover slip by sensing light or sound reflected from its closest surface to the objective or the distance between objective and sample holder [151–155]. These approaches however reach their limits when using oil immersion objectives due to a loss of contrast and reflectivity as the sensing light passes through the oil. Today, advanced autofocus systems use a laser or light emitting diode (LED) source coupled off-axis through the objective. The beam is reflected at the substrate, recovered with the objective and converted with a detector into an error signal. This signal can be used to adjust the position of the objective [156–158].

The majority of the above mentioned approaches was developed for tracking and imaging cells with confocal microscopy. In this thesis a very simple alternative to these techniques has been developed. It exploits the autofluorescence present in many photoresists. This solution requires no or little additional hardware as the fluorescence signal can be detected with the CCD camera with which most microscopes are equipped with. Moreover the solution can also be applied with non-parallel substrates and in case of resin and substrate having the same refractive index.
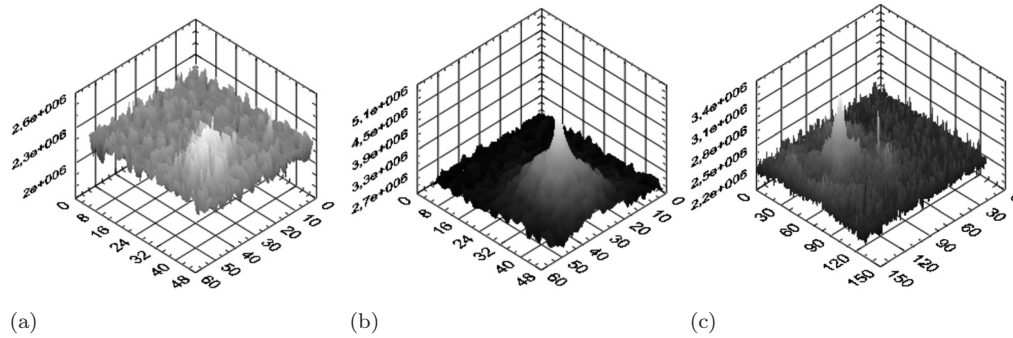

(a)   (b)   (c)

Figure 4.4: Autofluorescence signal of a photoresist coated glass slide at different focal planes imaged with the system's CCD camera: (a) weak signal at the substrate/photoresist interface (b) clear signal inside the photoresist (c) signal with halo at the photoresist/air interface (used resist: Ormocomp, laser power: 0.3 mW)

Figure 4.4 shows that the fluorescence signal intensity differs significantly with respect to the material into which the laser beam is focused. Accordingly, as depicted in Fig. 4.5 the interface position can be determined by vertically moving the focal volume of the laser beam along the z-axis at laser pulse energies well below the polymerization threshold. When the focal volume enters the photoresist layer, fluorescence light emitted by the photoresist is observed. At the glass/photoresist interface the fluorescence signal disappears. In the experiments the pulse energy setting turned out to be critical, if it was set too high, the autofluorescence of the immersion oil interfered with the resists fluorescence. Good results were achieved with an average power of 0.3 mW for Ormocomp and 0.6 mW for SU-8 2000. The accuracy of this method was limited by the sensitivity of the camera to approximately 1 µm.
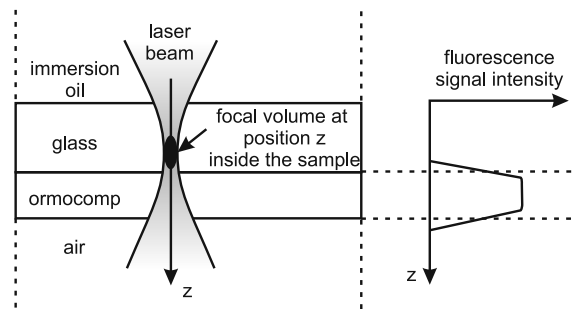
Figure 4.5: Determination of the position of the interface between the glass cover slip and the photoresist layer. The focal volume of the laser beam was moved vertically along the z-axis. When the focal volume enters the photoresist layer fluorescence light emitted by the photoresist can be observed. At the glass/photoresist interface the fluorescence signal disappears. (T. Woggon et al. [144])

4.1.4 Functional materials

In the early years of 3D-DLW, researchers relied in their studies on photoresists designed for conventional photolithography like SU-8. Some of them can be used for microoptical or microfluidic devices with respect to their optical quality or chemical strength. The use of such resists, however, limits the freedom of design as they were optimized for their original use, i.e. transferring a pattern with photolithography and not for high quality optics. Additionally the 3D-DLW process demands specific characteristics on a resist, e.g. low scattering losses after being exposed and a high two photon absorption (TPA) cross section.

These restrictions led to the development of numerous new material compositions. These have been optimized for 3D-DLW [159] in terms of an enhanced TPA cross section [160], incorporated metallic particles [161] or by employing photobleachable photoinitiators [162]. A very promising material class among these novel materials for 3D-DLW are the ORMOCER® hybrid polymers whose material characteristics can be tailored in a wide range. This allows to fabricate prototype systems which can be directly used after developing the resist.

The possibility to access this large number of specialized photoresists brings the same problem which is known from conventional photolithography. Each novel material demands to determine the exposure dosage parameters. In contrast to conventional lithography, however, the classical way of determining contrast curves is not applicable due to the threshold characteristic of the polymerization.

This problem can be addressed with writing test patterns with varying dosages [119]. The characteristic dosage dependent value for TPA 3D-DLW is the voxel size [163]. The dosage itself depends on the pulse energy and the focusing power of the optical system. Figure 4.6 shows a test pattern that allows to determine the TPA polymerization threshold and the thermal destruction threshold as the initial values marking the safe dosage interval. This serves as a basis for the following dosage tests. The safe dosage values can be subsequently applied in a second test pattern to determine the dosage dependent voxel extents. The focal plane is elevated step by step from the substrate with each written voxel or voxel-line (see. Fig. 4.7b). Voxels, which were written without contact to the substrate are tilted over or flushed
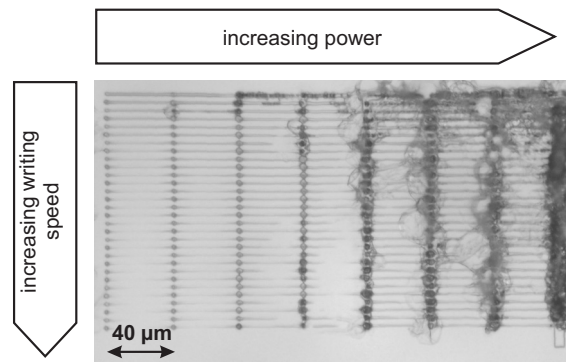
Figure 4.6: Microscope photograph of a test pattern for estimating the polymerization threshold power and thermal destruction power level for SU-8 2000.

away. The vertical dimension of a voxel can then be determined by counting the visible voxels and multiplying it with the step size. The use of such standardized patterns is thus a convenient way for finding the right exposure parameters for any unknown material with a minimal number of test exposures. The described method was used in this thesis to determine the dosage dependent extents of voxel-lines patterned with the 3D-DLW setup. The results plotted in figure 4.8 form the basis for the work in the following sections of this chapter.
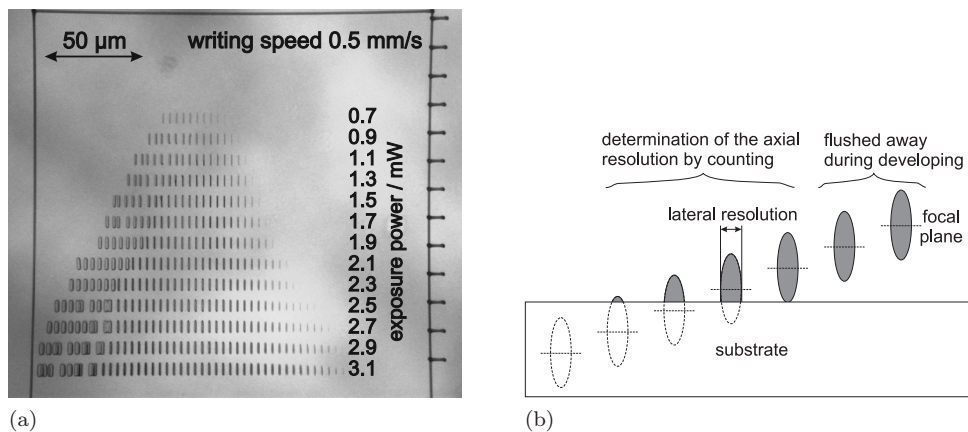

Figure 4.7: (a) Voxel line pattern in Ormocomp: The focal plane is elevated by 100 nm from the substrate with every voxel line. Voxel lines, which were written without a contact with the substrate are tilted over or flushed away. (b) The vertical dimension of a voxel can be determined by counting the visible voxels.

These test patterns conveniently deliver dosage values and resolution information but they lack any information on the structural integrity and shrinkage of a written structure. As with conventional photolithography, shrinkage of a resit can be compensated iteratively with writing a larger structure [159]. This procedure, however, is needed for each individual pattern which makes little or non-shrinking resists favorable. In addition to shrinkage, a lack of structural integrity during the development can rule out a specific resin for certain structures. Figure 4.9 shows an example for this with a direct comparison of a structure with cantilever features written in SU-8 2000 and Ormocomp. It shows that the little rigidity of Ormocomp

(a) Ormocomp

(b) Ormocomp
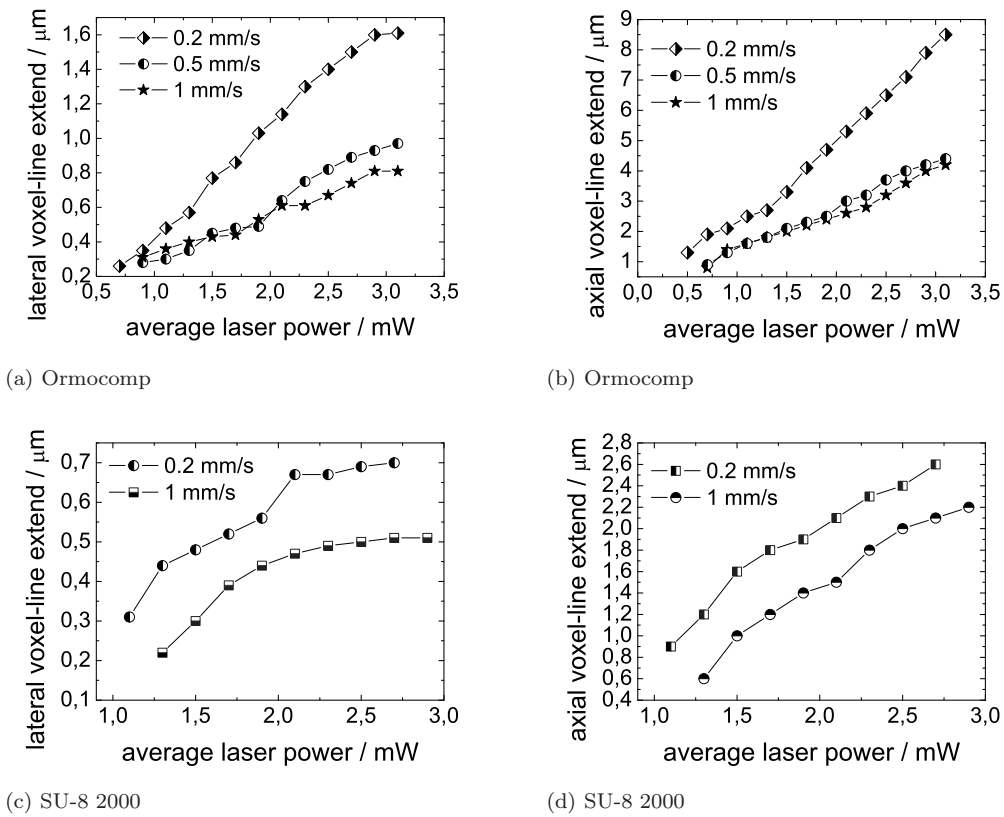

(c) SU-8 2000

(d) SU-8 2000

Figure 4.8: Dosage dependent extents of voxel lines patterned with the 3D-DLW setup (see 4.1) in Ormocomp and SU-8 2000

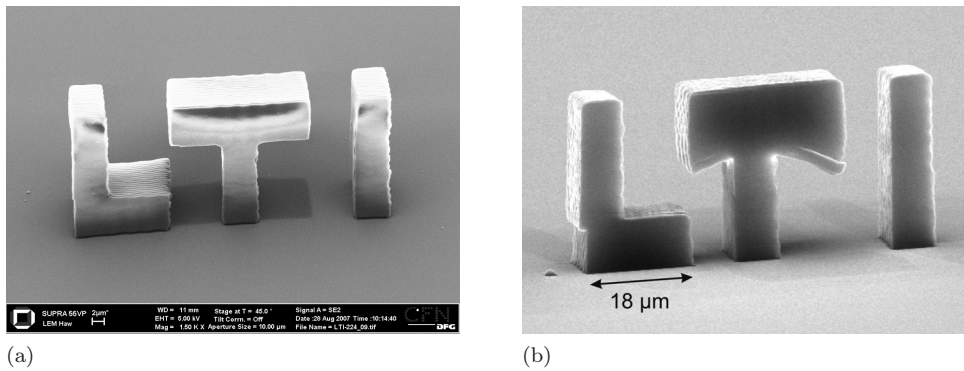prior hard-baking damages the structure during the development.

(a)

(b)

Figure 4.9: (a) Logotype patterned into SU8-2000 (written with $800\,\mathrm{nm}$ and $1.5\,\mathrm{mW}$ at $1\,\mathrm{mm\,s^{-1}}$ (b) Logotype patterned into Ormocomp. The freestanding cross beam of the letter T is bent downwards (written with $800\,\mathrm{nm}$ and $2.5\,\mathrm{mW}$ at $1\,\mathrm{mm\,s^{-1}}$

4.2   Rapid prototyping of DFB laser resonators

The most prominent feature of the 3D-DLW technology is the capability to polymerize sub-micron sized three-dimensionally defined voxels in a photo resin. These voxels can be serially stacked to form arbitrary structures. This makes 3D-DLW the perfect answer to the problem of combining sub-wavelength resolution and microstructure patterning in a single process step. A DFB resonator that provides optical feedback with 2nd order Bragg scattering in the red requires periodicities around 400 nm with a duty cycle around 0.5. Such structures are readily accessible with 3D-DLW. Accordingly the fabrication of such a microcavity laser by 3D-DLW was demonstrated first by S. Yokoyama et al. already in 2003. They structured a resin containing a dendrimer and the laser dye DCM [164]. The feedback structure featured a period of 1 µm. Later, in 2005 S. Klein et al. proposed to change the refraction index of a gain medium due to TPA to fabricate a distributed feedback laser with a grating period of 400 nm [165]. They dispersed the dye Rhodamine 6G as active material in a resin whose refractive index can be increased by TPA.

Both approaches used specifically composed photoresist/dye blends. Rapid prototyping would, however, require a resist which ideally is universally suited for integrating additional micro- and nanostructures and can be readily used after developing. This would reduce further processing needs. These demands also rule out SU-8, popular for MEMS devices as it is not an optimal choice for organic lasers because of its high refractive index and large optical losses. Other photoresists often lack chemical or thermal resistance.

Perfect candidates for 3D DLW prototyping can be found in the organic-inorganic material class ORMOCER®. These sol-gel materials can be tuned in their physical and chemical properties to comply with specific needs for medical (bio-compatibility) as well as for optical applications (refractive index control, low losses) (see 3.1.4). To emphasize the potential of ORMOCER®s for rapid prototyping applications the following describes the work conducted during this thesis for developing a 3D-DLW fabricating process for ORMOCER® DFB resonator gratings. The gratings fabricated with this process provided feedback for functional organic semiconductor DFB lasers. The following paragraphs elucidate the challenges that arose during this work and the found solutions.

4.2.1   Voxel-line stacking method for DFB resonator gratings

Fabricating a DFB grating by simply writing single parallel lines into a resin is hampered by two reasons. The first are fabrication tolerances of the substrate holder and the existence of residues which, as shown in figure 4.10a cause the cover slip to be tilted at a microscopic angle. This causes the focal volume to vertically move relative to the resin layer when the substrate position changes horizontally. Therefore, when patterning large areas the structure tends to be written partially inside the substrate or to lose contact to the substrate. This issue would normally require to additionally level the substrate surface with electromechanics or to map the topology of the substrate surface prior to writing the structure. The achievable accuracy with both approaches depends, however, directly on the uncertainty of the

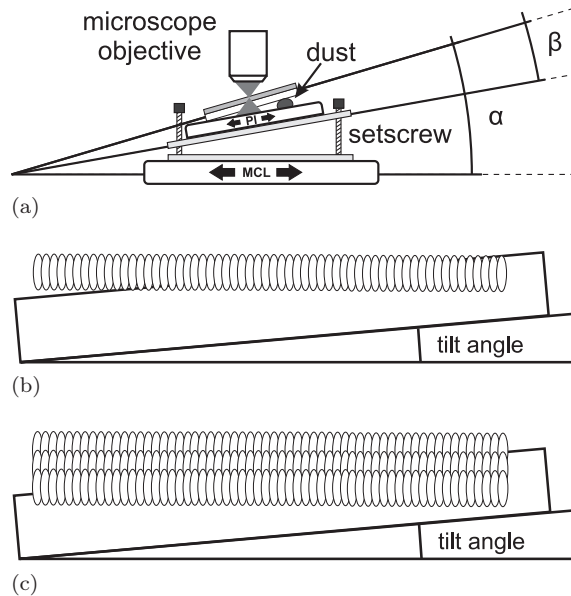employed interface position detection method.   For this work, however, a much

Figure 4.10: (a) Schematic representation of the factors leading to a tilted substrate sur-
face. The tilt angles are strongly exaggerated for better visibility. (b) Without
compensation, the tilted surface causes a structure to be written into the sub-
strate or loosing the contact to it. (c) The tilted surface can be compensated
with defining a baseplate consisting of several layers of stacked voxel-lines
with the bottom layer being written partially into the substrate.

simpler, yet reliable solution was employed. Instead of actively leveling, the angular
tilt of the substrate is compensated with a baseplate composed of several layers
of stacked voxel-lines with the bottom layers being situated partially inside the
substrate. This measure provides a coplanar starting plane for the DFB resonator
grating.

The second reason originates in the viscous character of resins like ORMOCER®
during development (see 4.1.4). This causes the thin voxel-lines to partly adhere to
each other during developing due to cohesive forces induced by surface tension on
a developing material while drying [166]. Figure 4.11a exemplifies this phenomenon
with 4.4 µm high and 800 nm wide parallel lines spaced at 5 µm. The example in
figure 4.11b shows that this effect also occurs for DFB resonators with 410 nm thin
voxel-lines spaced at 400 nm. Figure 4.11c visualizes that the small distance and the
large surface area in the deep groove between the voxel-lines pulls them together
randomly during development as it can be seen in the atomic force microscopy image
in figure 4.11d. This effect can be minimized by writing larger voxel-lines as depicted
in figure 4.11e and stacking them not only vertically but also horizontally to reduce
the aspect ratio and hence increase the mechanical stability during developing.

4.2.2 Fabrication of DFB resonator gratings

The findings described in the preceding sections of this chapter were used to fabricate
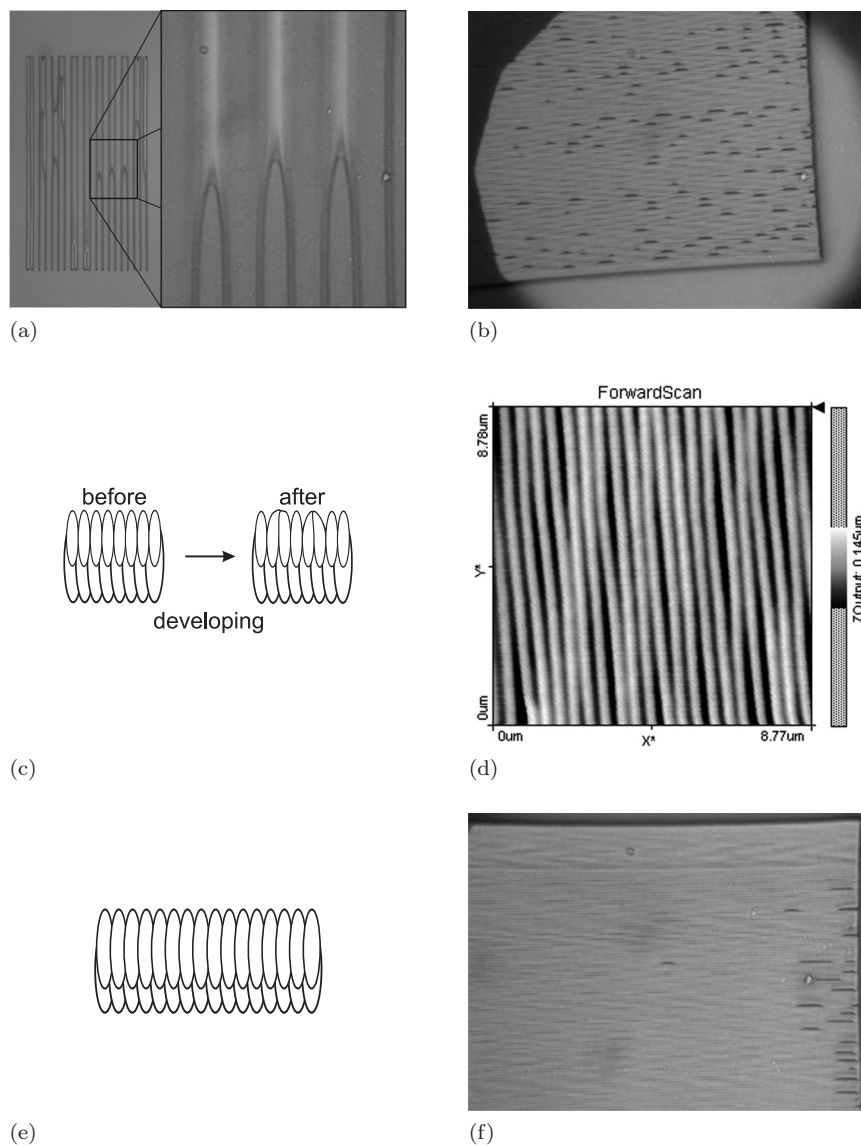an organic DFB laser based on a three dimensional direct laser written resonator

(a)

(b)

(c)

(d)

(e)

(f)

Figure 4.11: Voxel-line stacking prevents DFB grating lines from adhering to each other: (a) Microscope image of 800 nm wide and 4.4 µm high voxel-lines spaced at 5 µm. The lines were pulled together by capillary forces in the developer bath. (b) Microscope image of a DFB resonator grating with a large number of defects due to adhering grating lines. The grating consists of 410 nm thick voxel-lines spaced at 400 nm. (c) Schematic cross-sectional representation (to scale) of the geometry of the structure in (b). The small distance and the large surface area due to the deep groove between the voxel-lines cause them to randomly adhere to each other due to capillarity. (d) Atomic force microscope image showing the randomly adhered voxel-lines (e) Writing larger voxel-lines and stacking them not only vertically but also horizontally reduces the aspect ratio and hence increases the mechanical stability during developing. (f) Microscope image of an DFB resonator written with 490 nm thick voxel-lines spaced at 400 nm.

grating. The grating was patterned into ORMOCER$^{\circledR}$ US-S4, also referred to as Ormocomp (see 3.1.4, p. 38), because of its low refractive index and high transparency compared to SU-8. The Ormocomp resin was spin coated for 30 s with 3000 r/min from a droplet to a 50 μm thick homogeneous layer. A 170 μm thick BK7 glass cover slip served as substrate. A subsequent 2 min long pre-bake step at 80 °C on a contact hotplate promotes the resin adhesion and film homogeneity. Inscribing the grating into the resin with 3D-DLW started with defining a baseplate comprising six layers of parallel lines with a periodicity of 400 nm. The voxel-lines were written continuously with a width of 570 nm and a height of 2.5 μm at 2 mW time averaged laser power. The positioning stage was moved for this with a translation speed of 1 mm s^{-1}. The layers were vertically spaced at 600 nm with the first layers being placed below the interface between substrate and resin. This baseplate ensures proper adhesion of the grating and compensates surface deformations and mounting induced tilt of the cover slip.

The actual resonator grating was then written with the same periodicity as a seventh layer 600 nm above this baseplate. The voxel-line cross section dimensions were chosen to (0.49×2.3) μm^2 by setting the time averaged laser power to 1.8 mW. Immediately after the 3D-DLW exposure the sample was treated with a 5 min long post-bake step at 80 °C. Figure 4.12a shows the finished surface grating imaged with an atomic force microscope (*Zeiss NanoWizard II*) after being developed for 5 min with Ormodev [167]. The cross section in figure 4.12b reveals a periodicity of 400 nm with a height modulation of about 40 nm. The layer structure of the baseplate is visualized in the scanning electron micrograph in figure 4.12c. The complete structure spans an area of (200×200) μm^2. To finalize the sample preparation a 350 nm thick layer of the active material Alq$_3$ doped with 2.5 mol % of the laser dye DCM was deposited onto the resonator. Both materials were deposited simultaneously out of separate crucibles using a thermal vacuum vapor deposition at a pressure below 1×10^{-3} Pa. A schematic representation of the resulting organic semiconductor DFB laser structure is depicted in figure 4.13.

4.2.3 Optical characterisation

The fabricated DFB laser samples were characterized using the experimental optical setup which is shown schematically in figure 4.14. A frequency tripled actively Q-switched diode pumped neodymium:yttrium orthovanadate (Nd:YVO$_4$) laser (*Advanced Optical Technology AOT-YVO-20QSP*) operating at 355 nm acts as the pump source. It emits 500 ps long pump pulses at a repetition rate of 1.3 kHz. The pump pulse energy is set with a variable neutral density filter and measured online with a calibrated gallium arsenide phosphide (GaAsP) photodiode connected to an oscilloscope *(Agilent Infiniium 54810)*. A dichroic mirror and a lens direct and focus the pump laser onto the sample. The laser focal spot is elliptically shaped with a diameter of (300×200) μm^2. These dimensions were determined using the moving edge method [168]. To protect the Alq$_3$:DCM from degrading due to photooxidation (see 5.1.4, p. 80) the DFB laser sample is enclosed inside a vacuum chamber at a pressure below 5×10^{-3} Pa. The photoluminescence emission of the sample is collected by the focusing lens and coupled into an imaging spectrometer (*Acton*

(a)   (b)

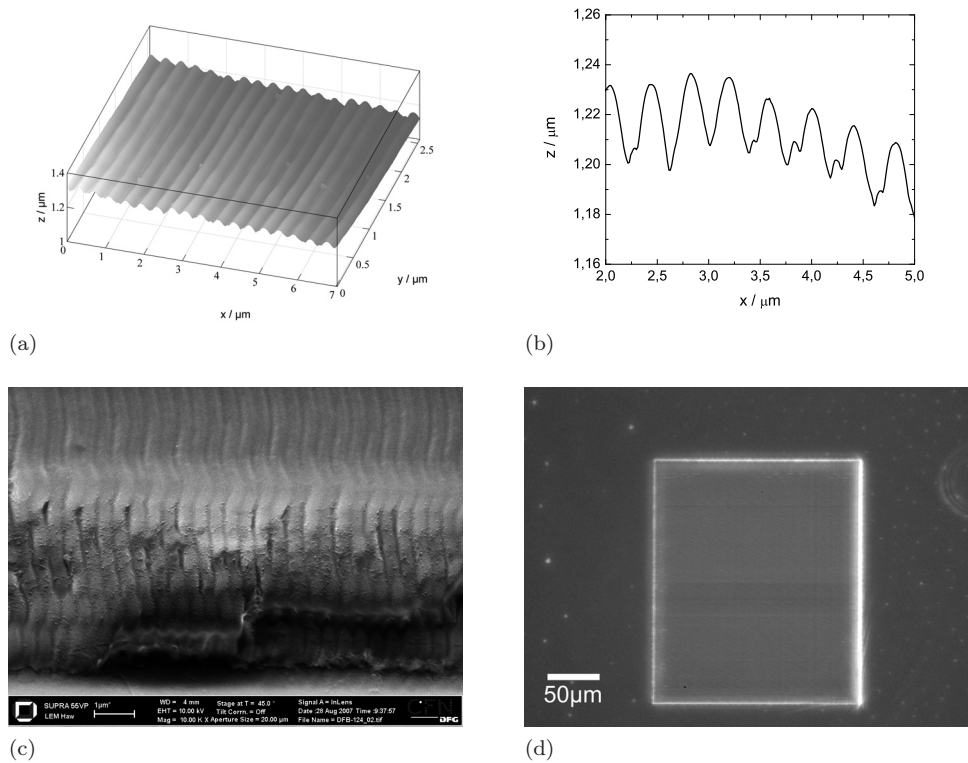(c)   (d)

Figure 4.12: (a) Atomic force microscope measurement of the resonator structure. (T.
Woggon et al. [144]) (b) Cross section at $y = 1.229\,\mu$m. The period of the
surface grating is 400 nm. The grating depth is about 40 nm. (c) Scanning
electron micrograph edge of a developed resonator grating (d) Optical micro-
scope image of the finished Alq$_3$:DCM DFB laser.
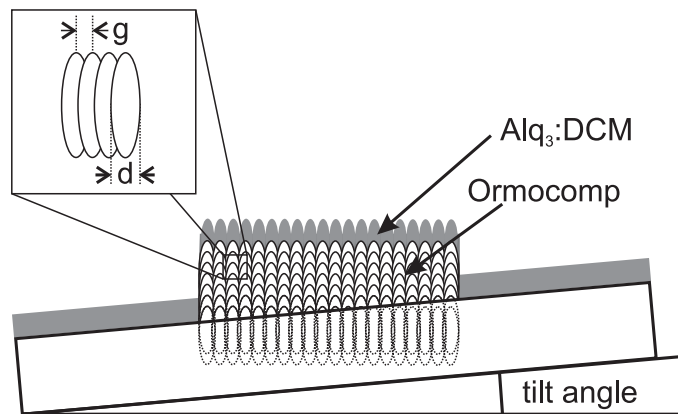
Figure 4.13: Resulting layer structure after the vapor deposition of the active material. The
Alq$_3$:DCM layer on the Ormocomp forms a slab waveguide. The depicted tilt
angle is exaggerated for clarification. Inset: By letting the voxels overlap
each other the grating periodicity g can be smaller than the voxel diameter
d. This allows to write larger voxels yielding a better mechanical stability
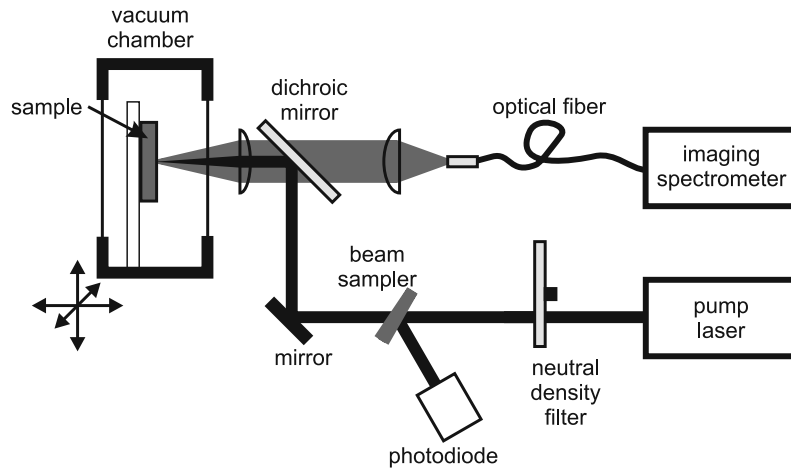during developing. (T. Woggon et al. [144])

Figure 4.14: Experimental setup for the optical characterization of the fabricated DFB laser sample. A frequency tripled 355 nm Nd:YVO$_4$ laser acts as the pump source. The pulse energy is set with a variable neutral density filter and measured online with a calibrated photodiode. A dichroic mirror and a lens direct the pump laser onto the sample. The photoluminescence emission of the sample is collected by the focusing lens and coupled into an imaging spectrometer via an optical fiber. (adapted from T. Woggon et al. [144])

Research Spectra Pro 300i with Princton Instruments PI MAX512) via an optical multimode fiber. To ensure a central and complete illumination of the DFB grating area the vacuum chamber can be translated with micron precision. A control algorithm for automated recording of spectrally resolved intensity maps allows an optimal alignment.

Figure 4.15a shows different emission spectra of the sample taken below and above the lasing threshold. The evolution of the lasing mode out of the photoluminescence spectrum with rising pump energy densities is clearly visible. The lasing wavelength is 634 nm with a spectral linewidth (FWHM) of 0.15 nm. This measurement was limited by the resolving power of the spectrometer. The corresponding characteristic threshold behavior can be seen in figure 4.15b. The laser starts to operate at a threshold energy density of about 175 µJ cm^{-2}. As shown in figure 4.16 the DFB laser emission shows also a high degree of polarization.
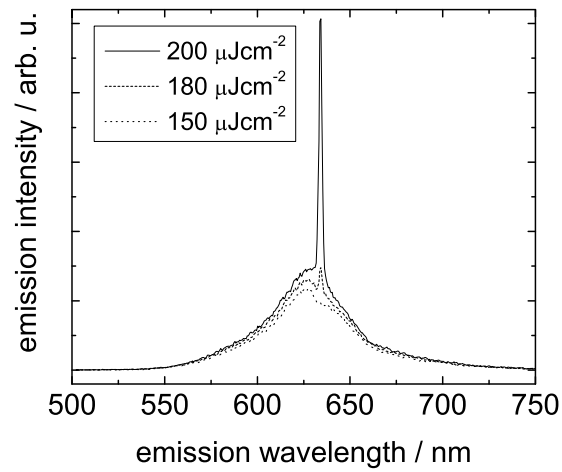
(a)
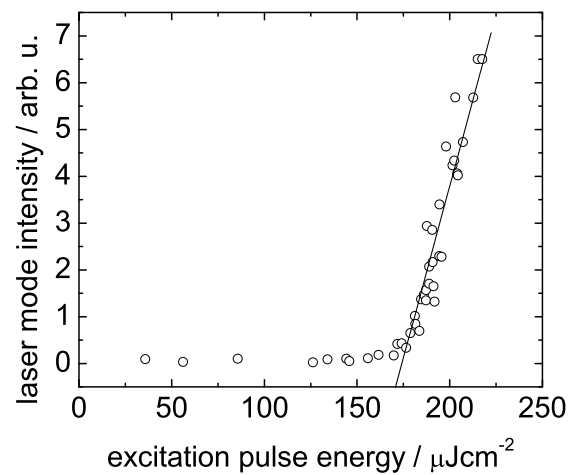
(b)

Figure 4.15: (a) Characteristic threshold behavior of the DFB laser. The threshold energy density is about $175\,\mu\mathrm{J\,cm^{-2}}$ (b) Emission spectra of the DFB laser taken at excitation energies above and beneath the lasing threshold. (T. Woggon et al. [144])
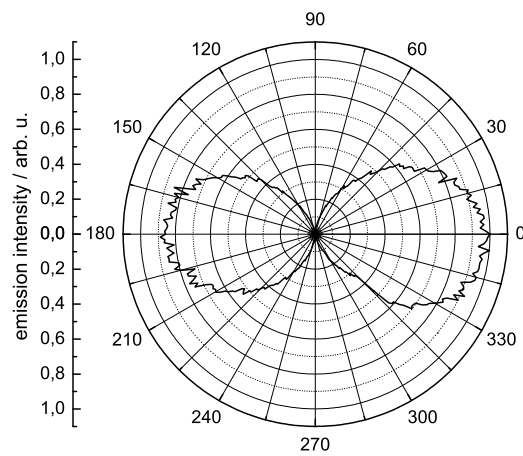
Figure 4.16: Polarization dependent intensity of the DFB laser sample showing a high degree of polarization. The plotted data as been acquired by inserting a motorized polarizer in front of the optical fiber to the spectrometer and integrating the detected spectrum for different angular positions of the polarizer. (T. Woggon et al. [144])

4.3 Towards rapid prototyping of complex microoptical systems

Microoptical devices can be characterized mainly by their physical dimensions. Examples for such devices are classical optics like mirrors, prism and lenses with micron dimensions. These devices can be combined to fully functional systems, e.g. miniaturized spectrometers [169] or length measurement sensors [170]. A field that attracted a lot of attention in the recent years are microring resonators, especially microtoroids due to their high Q-values which enable numerous applications in nonlinear optics and ultra sensitive bio-sensing [171]. Common to all of these approaches for microoptical systems is that, although the single elements measure only microns, the whole system usually extends over several millimeters. 3D-DLW has the potential to become a powerful prototyping tool in the development process for such integrated systems. This however requires to extend the capabilities from patterning the rather small areas sufficient for nanostructures like DFB resonators or photonic crystals to largely extended structures.

In the above sections the 3D-DLW pattering was done by employing only the travel range accessible with the *PI P-563.3CD* nano-positioning table. It is obvious that this area is far to small for the targeted prototyping of lab-on-chip devices occupying square centimeter areas. This requires either a larger nano-positioning system or the ability to stitch such a structure together from single patches. As most extended components in lab-on-chip application schemes allow for micron tolerances the use of a long travel nano-positioning setup is economically unviable. The 3D-DLW setup used for this thesis is therefore equipped with an additional scanning table (*Märzhäuser Scan 120x100*). This extends the available scan area to $(100 \times 120)\,\text{mm}^2$ with micron positioning accuracy.

Independently from the choice made for extending the travel range, the writing of extended structures requires additional measures to compensate uneven substrate surfaces. The already employed method of writing the structure base partially into the substrate compensates these unevennesses only for small writing areas. This can be solved by approximating the surface as a plane defined by the interface location measured at three distant points as depicted in figure 4.18a. This approximation yielded good results for compensating a tilted substrate and allowed for automated patterning of waveguide structures extending up to 8 mm. Figure 4.17a and 4.17b shows such an optical rip waveguide with an attached total internal reflection coupling mirror patterned into Ormocomp. The waveguide was build by attaching multiple 200 µm long segments with an overlap of 5 µm. Figure 4.17c shows a transition between two segments. The visible step on top of the waveguide is the result of the readjustment of the interface position. The design freedom provided with 3D-DLW is illustrated in figure 4.17d with a scanning electron micrograph of freestanding rip waveguides. This enables to fabricate complex optical interconnecting systems featuring multiple layers of crossing individual waveguides.

For larger patterns the plane approximation, however, failed because of tension induced ripples of the slide due to the mounting. This and other causes of such defocusing are well known in the field of confocal microscopy with multiple proposed solutions for automatic focus hold systems since the 1980s which continuously mea-
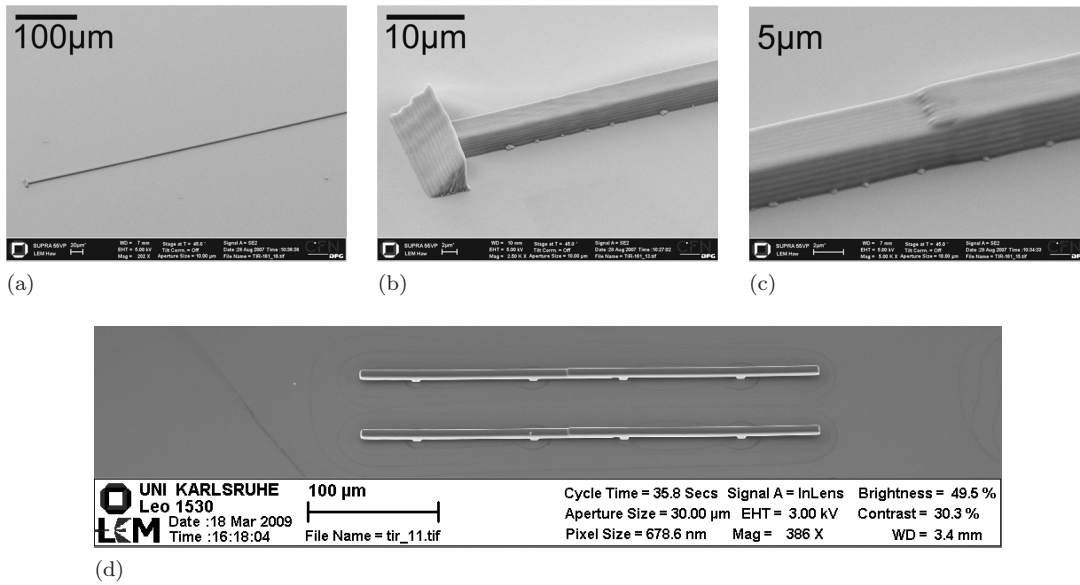
(a)

(b)

(c)

(d)

Figure 4.17: Extended integrated rip waveguides fabricated with 3D-DLW: (a)-(b) Scanning electron micrograph of an optical rip waveguide with attached total internal reflection coupling mirror which was patterned into Ormocomp. The waveguide cross-section measures $(5 \times 5)\,\mu\text{m}^2$. (c) Scanning electron micrograph of transition were two segments overlap by $5\,\mu\text{m}$. The visible step on top of the waveguide is the result of the readjustment of the interface position. (d) Scanning electron micrograph of freestanding rip waveguides which illustrate the design freedom available with 3D-DLW.

sure (see 4.1.3) and correct the distance between objective and substrate surface. Although the simple solution of approximating a plane worked satisfactory for this thesis, it cannot compensate deformations with large area substrates were the gravitational force of glass weight, mass of the resin, dynamic adhesive forces caused by the immersion oil (see figure 4.18b) and thermal expansions/shrinks of the involved object carrier parts lead to unpredictable deformations of the substrate. An automated focus hold system thus has to be considered as a mandatory part of a 3D-DLW production system.

The optimizations made in this work allow to conveniently prototype microoptical systems. As an example, Figure 4.19 shows an integrated waveguide coupled organic photodiode. Figure 4.19a shows a schematic of the device structure. The photodiode with a circular active area of $200\,\mu\text{m}$ in diameter was photolithographically defined on a $1\,\text{mm}$ thick glass substrate with a indium tin oxide coating [172]. The $700\,\mu\text{m}$ long waveguide and the attached TIR mirror were written in SU-8 2000 on a $170\,\mu\text{m}$ thick glass cover slip with 3D-DLW. The cover slip was then aligned and bonded to the photodiode substrate. A blocking layer between the two substrates prevent stray light and substrate modes from reaching the photodiode.

Light from a $532\,\text{nm}$ laser is coupled into the end facet of the rip waveguide through an optical fiber which can be moved with micropositioning actuators. The photocurrent is recorded while the fiber is displaced several micron starting from the position yielding the highest photocurrent. The result is plotted in figure 4.19b.

(a)   (b)
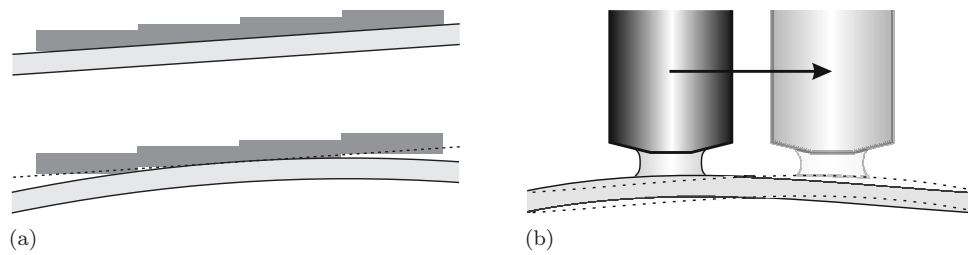
Figure 4.18: (a) A tilted substrate can be leveled by measuring the interface position at
          three reference points and spanning a correction plane through them. This
          method, however, fails for bent substrates. (b) For large substrates a contin-
          uous autofocus is required as the surface can be deformed due to the capillary
          force of the immersion oil.

It shows that only light coupled into and guided by the waveguide reaches the
photodiode.

(a)   (b)
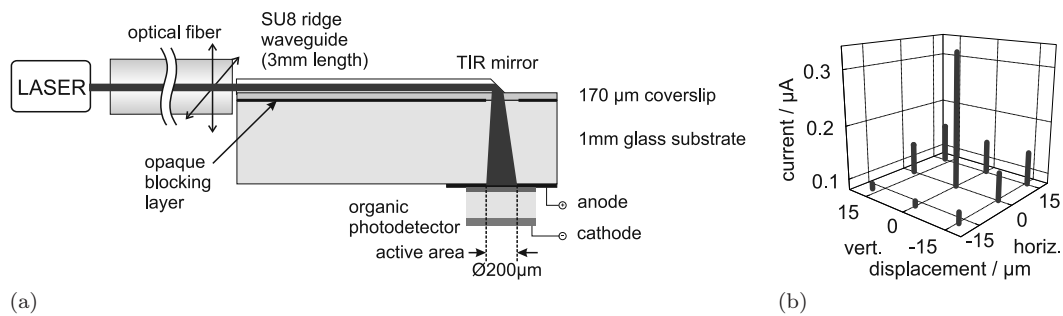
Figure 4.19: Schematic representation of the structure of an integrated organic photodiode
          coupled to an optical waveguide through a TIR mirror. The blocking layer
          prevents that stray light and leaky waveguide modes reach the diode. (b) Plot
          of the photocurrent measured with respect to the displacement of the optical
          fiber from the waveguide entrance facet.

4.4 Perspective: Rotational-symmetric structures

Rotational-symmetric structures attract a growing interest for providing the feedback for low threshold organic lasers and as microoptical sensing elements. Circular Bragg gratings provide, in contrast to other surface gratings, nearly full two-dimensional feedback [29,30]. Low-threshold organic lasers have been demonstrated also with microring and microdisk resonators [173] as well as with freestanding microtoroid resonators [174].

In the recent years different fabrication methods for freestanding microring resonators with high quality factors (high-Q) have been proposed [175,176]. All these approaches, however, still require multiple processing steps for integrating them into microoptical systems [177]. Additionally they all exploit self-organizing effects which limits the influence on shaping the resonator cross-section. Koechlin et al. demonstrated in 2009 that two-dimensional direct laser writing can be a viable method for fabricating integrated waveguide coupled planar microring resonators [178]. The 3D-DLW thus suggests itself for the fabrication of rotational-symmetric resonators as it not only allows a great freedom in design but also the simple integration of high-Q microtoroids in microoptical systems.

Obtaining high Q-values in microtoroids requires devices with a very low surface roughness. The schematic representation in figure 4.20 shows the most common 3D-DLW scanning methods (see 4.1.2, p. 51) applied for annular shapes. The surface quality with 3D-DLW patterning depends strongly on the employed scanning method. R. Guo et al. employed the voxel-by-voxel scanning approach depicted in figure 4.20a for the fabrication of microlenses with smooth surfaces [143]. However, the employed tightly spaced voxel pattern required them to pattern at very low speeds of $(4 \text{ to } 16)\,\mu\text{m}\,\text{s}^{-1}$. Comparing the amount of lines theoretically needed for patterning a circular shape with the different methods, the annular vector scan approach clearly stands out as the best option to significantly speed up the fabrication process while maintaining a smooth surface.
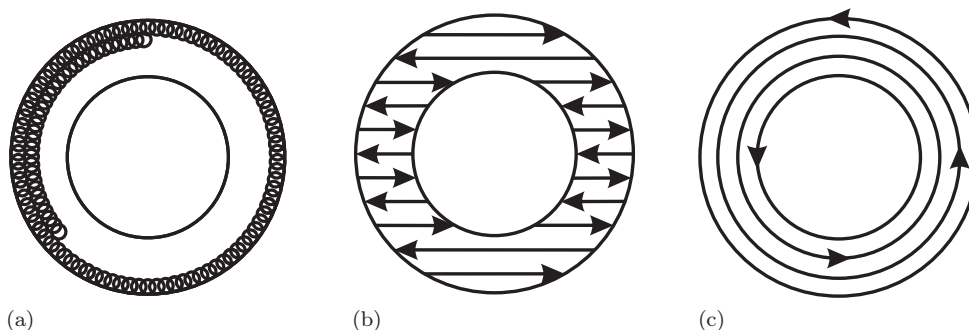

(a) (b) (c)

Figure 4.20: Comparison of different scanning modes for direct laser writing: (a) voxel-by-voxel mode (b) parallel line scanning mode (c) annular scanning mode. (adapted from C. Eschenbaum, T. Woggon et al. [150])

The required circular movement can be obtained by moving two axes simultaneously with a phase-shift of $\pi/2$ on a sinusoidal shaped curve. The writing speed with this approach is limited mainly on how well the motion control feedback loop

parameters are adapted to the mechanical system. Without optimizing these parameters a result like it is shown in figure 4.21a can occur. The employed *PI E-710.2* controller thus provides a costly upgrade option to automatically adapt these parameters to the desired motion. This solution, however, increases fabrication time as for each programmed motion the optimal parameters are determined iteratively with multiple initialization runs.
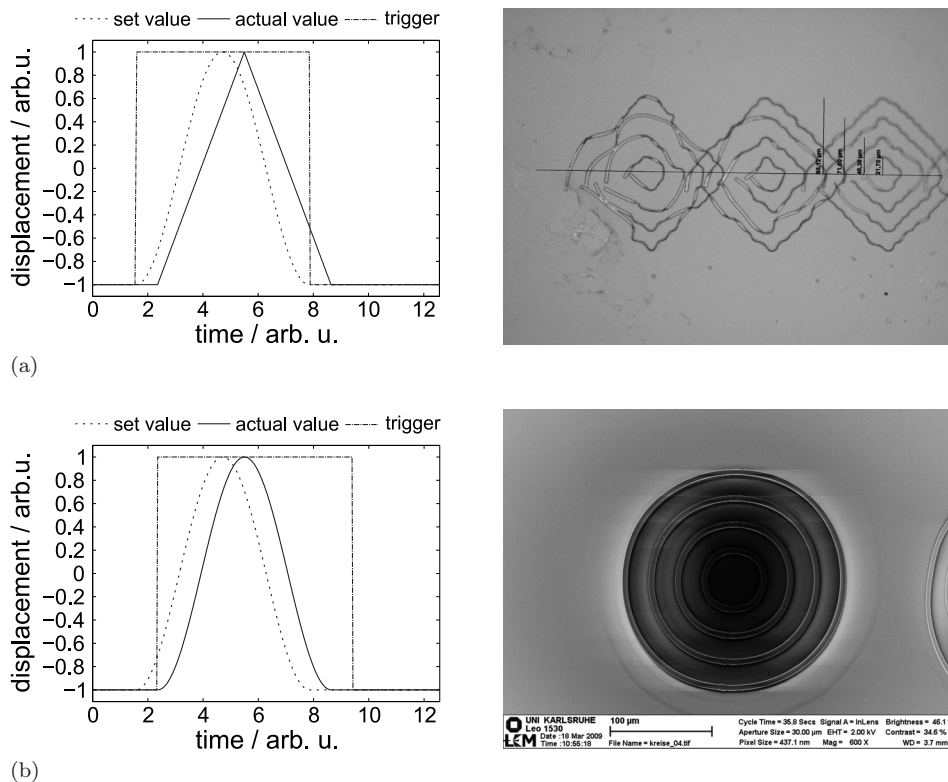

(a)

(b)

Figure 4.21: Set point/actual-value comparison for annular vector scanning: (a) Acceleration limit is too low, shutter opens early: The microscope image shows the resulting rectangular pattern with open lines. (b) Optimized control parameters, the stage accurately follows the set values, the trigger delay properly matches the delayed stage movement: The SEM image shows the resulting perfectly shaped circles.

In this thesis it was found that a manual optimization of the feedback loop parameters is a more feasible approach to realize a high speed fabrication of circular shapes. The feedback loop parameters were therefore optimized for a circular movement. This was done by measuring the resonance frequency of the mechanical system for different amplitudes and writing velocities and iteratively adjusting the control parameters in order to maintain the lowest possible positioning error. The result of such an optimization can be seen in figure 4.21b. The so obtained set of optimized process parameters is stored in the control software which programs the piezo controller with the best solution dependent on the pattern to write.

This optimization enabled circular writing speeds of $1.5\,\mathrm{mm\,s^{-1}}$ at $1\,\mathrm{mW}$ exposure laser power. This remarkable result excels the fabrication speed to an order of magnitude higher values than the results of Guo et al. [143]. A single freestanding

microtoroid as shown in the SEM picture in figure 4.22 can be fabricated in less than 10 min. These microtoroids were written into a 50 µm thick SU-8 2050 layer glass substrate.
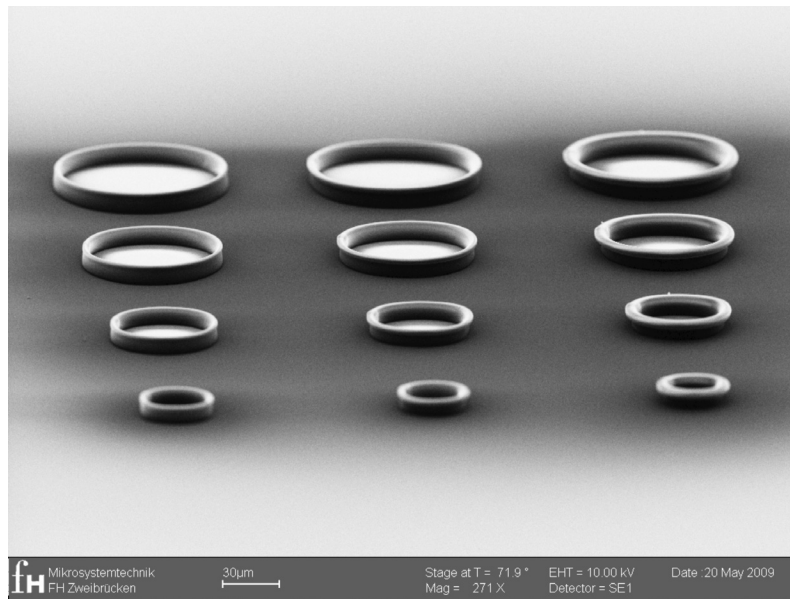

Figure 4.22: SEM micrograph of different microtoroid ring resonators with varying diameters and cross-sections

4.5   Conclusion

The work presented in the preceding sections of this chapter illustrated key aspects and proposed solutions for applying the 3D-DLW patterning technology as a tool for rapidly prototyping integrated microoptical systems. It was demonstrated that a vector scanning writing strategy in conjunction with an optimized electromechanical system enables a considerable increase of the fabrication speed. The suggested method of detecting the glass/resin interface position by exploiting the resin auto-fluorescence requires little or no extra hardware in a 3D-DLW system and works independently of the refractive indexes of substrate and resin. Using the test pattern for characterizing unknown photoresists allows for a simple and fast adaption to the emerging number of novel photosensitive materials.

The functional DFB laser fabricated in this work proves the applicability of 3D-DLW for rapidly prototyping integrated organic laser light sources. The required nanostructures were patterned into the organic-inorganic hybrid material Ormocomp. An optimized voxel-line stacking processing strategy was developed for this. This strategy effectively compensates microscopic tilted substrate surfaces and prevents voxel-lines from collapsing due to capillarity during developing.

The proposed solution for leveling surface deformations by approximating a correction z-plane combined with developing a stitching strategy enabled the prototyping of integrated microoptical systems with extents of multiple millimeters. The demonstration of a functional integrated waveguide coupled organic photodiode emphasizes the applicability of 3D-DLW for this purpose. The extension made in this work enable a high-speed processing with simultaneous nonlinear movement of two writing axes. It allows to rapidly prototype freestanding microtoroids and other arbitrary annular shaped structures which are not possible with conventional self-organizing methods.

In summary, the developed patterning capabilities for micro- as well as nano-structures using the glass like ORMOCER® Ormocomp provides the basis for the rapid prototyping of organic lasers and all-integrated optical circuits.

Chapter 5

Organic lasers for spectroscopy

Abstract[1]

The following chapter addresses key questions of substrate materials, operating lifetimes and temperature stability of as well as tuning and pumping schemes for organic lasers. It presents application oriented solutions for the usage of organic semiconductor lasers in spectroscopy. In particular it describes the application of organic lasers for spectrally resolved transmission measurements and for fluorescence excitation.

5.1 Optimization of organic DFB lasers

Up to today research activities on organic lasers were often concentrated on fundamental work on improving the emission characteristics. Although parameters like linewidth, threshold, spectral coverage and tunability are the most prominent for describing an organic laser device, they are only one part of the picture based on which one has to judge the applicability of this novel technology for a specific application. Transferring the technology of organic lasers from the controlled laboratory environment to a practical application needs additional activities not covered in fundamental research.

Apart from quantifying the influence of environmental factors on performance and lifetime of an organic laser, a working combination of the various singular approaches for such devices proposed in literature has to be found. The latter is necessary as researchers tend to compare their results in absolutes while concentrating on single aspects, e.g. highest output powers, lowest threshold or largest tuning range. Whether or not the improvement of a single performance parameter had a negative influence on others is often not investigated.

This section evaluates the influences of different substrate materials and environmental changes on the performance and lifetime of organic lasers. It proposes solutions for materials, encapsulation methods and optical system setups which, when combined, enable the use of organic lasers for spectroscopy applications.

5.1.1 Substrate material

As elucidated in the fundamentals in chapter 2.2 (p. 17) a high index contrast of the active material waveguide favors low threshold DFB laser operation. Accordingly, from the experimenters view the perfect substrate material would be vacuum or air. As this makes solution or vapor deposition processing of organic gain materials quite difficult, an optical transparent, low refractive index substrate is required. Glass is an excellent choice for research purposes due to its high resistance to solvents and cleaning processes which allows the multiple use of the same DFB grating with different organic gain materials. For the targeted mass volume applications, however, a low cost replication process with polymer substrates is desired.

Despite its unique features, PMMA unfortunately turned out to be a non-favorable material for this application at a very early stage of this thesis. One reason is the low chemical resistance of the material against acids, bases and solvents like alcohols, acetone or benzole. Another reason is the considerable water absorption. These problems may be solved with an additional surface treatment or with one-time use as disposable devices. A more critical point which emerged in experiments is the vast number of PMMA derivates available. Although they exhibit similar optical characteristics, the different material compositions can lead to unpredictable results in device performance.

The photographs depicted in figure 5.1 show two samples of DUV lithographically defined waveguide coupled DFB resonators with a layer of Alq$_3$:DCM on top. The substrate material is a strongly cross linked PMMA variant(*Notz Plastics Hesaglas HT*). The device geometry is the result of a work from Mathias Bründel [179] who
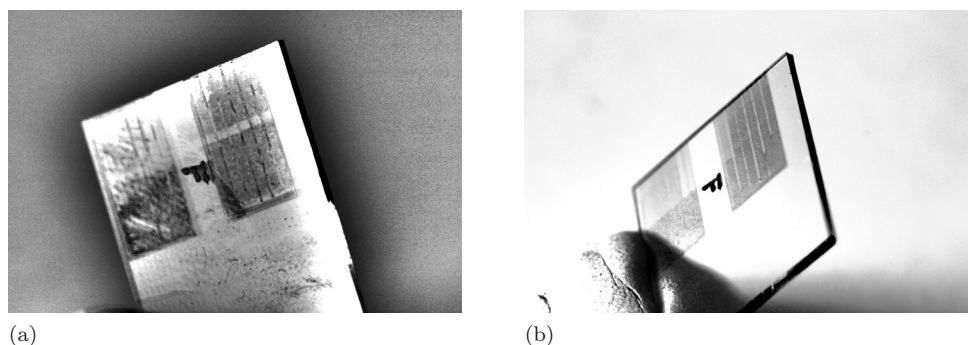
(a)   (b)

Figure 5.1: Excessive degradation of the active material on PMMA. Both samples comprise DUV lithographically defined waveguide coupled DFB resonators with an layer of Alq$_3$:DCM on top. A pump laser spot has been scanned over a selected area. Although being in a vacuum, the Alq$_3$:DCM is bleached throughout the scan area.

successfully demonstrated laser operation. Instead of *Hesaglas HT*, he used the weakly cross linked *Hesaglas LT* also from *Notz Plastics*. The devices in figure 5.1 as well as the devices from Mathias Bründel have been optically characterized using the same setup described in 4.2.3 with scanning a selected area with the pump laser spot. Although specified with the same optical characteristics, the *Hesaglas HT* based devices failed to show laser operation[2]. Moreover, after the experiment the organic active material was bleached throughout the scan area. This effect could not be observed with different substrate materials at the same pump power level. A possible cause could be volatile products of a photoinduced scission of specific side groups which were added to the PMMA homopolymer to achieve better cross linking. A detailed explanation for this phenomenon would require thorough investigations starting with a confinement and detailed analysis of any reaction products. This would, however, have gone far beyond the scope of the present thesis.

The observed strong influence of the different cross linking grades alone on the experimental results imply that the material composition of the substrate is a parameter which can not be neglected. As stated in 3.1.1 (p. 36) PMMA is available in a large variety of formulations. The ASTM standard 788-04 for PMMA [180] specifies four groups in accordance with their composition. Each group comprises of up to four classes and each class can be divided further into individual grades. Thus, the advantage of PMMA for industrial applications of being widely available at low costs paradoxically hampers microoptical application engineering with a large set of unknown material parameters.

In the search for a viable alternative to PMMA, experiments were conducted for this thesis using Ormocomp and Topas as substrate materials. The results of Martin Punke for organic DFB lasers replicated into PMMA were used as a reference. The Topas DFB resonator was fabricated by hot embossing using the same nickel imprinting tool as for the PMMA based devices. The Ormocomp resonator was fabricated with UV NIL using a Topas replica as master. The measured laser characteristics of these devices are plotted in figure 5.2. Evidently, the devices based on

---

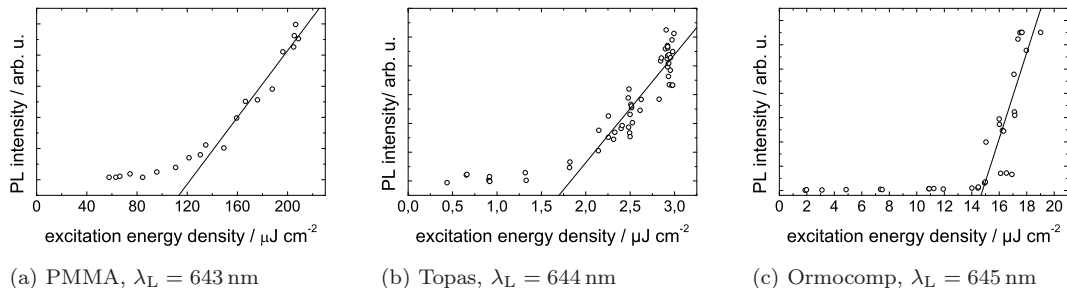[2]amplified spontaneous emission could be observed at 622 nm

(a) PMMA, $\lambda_L = 643\,\text{nm}$ (b) Topas, $\lambda_L = 644\,\text{nm}$ (c) Ormocomp, $\lambda_L = 645\,\text{nm}$

Figure 5.2: Laser thresholds of devices with similar peak wavelengths λ_L which are fabricated with replicated resonators using the same master but different polymers: (a) DFB resonator hot embossed into PMMA (data taken from Punke et al. [91]) (b) A Topas based DFB resonator fabricated by hot embossing using the same nickel tool as for the PMMA based devices yields a 100-fold lower threshold than the PMMA based device. (c) Although it can be assumed that the Ormocomp UV NIL replica of a Topas replica exhibits more defects, the laser threshold is still 10 times lower compared to the PMMA based device.

these alternative polymers perform significantly better than the PMMA based device, even with the second replica in the Ormocomp. Given the better performance of Ormocomp and Topas they were preferred to PMMA as substrate material for DFB lasers for the present thesis.

5.1.2   Impact of ambient temperature variations

The temperature range in which organic lasers can be operated is primarily limited by the glass transition temperature of the employed polymers. The influence of the typically large thermal linear expansion coefficients and thus the large thermo-optical coefficients of polymers imply a huge impact of temperature variations on the optical performance of an organic laser device. Kozlov et al. conducted a thorough investigation on the thermal properties of the gain material Alq_3:DCM in 1998. They used a $2\,\text{mm}$ long Alq_3:DCM slab waveguide laser with cleaved edges which served as cavity mirrors [5]. It was found that neither the threshold energy nor the differential quantum efficiency is significantly affected when varying the temperature between $273\,\text{K}$ and $413\,\text{K}$. They also found the emission wavelength being independent of the temperature although the provided data shows some variation. The authors compared the organic laser to a GaAs based laser diode which legitimates their conclusion of the wavelength being temperature independent quite well. The experiment, however, was not suited to provide any information on the temperature behavior of the Alq_3:DCM. The reason for this is the fabry-perot type of the used resonator which was fabricated on an InP substrate. The linear thermal expansion coefficient of this material is approximately $\alpha_{\text{InP}} = 5 \times 10^{-6}\,\text{K}^{-1}$ [181] which yields a length change of

$$\frac{\mathrm{d}L}{\mathrm{d}T} = \alpha_{\text{InP}} L_0 = 12\,\text{nm}\,\text{K}^{-1} \qquad \text{with } L_0 = 2\,\text{mm} \tag{5.1}$$

Calculating the free spectral range of a fabry-perot type resonator [182] of 2 mm length, however, results in a value of only 64 pm. This makes the spectral gain to the main determining factor of the emission wavelength.

The impact of the linear thermal expansion of the substrate can be minimized when using a distributed feedback resonator. With this resonator the differential expansion has to be integrated only over a single grating period. For a grating with a periodicity of 400 nm structured in COC the grating period would change with only

$$\frac{\mathrm{d}L}{\mathrm{d}T} = \alpha_{\mathrm{COC}} L_0 = 24\,\mathrm{pm}\,\mathrm{K}^{-1} \qquad \text{with } L_0 = 400\,\mathrm{nm},\ \alpha_{\mathrm{COC}} = 6 \times 10^{-5}\,\mathrm{K}^{-1}. \quad (5.2)$$

Town et al. published some data on the thermal dependence of the emission wavelength of an organic semiconductor laser with the active polymer MEH-PPV on a silica DFB grating resonator in 2005 [183]. They found a large temperature dependency of the wavelength with a tuning coefficient of $\mathrm{d}\lambda/\mathrm{d}T = -0.4\,\mathrm{nm}\,\mathrm{K}^{-1}$ mainly attributable to the thermo-optical coefficient of the MEH-PPV.

Also in 2005, Zhu et al. went a step further and eliminated the thermal length change of the resonator by using a holographic pump scheme for a gain modulated organic DFB laser [184]. They achieved a 5.5 nm broad wavelength tuning range around the emission wavelength of 599 nm in Rhodamine 6G doped $\mathrm{ZrO_2}$-$\mathrm{TiO_2}$-ORMOSIL films with a temperature variation between (293 to 393) K.

These three studies indicate that the chemical structure and morphology of the active material strongly influences the temperature dependence of the emission wavelength for different organic lasers. The impact of temperature variations is of key importance for measurement applications outside an air-conditioned laboratory. The temperature dependence of the DFB lasers specifically used in this study was therefore determined to obtain a more reliable information. Accordingly, the emission wavelength of an $\mathrm{Alq_3}$:DCM laser device on a BK7 glass ($\alpha_{\mathrm{BK7}} = 8.3 \times 10^{-6}\,\mathrm{K}^{-1}$) resonator was measured in a temperature range from 295 K to 335 K. For this experiment the setup used in section 4.2.3 (p. 60) was extended with a heating capability as figure 5.3 represents schematically.

The sample device is mounted on a thermoelectric heater. The temperature is measured with a positive thermal coefficient (PTC) thermistor which is pressed onto the active layer by a spring loaded bracket. Its resistance is measured with a *Keithley 283* source-measure unit (SMU). The probe current of 1 mA was sourced only during the data acquisition to prevent unwanted heating of the thermistor.

Figure 5.4 plots the laser emission wavelength and FWHM data which has been acquired for different device temperatures. Conducting a linear regression curve fit for the heat up and respectively for the cool down phase yields a temperature wavelength tuning coefficient of

$$\left(\frac{\mathrm{d}\lambda}{\mathrm{d}T}\right)_{\mathrm{BK7}} = (-0.0120 \pm 0.0011)\,\mathrm{nm}\,\mathrm{K}^{-1} \qquad (5.3)$$

With respect to the resolution of 0.2 nm of the employed spectrometer the FWHM can be regarded as being temperature independent. Any significant broadening can only be observed during a transition between two pixels of the spectrometer CCD chip.
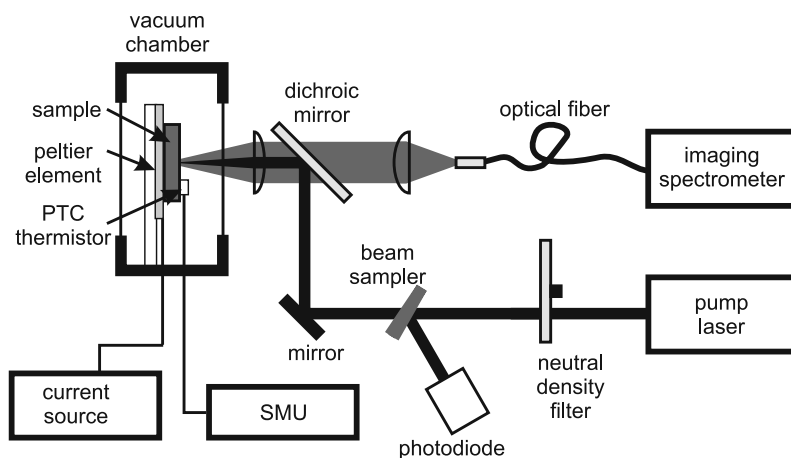
Figure 5.3: Experimental setup for measuring the temperature dependence of the emission wavelength. The sample is heated with a peltier element. The temperature is measured with a PTC thermistor. The resistance is acquired with a source-measure unit.
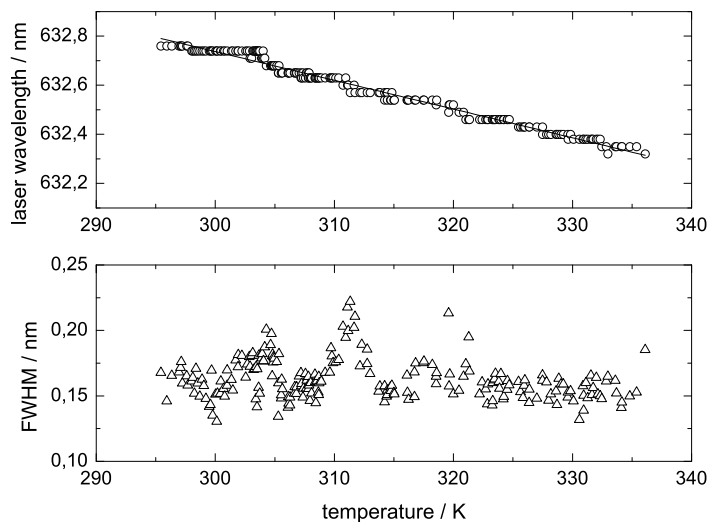

Figure 5.4: Temperature dependence of the emission wavelength and linewidth of a second order Alq_3:DCM DFB laser on a BK7 glass substrate

Encouraged by these findings the question arose how the picture would change when a polymer substrate is used that exhibits a much higher CTE compared to glass. This would be critical as in the perspective of low cost applications it would be advantageous to fabricate the DFB gratings on polymer substrates. To verify if the high CTE of a Topas substrate ($\alpha_{\text{Topas}} = 6.0 \times 10^{-5}\,\text{K}^{-1}$) significantly affects the temperature dependency, the aforementioned experiment was conducted with an Alq_3:DCM organic laser device with a Topas resonator. Additionally the temperature measurement parameter range was increased to cover 285 K to 385 K. To check if the heating induces any morphology changes a second data set was recorded during a passive cooling. The linear fits applied on the measured wavelength data
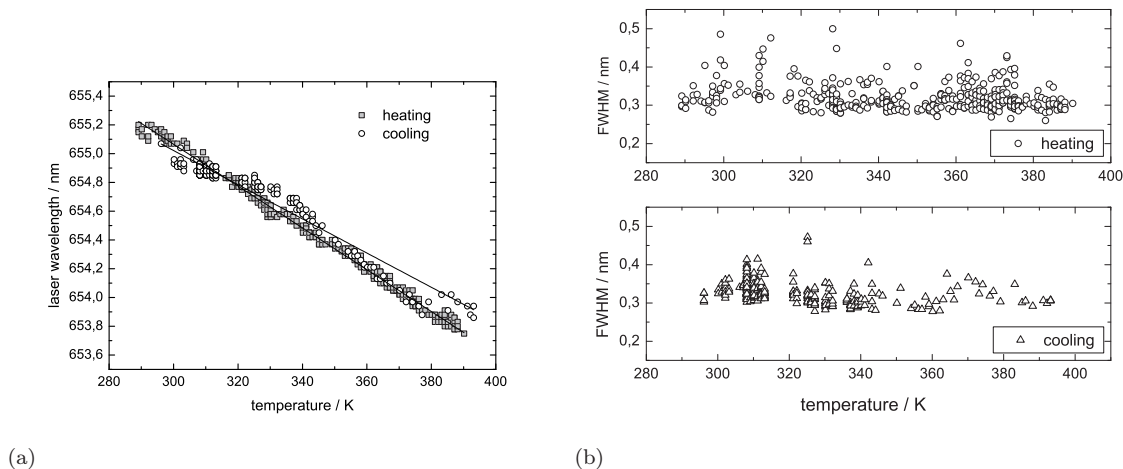
(a)   (b)

Figure 5.5: Temperature dependence of the emission wavelength and FWHM of a second order Alq$_3$:DCM DFB laser on a Topas substrate

displayed in figure 5.5a yield tuning coefficients of

$$\left(\frac{\mathrm{d}\lambda}{\mathrm{d}T}\right)_{\text{Topas,heating}} = (-0.0120 \pm 0.0017)\,\mathrm{nm\,K^{-1}}$$

$$\left(\frac{\mathrm{d}\lambda}{\mathrm{d}T}\right)_{\text{Topas,cooling}} = (-0.0146 \pm 0.0055)\,\mathrm{nm\,K^{-1}}$$

The temperature tuning curves exhibit no measurable change of the slope indicating that no phase changes took place. The difference in $\mathrm{d}\lambda/\mathrm{d}T$ between the heating and the cooling phase for the Topas is mainly attributed to the different time scales of the two processes. The active heating under vacuum was much faster than the passive cooling resulting in two different delays for the thermistor response. Due to the only marginal difference it can be assumed that the laser devices were not irreversibly damaged by the heating process.

These results correspond very well with the results for a BK7 substrate. This allows to conclude that the CTE of the substrate material does not significantly influences the temperature dependence of the emission wavelength of organic Alq$_3$:DCM DFB laser devices.

5.1.3   Tuning and pumping schemes

An eminent feature of organic DFB lasers is the easiness of how their emission wavelength can be tuned. Among the various approaches for continuously tuning covered in chapter 2.2.7 (p. 31) an elegant one is to use a wedge shaped active material waveguide layer, e.g. fabricated with a rotating shadow mask evaporation process [13]. Such an organic laser can be tuned during operation by varying the pump spot position. For the studies covered in this chapter this method was therefore employed to fabricate a DFB laser device with a continuous tuning range of more than 10 nm. As resonator served a textured glass substrate with an one-dimensional second-order distributed Bragg reflector surface grating patterned with

laser interference lithography and reactive ion etching [185]. An evaporated wedge-shaped layer of the organic semiconductor Alq_3 with $2.5 \, mol \, \%$ of the laser dye DCM provided optical confinement and gain.

Such a tunable laser sample is preferably moved relatively to the pump beam to have all emission wavelengths placed on a coaxial beam path. This suggests the pump scheme that is depicted in figure 5.6a. Neglecting any saturation effects and evaluating the Lambert-Beer law with the refractive index data given in figure 3.4, a $350 \, nm$ thick Alq_3:DCM layer transmits $22 \, \%$ at $350 \, nm$. Thus, apart from directing reflexes of the pump laser back into its cavity the major downside of this setup is the need for a high quality and thus expensive long pass optical filter. This issue can be addressed by pumping the laser non-perpendicularly and employing a beam dump to eliminate the pump beam reflexes. Such a setup, as depicted in figure 5.6b requires only a low-cost long pass filter as it only has to block scattered pump light. Although the latter approach involves higher optical losses due to Fresnel reflections for some encapsulation methods (see 5.1.4), it was used for all following studies due to the efficient pump light suppression.
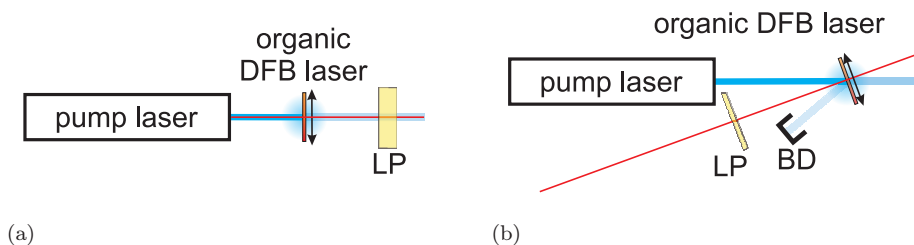

Figure 5.6: Geometric setup for exciting organic DFB lasers: (a) Coaxial pumping allows very compact systems but requires a high quality pump light filter. (b) Pumping under an angle with respect to the DFB laser emission allows very efficient pump light suppression with low-cost filters.

5.1.4   Encapsulation and degradation

The fluorescence intensity of dye molecules in organic gain materials is known to degrade during excitation. This photobleaching phenomenon originates from a photochemical modification of the dye causing the irreversible loss of its ability to fluoresce. The photobleaching kinetics, e.g the number of emitted photons before a dye molecule is destroyed, depend both on the structure and on the environment of the molecule.

There are various theories on the photochemical processes accountable for this photobleaching. Among these, the photodynamic interaction of molecular oxygen (O_2) with fluorophores in an excited triplet state is regarded as the main cause [186]. The interactions between oxygen and fluorophore triplets can produce singlet oxygen which, when decaying, can create damaging free oxygen radicals. Additionally, triplet fluorophores are also highly reactive and may react with organic molecules in the embedding matrix [186].

Besides molecular oxygen, the intrinsic incorporation of water in the organic matrix is negatively affecting the operational lifetime. Papadimitrakopoulos [187] et al. found in their experiments that freshly sublimed Alq_3:DCM thin films are saturated with water in less than 2 min under laboratory conditions. In experiments, organic lasers are therefore often operated inside a vacuum or nitrogen purged chamber. For the targeted applications outside the laboratory those solutions are of course not feasible. Such applications require a suitable encapsulation which provides a sufficient barrier against oxygen and moisture.

The activities in OLED research produced a broad spectrum of methods for device encapsulation. These range from glass covers and single barrier layer approaches up to complex multiple barrier layer systems. Graff et al. provide a comprehensive insight into this technology branch in the book *Flexible Flat Panel Displays* edited by Gregory Crawford [188].

A benchmark for the protection level provided by different methods are the rates at which water vapor and oxygen permeate the barrier. Literature states for a sufficient encapsulation of OLEDs values of $1 \times 10^{-6} \, g \, m^{-2} \, d^{-1}$ for the water vapor transmission rate [189, 190] and $1 \times 10^{-5} \, L \, m^{-2} \, d^{-1}$ for the oxygen transmission rate [189] respectively. Unfortunately, these findings can not be applied directly to organic semiconductor lasers as for OLEDs the oxidation of the metallic cathode is accredited to be the critical lifetime limiting factor. The degradation of the organic materials is not accounted for the operational lifetime. This assumption is justified with the low electron affinity and thus the high reduction potential of the cathode materials used for OLEDs.

Regarding the lifetime of organic lasers there are only few published results. They range from 3.6×10^6 pulses for an unprotected polymer laser [191] to 2×10^7 pulses for a polymer laser operated in vacuum [5] till emission intensities drop to 50 % of the initial value. Kozlov et al. published a lifetime of $>1 \times 10^6$ pump pulses for an Alq_3:DCM based laser operated in a nitrogen purged chamber as well as for a device with a thin silver layer as encapsulation [5]. Richardson et al. achieved a lifetime of 1.6×10^7 pulses by gluing a 150 µm thick silica cover slip onto a polymer DFB laser with an optical adhesive [192].

In this work the laser devices have been encapsulated for protection under a pure nitrogen atmosphere. The samples were put on an aluminum backplate with a petri dish bonded on top using an epoxy resin. With this approach the optical waveguide properties of a DFB laser sample are not affected. This method has also the extra benefit of being able to reuse the same substrate for further experiments.

The quality of this encapsulation approach was quantified by determining the operational lifetime of an encapsulated Alq_3:DCM laser. The laser was optically pumped by an actively Q-switched frequency tripled neodymium-doped yttrium lithium fluoride laser (*Newport Explorer Scientific*) with an emission wavelength of 349 nm at a repetition rate of 2 kHz while the number of pump pulses and the corresponding emission spectrum were recorded with a computer. The results plotted in figure 5.7 show that this encapsulation enables an operational lifetime of 1×10^6 pulses without a change in the emission characteristic. With accepting a slight blue-shift of 0.1 nm the operational lifetime increases to 1×10^7 pulses. Taking a drop of the intensity to 50 % of the initial value as criteria for the benchmark, the
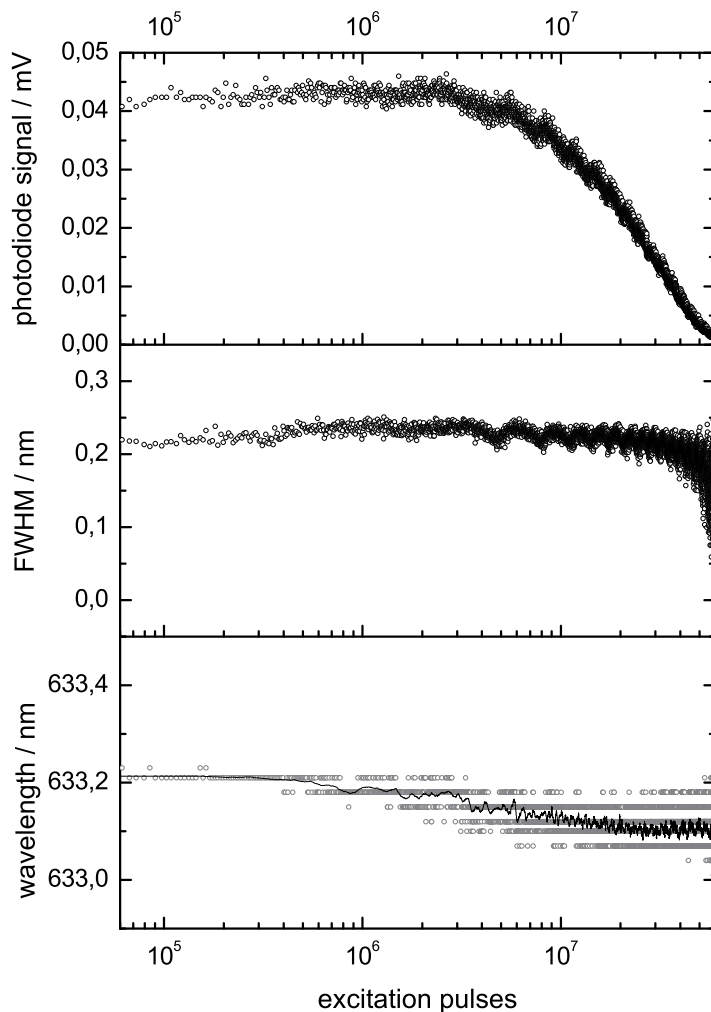
Figure 5.7: Degradation characteristics of an encapsulated Alq_3:DCM DFB Laser: The encapsulation yielded an operational lifetime of 1×10^6 pulses without a change in the emission characteristic. When a slight blue-shift of $0.1\,nm$ can be accepted, the operational lifetime increases to 1×10^7 pulses. Taking a $50\,\%$ drop as benchmark criteria the lifetime is 2×10^7 pulses.

lifetime reaches 2×10^7 pulses. This value accounts only for the lifetime for a single pump position. The accumulated lifetime of the whole chip can easily compete with current high repetition rate flash lamps (8×10^7 to 1.2×10^9 pulses [193]).

It has to be noted that this result can only be seen as an indicator that the encapsulation efficiently prevents photooxidation as it is the dominant degradation process. A deeper understanding of the photophysical process can not be deduced from the acquired data. At most, the decrease in wavelength may be attributed to a decrease of the effective refractive index according to equation (2.32). This deduction is, however, quite speculative in the light of the complex photochemical and photophysical properties of the active material Alq_3:DCM. There are four dif-

ferent isomers of the host Alq_3 which can form three different crystal phases. Each of these phases exhibits different photophysical properties [194–196]. The laser dye DCM also comprises two isomeres with different optical properties, whose ratio can change due to photoisomerization [197]. Last but not least, complexity rises with incorporating the DCM dye into the Alq_3 matrix environment where the morphology additionally extends the parameter realm [198, 199].

The employed encapsulation gives a high barrier quality to effort ratio. Encapsulated samples could be stored more than 12 months without a significant decay. Based on the good performance and the easiness of the employed encapsulation approach it was thus preferred in this work against other solutions. The employed encapsulation approach has, however, also a major downside. As it can be clearly seen in figure 5.8, the use of a protective atmosphere leads to pump light losses due to Fresnel reflection at the multiple interfaces between media with low and high refractive indexes.

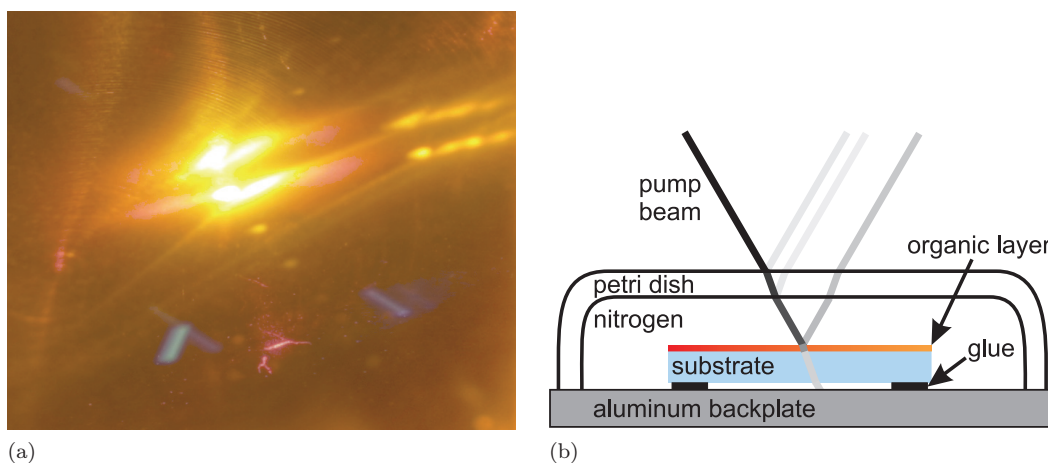(a)   (b)

Figure 5.8: (a) High dynamic range photograph of an optically pumped encapsulated organic laser. The clearly visible multiple reflections of the pump laser beam are caused by multiple transitions of the pump beam from a high to a low refractive index medium. (b) Schematic of the main reflection losses. The grayscale value of each beam represents its intensity with respect to the incident beam.

With a non-perpendicular excitation the situation can be even worse depending on the polarization of the pump light. To estimate these losses and to determine the optimal pump beam angle the angular dependent pump light transmission for a air/glass/nitrogen/Alq_3:DCM optical path was calculated using the Fresnel equations (see 2.1.1). The complex refractive index values used for the calculation are listed in table 5.1. The resulting curve is plotted in figure 5.9a. As expected the transmission for purely TM polarized pump light has a maximum at the Brewster angle of glass. In the used setup, however, the pump laser polarization vector was rotated due to metal beam steering mirrors. Thus in the experiments it was ensured that the pump beam angle does not exceed 30° to keep losses reasonable.

A solution to this issue for future applications, where pump power might be critical, e.g. when pumping with laser diodes, would be to use a directly applied low refractive index coating. The advantage of such a low index encapsulation coating

material	complex refractive index
air, nitrogen	1
glass	1.54
Alq_3:DCM	$1.75 + 0.12i$ [53]

Table 5.1: Complex refractive indexes used for calculating the refraction losses due to the encapsulation.
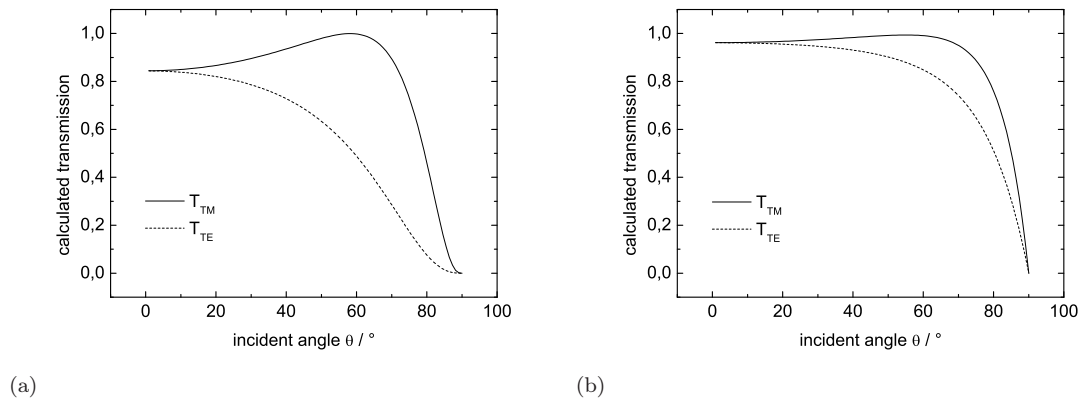

(a)

(b)

Figure 5.9: Calculated angular dependent pump light transmission for (a) glass/nitrogen and (b) low index ($n = 1.34$) layer encapsulation

reveals when calculating the curve for a coating using the amorphous fluoropolymer CYTOP with a refractive index of 1.34 which is plotted in figure 5.9b.

5.1.5   Spectral mode reduction

Besides a concurrent operation of TE and TM laser waveguide modes, that can be easily separated with a polarizer, one result of the theoretical view on one-dimensional DFB resonators given in chapter 2.2.2 is the possibility for multiple lateral modes with different wavelengths whose out coupling light beams are arranged in a fan-shape emission pattern as it is described in detail in the work of Stefan Riechel [53]. This behavior is problematic for aligning an optical system, e.g. to monitor the output beam it can not be assured that the signal and the reference detector are illuminated by the same spectral mode.

   This problem can be addressed by placing apertures into the optical path which block the unwanted modes. Figure 5.10 shows the optical setup that was used to demonstrate the effectiveness of this approach. The emission of an organic DFB laser was directed onto a CCD camera based beam profiling system (*Coherent LaserCam HR*) with two variable apertures placed at the optical axis between laser and camera.
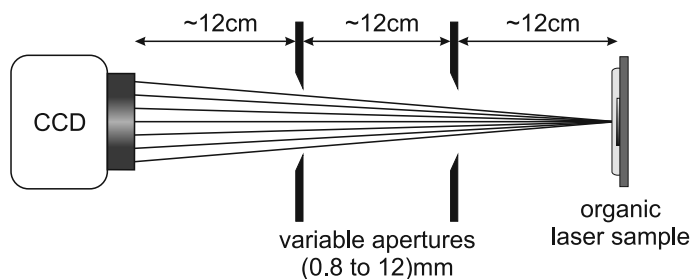

Figure 5.10: Optical setup for discriminating unwanted lateral modes with apertures: Two apertures are placed into the light path between an encapsulated organic DFB laser sample and a CCD beam profiling camera. The grating groves point out of the drawing plane.

   The measured intensity distribution on the CCD sensor for various aperture sizes is depicted in figure 5.11. Figure 5.11a shows, that with fully opened apertures the broad line shaped distribution typically for a 1D DFB laser is observed at the CCD. The multiple stripes parallel to the main emission originate from multiple reflections at the encapsulation glass or from independent resonator modes excited by a too large pump spot. The weak interference fringes in the main emission intensity distribution indicate that the multiple lateral modes interfere with each other. Accordingly, in analogy of blocking Fresnel zones [37], reducing the apertures results in the typical Fresnel diffraction interference pattern shown in figure 5.11b with two peaks at the outer edge of the intensity pattern. With the apertures set to the minimum size the output beam reduces to a well defined single spot as shown in figure 5.11c. The intensity profiles along the x-axis and the y-axis of this reduced output beam are plotted in figure 5.12. It shows that removing the interfering outer laser modes with the apertures yielded an increase in intensity along the beam path by 20 %. In consistence with these measurements is the observation that, as plotted in figure 5.12c, obstructing the outer modes of the fan-shaped emission pattern with apertures also drastically narrows the spectral distribution of the DFB laser output beam compared to an undisturbed beam whose spectrum is plotted in figure 5.12d. The exemplary spectrum of the undisturbed beam was extracted from the

measurement data acquired in the fluorescence excitation experiment which will be
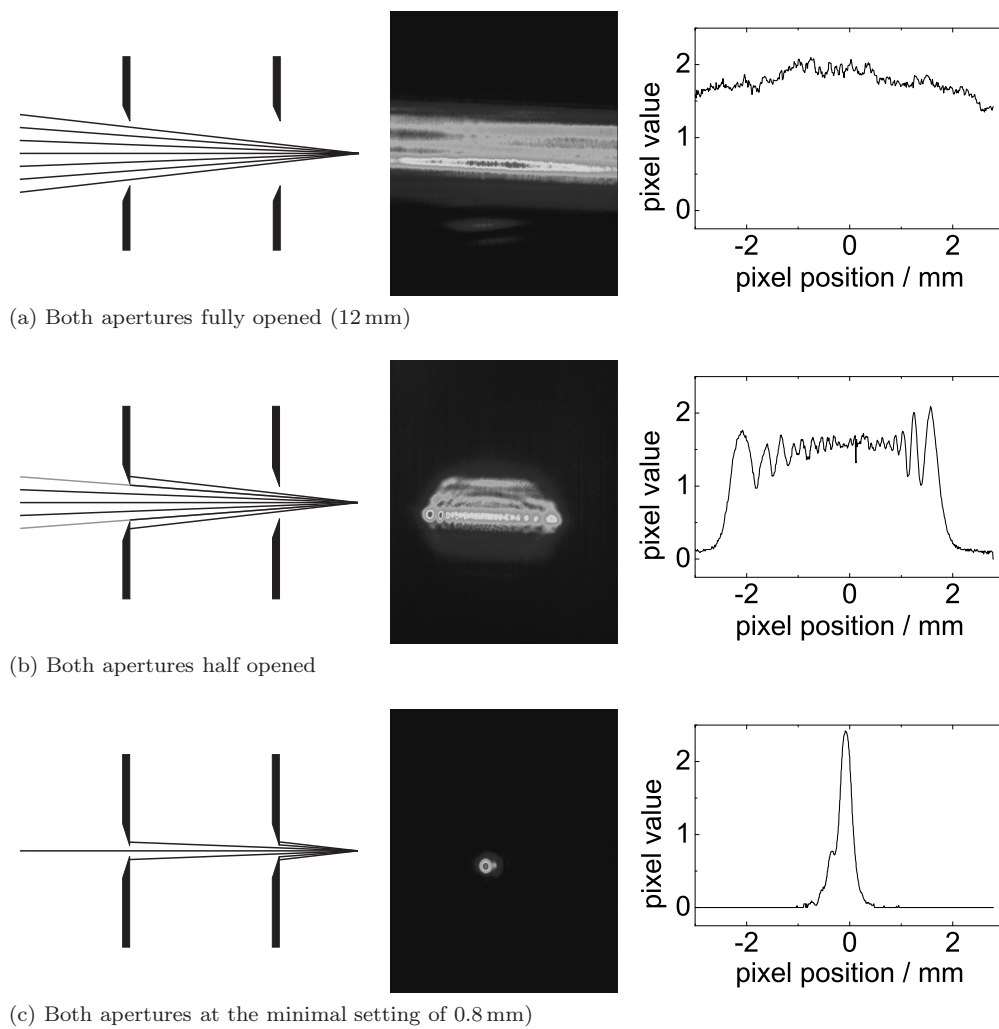described in 5.3.

(a) Both apertures fully opened (12 mm)

(b) Both apertures half opened

(c) Both apertures at the minimal setting of 0.8 mm)

Figure 5.11: Intensity distribution on the CCD sensor for various aperture sizes.

(a) x-axis intensity profile

(b) y-axis intensity profile

(c) Spectrum of an aperture limited beam

(d) Spectrum of an undisturbed beam
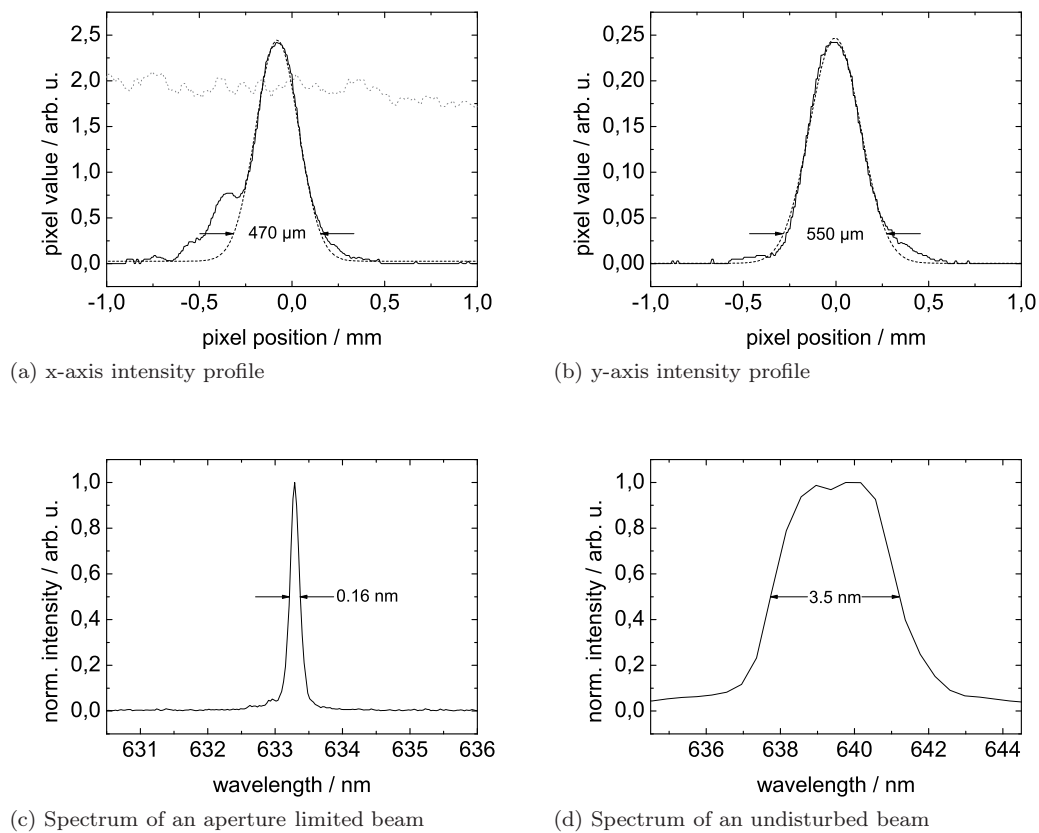
Figure 5.12: Intensity profiles along the x-axis and the y-axis of the output beam after blocking unwanted lateral modes with apertures. A Gauss function curve was fitted to the profiles. The $1/e^2$ widths of the Gauss curves are annotated in the plot. The removal of interfering laser modes with the apertures increases the intensity along the beam path by 20 % compared to the profile of a beam with fully opened apertures (gray dashes in (a)). (c) Filtering the lateral modes with apertures drastically narrows the spectral distribution of the DFB laser beam compared to an undisturbed beam (d).

5.2   Organic laser based spectrophotometer

The previous findings were applied for assembling the first high resolution transmission spectrophotometer which uses a tunable organic laser as light source. Figure 5.13 shows a schematic representation of the optical setup employed for this. The laser source part of the spectrophotometer comprises the same DFB laser sample and pump source that were already used for the experiments described in the sections 5.1.4 and 5.1.5 of the present chapter. A linear positioning stage moves the sample relatively to the pump beam to tune the organic laser.

To ensure reproducible results the stage itself is equipped with a *Newport 850G* actuator. The stage is controlled with a *Newport ESP 300* motion controller. This combination of positioning hardware yields an accuracy of better than one micron. The organic laser emission is directed through two 0.8 mm apertures for lateral mode reduction and alignment. A polarizer (P) selects the TE mode and a 385 nm long pass filter (LP) suppresses residual light from the UV pump laser.
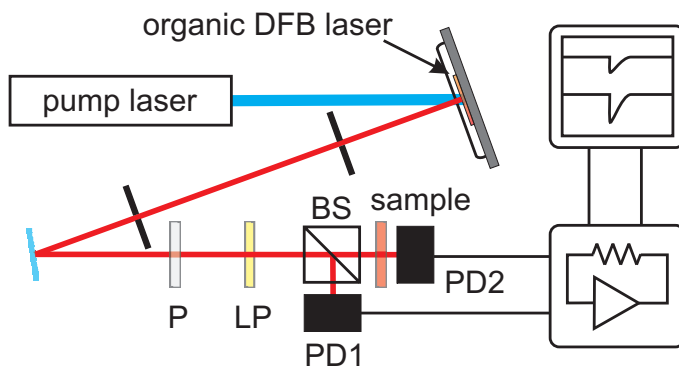

Figure 5.13: Schematic representation of the optical setup and the detection scheme of the organic laser based transmission spectrophotometer. The organic laser is optically pumped with a pulsed UV laser. Tuning of the emission wavelength is achieved by moving the sample relatively to the pump laser beam. The organic laser emission is directed through a polarizer (P) and a 385 nm long pass filter (LP). Subsequently the beam is split into a probe and a reference beam using a polarization-insensitive 50:50 beam splitter (BS). Probe and reference beam are detected using two silicon photodiodes (PD). The photocurrents of both diodes were measured with an oscilloscope using transimpedance amplifiers. (T. Woggon et al. [200])

The transmission spectrophotometer was calibrated by measuring the pump position dependent emission wavelength with a 300 mm imaging spectrograph with a resolution of 0.1 nm (*Acton Research SpectraPro-300i*, 1200 grooves per mm grating). Figure 5.14 shows the resulting relation for a displacement step size of 2 μm. The discrete steps of approximately 0.03 nm observable in the data curve originate in the limited resolution of the spectrograph and mark transitions between two pixels of its CCD detector (*Princeton Instruments PI-Max 512*). A second order polynomial function fit was applied to the data to serve as the calibration curve for the following measurements.

The photometer part employs a polarization-insensitive 50:50 beam splitter (BS, *Thorlabs CM1-BS1*) to divide the laser beam into a probe and a reference beam.
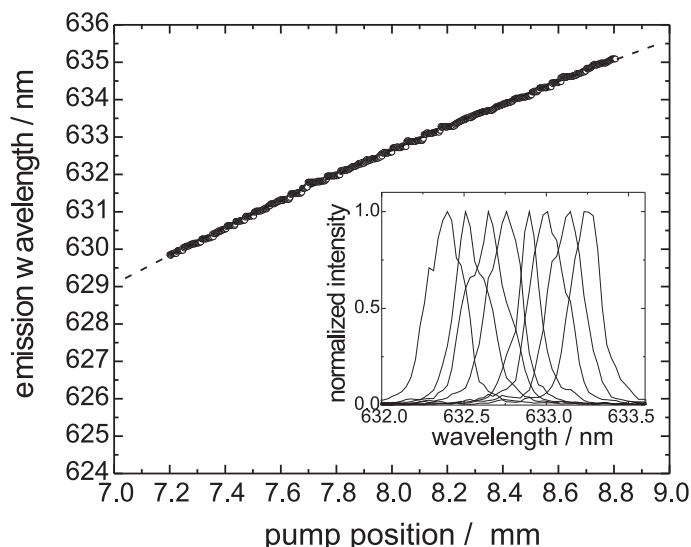
Figure 5.14: Emission wavelength calibration in relation to the excitation spot position for the organic laser. The inset shows a selection of the respective laser spectra. (T. Woggon et al. [200])

Both beams are detected with single pulse resolution using two silicon photodiodes (PD) which are connected to two transimpedance amplifiers with a transfer ratio of $1\,\mathrm{V\,nA^{-1}}$. The amplified photodiode signal is read out with a 200 MHz oscilloscope (*Tektronix TDS 2024*). The pump position and the photodiode readings are recorded by a computer.

5.2.1 Measurement of a narrow band optical laser line filter

To quantify the performance of this system, it was used to measure the transmission properties of a $(632.8 \pm 0.2)\,\mathrm{nm}$ laser line filter with a FWHM of $(1.0 \pm 0.2)\,\mathrm{nm}$ (*Thorlabs FL632.8-1*). The spectral data was obtained with a displacement step size of $5\,\mathrm{\mu m}$. This translates to a wavelength interval of approximately $0.016\,\mathrm{nm}$. The photodiode signals were averaged over 64 pump pulses. The pump frequency was set to 200 Hz. A zero signal and a baseline curve were measured to account for residual stray light and the position dependent inhomogeneous output power of the laser. Applying these corrections to the measured data delivers the curve that is plotted as a solid line in figure 5.15. The curve maximum is located at 632.7 nm with a transmission value of 0.71. The FWHM can be determined to a value of 1.16 nm.

To evaluate the quality of this result the filter transmission spectrum was additionally measured using a *Varian Cary 5 VIS* spectrophotometer to obtain reference data for comparison. The spectrophotometer data acquisition interval was set to the smallest available value of 0.005 nm for optimal results. The spectral bandwidth was set to the fixed value of 0.025 nm. To minimize the incident angle the reduced slit height setting was also applied. Together with an integration time of 0.500 s the combination of these settings assured optimal results [201]. Figure 5.15 plots the transmission curve which has been measured with these settings as a dashed line.
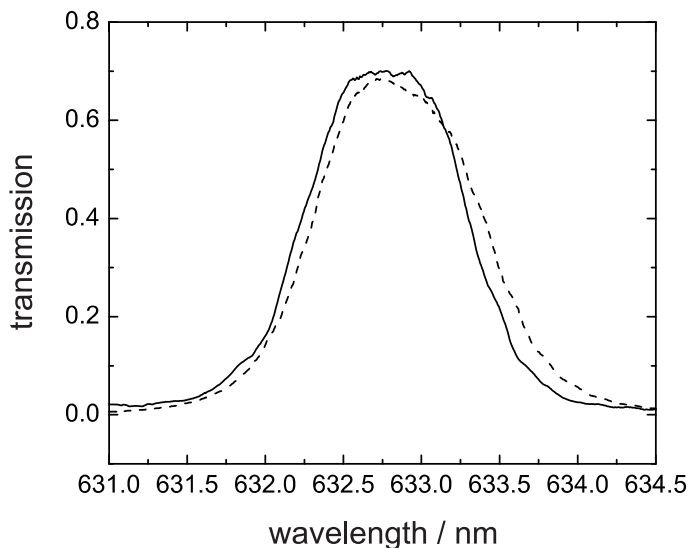
Figure 5.15: Comparison of the filter transmission curve measured using the tunable organic semiconductor laser (solid) and a *Varian Cary 5* photospectrometer (dashed). Both measurements were baseline and zero corrected. (T. Woggon et al. [200])

It shows a peak wavelength of 632.74 nm and a FWHM of 1.2 nm. Considering the measuring accuracy both measurements are evidently in a good agreement.

The organic laser setup measures the transmission value by integrating the photodiode signals over a single pump pulse. This allows integration times well below a millisecond per datapoint due to the photodiode and read-out electronics. With the 5 ns long pump laser pulses integration times of several nanoseconds are theoretically possible with faster detection electronics. The in this thesis applied averaging over 64 single measurements yields an acquisition time of 0.32 s per datapoint. This is already much faster than the 0.500 s for acquiring a datapoint with the *Varian Cary 5 VIS* spectrophotometer.

5.2.2 Absorbance measurements

For absorbance measurements not only a high spectral resolution is desired but also a high dynamic range, especially when monitoring kinetics of chemical reactions or bacteria growth. To estimate if the organic laser based spectrophotometer provides enough sensitivity for such applications a series of absorbance measurements of different non-reflecting neutral density optical filters were conducted. The measurements were done with a fixed wavelength setting of 632 nm. As shown in figure 5.16 even with the standard Si photodiode detectors optical density (OD) values up to 5 can be measured with a maximum error range of OD ±0.02 below and ±0.2 above OD values of 4.

The sensitivity of the employed system setup is mainly limited by the 50:50 beam splitter cube. The equal split of the organic laser output causes the reference diode to saturate at high pump pulse energies. Experiments with a variable beam splitter showed better results, however, due to the high pump pulse energies a significant
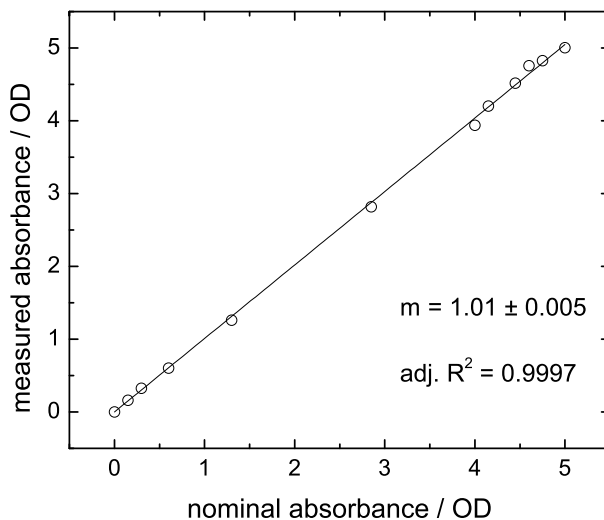
Figure 5.16: Relation between the nominal absorbance of non-reflecting neutral density optical filters to the value measured using the organic semiconductor laser based transmission spectrometer. (T. Woggon et al. [200])

level of stray light interfered with the probe beam. This indicates, that with a proper stray light suppression, a variable beam splitter and optimized detectors, e.g. photomultiplier tubes, the organic laser can be used for spectrally resolved linear absorbance measurements in optically highly dense media.

5.3 Fluorescence excitation of dyes with a tunable organic laser

The fluorescence excitation of fluorophores is regarded to be an essential optical read-out method in biological confocal microscopy as it can be more sensitive and specific than absorbance or reflectance [202]. In life science applications, fluorescence is typically used as a non-destructive way of tracking or analyzing biological molecules in cells. Popular applications are for example flow cytometry and cell sorting [203]. Whereas some proteins or small molecules in cells exhibit intrinsic fluorescence, in general, cells have to be labeled by attaching an extrinsic fluorophore to them. These fluorophores are preferably excited in experiments using a laser light source as these combine high optical energy levels with a spectrally narrow emission. The importance of the latter can be explicated with the help of the absorption and emission spectral data of the popular dye Cy5 [204] which is shown in figure 5.17.

(a)   (b)
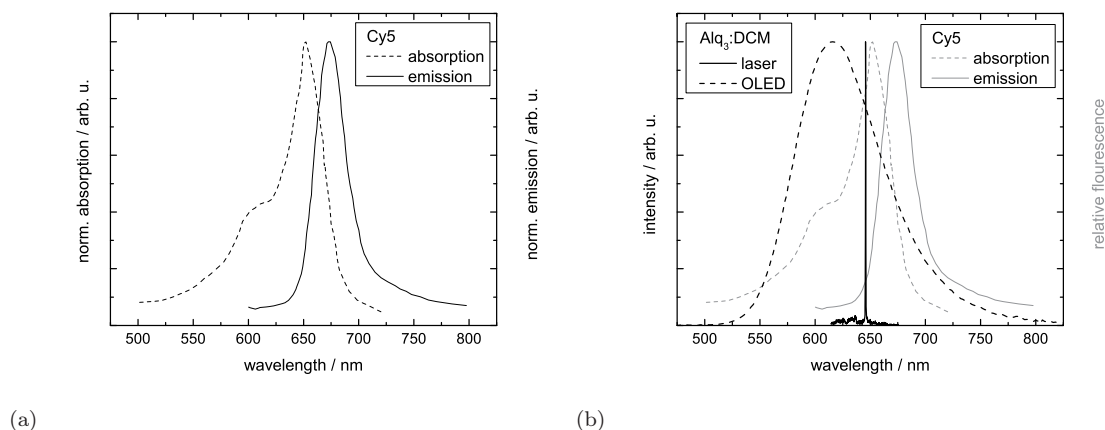
Figure 5.17: (a) absorption and emission spectra of the dye Cy5 [204] used for labeling nucleic acids or protein molecules. (b) The use of a spectrally narrow laser source over a spectrally broad emitting OLED as excitation source enables significantly increased signal-to-noise ratios as the dye can be efficiently excited at the absorption maximum without the excitation light spectrally overlapping with the dye emission.

Cy5 exhibits, like many dyes, only a small Stokes shift. Exciting it with a spectrally narrow laser source as it is implied in figure 5.17b allows to significantly increase the signal-to-noise ratio due to the dye being excited efficiently at its absorption maximum without the excitation light spectrally overlapping into the dye emission. Exciting with a spectrally broad emitting light source, e.g. an OLED, would require optical filters to spectrally block the excitation light.

Commercial dyes are therefore designed for excitation wavelengths available by solid-state or gas lasers. But some times even these, often patent protected dyes still have a significant mismatch between their absorption maximum and the laser wavelength they are designed for. For example the dye AlexaFluor® 568 designated to be excited with the 568.2 nm line of krypton ion gas lasers has its absorption

maximum at 578 nm.

Due to their effortless tunability organic lasers could be of great benefit for fluorescence excitation applications as they not only allow to excite a set of multiple dyes with the same laser source but also to perfectly match the absorption maximum of them. Astonishingly, albeit the many publications on low threshold organic lasers, so far not much literature can be found on exciting dyes with them. Thus, for the consistency of this work a basic experiment was set up to demonstrate the applicability of organic lasers for fluorescence excitation experiments. The setup is depicted schematically in figure 5.18a.
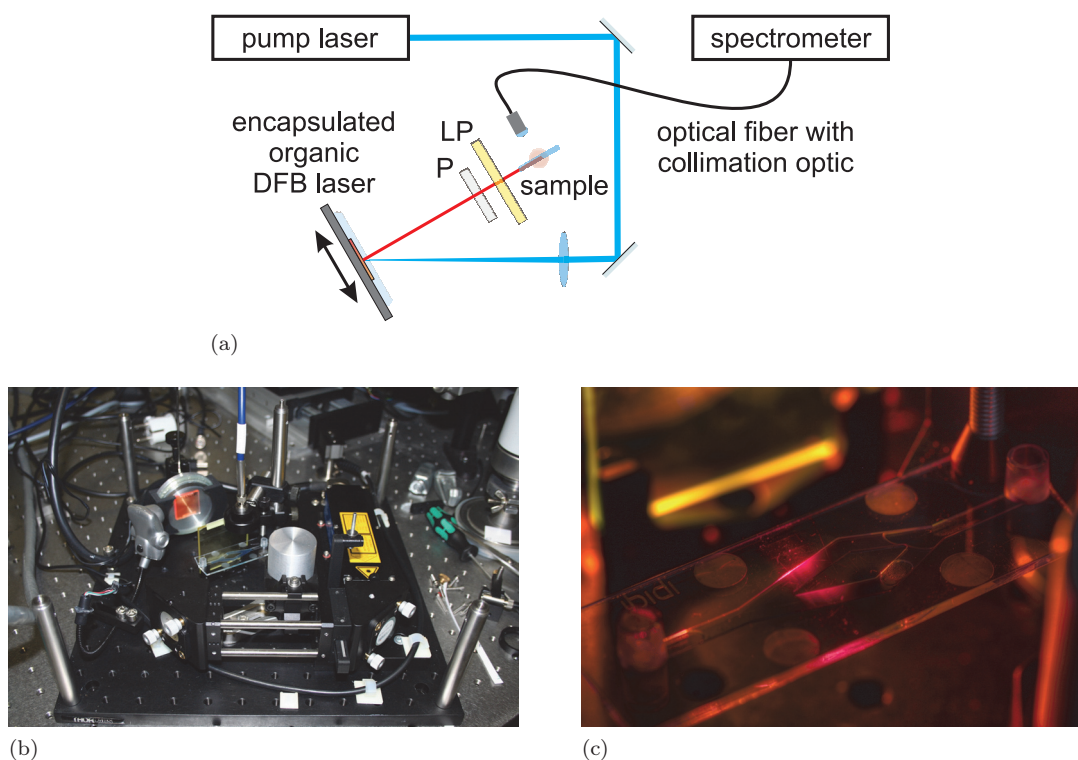
Figure 5.18: (a) Schematic of the experimental setup for fluorescence excitation of dyes with a tunable organic laser. As no apertures were employed, all TE laser modes are used to excite the dye. TM laser modes are blocked by a polarizer (P). (b) Photograph of the experimental setup: Although standard laboratory optical components are used, the system has a very compact footprint. This shows the great potential for a further size reduction using integrated optics. (c) HDR image of a 0.5 % solution of FluoSpheres® dark red (660/680) in H_2O inside a 1 μm microscopy capillary slide excited with the tunable organic laser.

It is based on the optical setup used in chapter 5.2 of this thesis and employed the same encapsulated laser sample. The laser light of the tunable organic laser was coupled into a microchannel slide (*ibidi μ-Slide y-shaped*) through a side facet without any collimation optics. The microchannel was filled with a dye solution composed of 0.5 % FluoSpheres® dark red (660/680) dissolved in water. The fluorescence emission is detected from the top (side scatter channel) using a multi-mode optical fiber with collimation optics. The fiber connects an imaging spectrometer

(*Acton SpectraPro 300i*) with an intensified CCD detector (*Princeton Instruments PI-max 512*).

As this setup is clearly not optimized for fluorescence detection all accessible spectral modes of the organic laser where used by omitting the filter apertures. This results in a higher usable excitation energy. The excitation laser line broadened to a FWHM of 3.5 nm which can still be considered as a narrow excitation.

Figure 5.19a depicts a series of fluorescence spectra measured with this setup. Each data set was recorded with a different excitation wavelength of the organic laser. The above claimed benefit of being able to tune the organic laser towards the absorption maximum of the FluoSpheres® displays itself clearly with the relative increase of the PL signal.
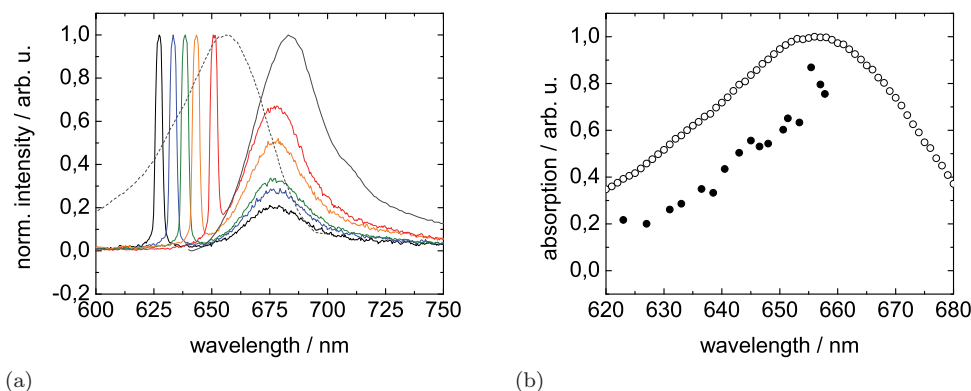

(a)   (b)

Figure 5.19: (a) Fluorescence spectra of a 0.5 % solution of FluoSpheres® dark red (660/680) in H_2O at different excitation laser wavelengths of a tunable organic laser. The gray curves represent the absorption (dashed) and emission (solid) spectral data published by *Invitrogen GmbH*. All spectra have been normalized to the same intensity for comparison purposes. (b) The plot of the ratio of the laser line maximum and the PL maximum of the dye emission (filled circles) agrees qualitatively well with the absorption curve provided by *Invitrogen GmbH* (empty circles).

5.4 Conclusion

The work described in the present chapter was dedicated to quantifying the claimed huge potential of organic lasers for spectroscopy applications. As this goal required to actually test such lasers in a spectroscopic setup the laboratory stage technology principle of organic lasers was successfully transferred into a durable laser device. This device can not only be operated outside a controlled laboratory environment but also maintains the advantage of the low-cost fabrication capabilities of organic materials.

The development process towards this device included considerations on substrate materials, evaluation of temperature influences, an increase of the lifetime and the design of the peripheral optical setup for optical pumping. The results with PMMA in the studies on different substrate materials showed that polymers that are very well suited for microoptical devices may be incompatible with organic gain materials. The studies also showed that the materials Ormocomp and Topas are excellent alternatives.

The conducted experiments on the influence of changes in the ambient temperature showed that the high CTE of a polymer substrate has no measurable influence on the laser characteristic compared to a glass substrate. The proposed encapsulation approach yields, despite the simplicity, operational lifetimes which can easily compete with current high repetition rate flash lamps.

The proposed approach of spatially limiting the fan-shaped emission beam of 1D DFB lasers with apertures is a low-cost solution to narrow the organic laser emission spatially and spectrally. Obstructing the outer modes reduced also interference losses which resulted in a 20 % intensity gain.

The developed organic laser device was used to build the first organic laser based spectrophotometer. It was applied for measuring the transmission properties of a 1 nm narrow laser line filter and neutral density filters with attenuation values of up to OD 5. The successful excitation of a fluorescent dye with the tunable organic laser emphasizes clearly the applicability of these devices for a key method in bioanalytics.

The illustrated spectroscopy application demonstrations were set-up with standardized laboratory optics and optomechanics. Silicon photodiodes and low cost transimpedance amplifiers were used for detection. The sensitivity and high resolution already possible with these suboptimal setups clearly show the applicability of organic lasers for spectroscopy. Additionally, the small footprint of the fluorescence excitation setup shown in the photograph in figure 5.18b shows evidently that, even without being fully integrated lab-on-chip systems, small and sturdy bench top or even portable laser induced fluorescence based sensing systems for the use in everyday lab life are already possible.

In summary, the work presented in this chapter clearly demonstrates that organic lasers are applicable for sensing applications.

Chapter 6

High speed wavelength switching

Abstract[1]

The tuning of position-dependent distributed feedback lasers by translating them with linear positioning stages is a convenient way to change the pump position while maintaining a coaxial output beam. The wavelength setting speed with this straightforward approach, however, is restricted by the translation speed of the micropositioning system. This causes the worst case wavelength access time to increase linearly with the tuning range. Especially with prices for positioning systems rising nonlinearly with their speed this poses a problem for applications which require a fast switching between emission wavelengths. This chapter describes a novel mechanical tuning method for position-dependent distributed feedback lasers. The method enables high-speed tuning with wavelength access times under 10 ms independently of the tuning bandwidth. The proposed concept has very little hardware requirements while being comparable to a linear tuning approach regarding accuracy in wavelength setting and long term wavelength drift.

---

[1]Parts of this chapter have already been published in:
(a) **T. Woggon**, S. Klinkhammer *et al.*, *Compact spectroscopy system based on tunable organic semiconductor lasers*, Appl. Phys. B. **99**(1), 47–51 (2010)
(b) **T. Woggon**, S. Klinkhammer *et al.*, *Variable laser light source on the basis of variable optical pulse excitation and method for operating same*, European patent application EP2287980A1 (2009).

6.1   Limitations of linear pump position change

The tuning of pump position dependent organic lasers via linear positioning stages faces its limits when different emission wavelengths in a broad available spectrum have to be addressed in a very short time span. The main reason for this problem is the micrometer translation system. It causes the worst case wavelength access time to increase linearly with the tuning range. The tunable DFB laser devices prior used in this work exhibit an emission wavelength gradient of about $30\,\mathrm{nm\,cm^{-1}}$. Covering the whole visible spectrum requires a wavelength span of $400\,\mathrm{nm}$. This implies a translation path length of $14\,\mathrm{cm}$. Even with a high speed translation stage at a speed of $50\,\mathrm{cm\,s^{-1}}$ and an acceleration of 5g [205] it would take $380\,\mathrm{ms}$ to move from end to end. This and the involved extensive hardware costs make this approach impractical for any applications requiring fast and accurate scanning at multiple wavelengths. Scanning the pump laser beam by deflecting it with rotating polygon mirrors or paddle mirrors [206] can be a very fast, a steady coaxial output beam is however not possible. Additionally, the pump spot shape depends strongly on the deflection angle [207].

6.2   A nonlinear approach for high speed mechanical tuning

6.2.1   Eliminating the acceleration problem

A solution to this problem was found in this work by mounting a DFB laser on a rotating disc. While spinning, it is optically excited with time synchronized pulses from a pump laser. The constant spin provides high velocities for the relative pump spot movement while the sample has to be accelerated only once. The benefit of this approach can be eminently shown by simple math. To match a translation speed of $50\,\mathrm{cm\,s^{-1}}$ in a circular motion on a radius of $22\,\mathrm{mm}$, which corresponds to a circumference of $14\,\mathrm{cm}$, a revolution frequency of only $4\,\mathrm{Hz}$ suffices.

The following will exemplify that a rotating disc approach can be realized using low cost components while easily surpassing the performance achievable with linear translation stages regarding wavelength setting time. For the experiments a DFB laser sample was fabricated which exhibits a particularly low emission wavelength gradient of only $10\,\mathrm{nm\,cm^{-1}}$. The active area of the sample spanned an area of $(25 \times 25)\,\mathrm{mm^2}$. It was mounted of axis on a disc as shown in figure 6.2a together with a dummy laser device substrate on the opposite side in order to balance masses. The geometry of the sample holder diminishes the visible area of the DFB laser sample to $(22 \times 22)\,\mathrm{mm^2}$.

For practical reasons and to prevent further unbalances it was omitted to encapsulate the samples. The laser mount was rotated by a brushless DC motor (ESky EK5-0002B). This kind of motor is widely used for propelling model aircrafts and cars and thus available at quite low costs. The motor is driven and controlled with an 8bit RISC microcontroller unit (Atmel ATMEGA8 [208]) based motor driver stage from *HiSystems GmbH*. It comprises a standard triple half-bridge power stage

as schematically depicted in figure 6.1a for driving the motor phases. The rotational speed is controlled by pulse width modulating (PWM) the phase currents. The PWM frequency is generated with the internal timers of the MCU. The motor
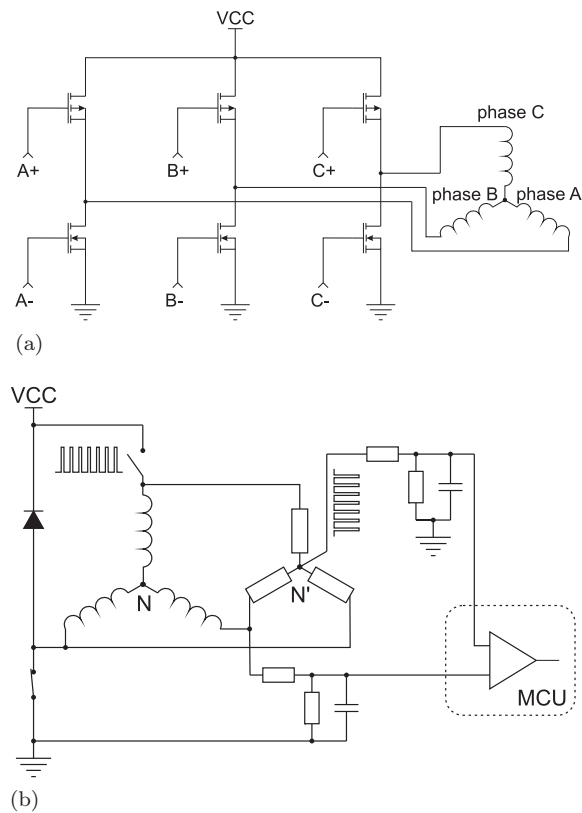

(a)

(b)

Figure 6.1: (a) Schematic of the electronic circuit for the used triple halfbridge powerstage used for driving the brushless DC motor phases. (b) Schematic of the electronic circuit used for the motor phase commutation timing. The zero crossing of the voltage induced by the unpowered phase is detected by comparing it with the potential at the virtual neutral point N'. The comparison is done with the on-chip comparator of a microcontroller unit (MCU) after filtering the signals with a low pass filter.

phases are electronically commutated by using back electromagnetic force (EMF) sensing [209]. The zero crossing of the voltage induced by the unpowered phase is detected by comparing it with the potential at a virtual neutral point using the on-chip analog comparator of the ATMEGA8 as depicted in figure 6.1b. This approach for timing the phase commutation results in a very stable closed loop operation of the system. The motor driver stage's settings are controlled through a serial interface line. This mechanical setup was successfully tested with revolution frequency values up to 220 Hz. These tests have, however, been conducted inside a safety cabinet and not in an optical setup. During the actual optical characterization the revolution frequency was limited in the controller code to a maximum of 100 Hz for safety reasons. For the optical characterization this spinning disc setup was integrated into the setup used in chapter 4.2.3 (p. 60) in front of the vacuum chamber with an extra focusing lens. A schematic of the experimental setup is depicted in figure 6.3. The sample mount was aligned in a way that when operating in free running mode the

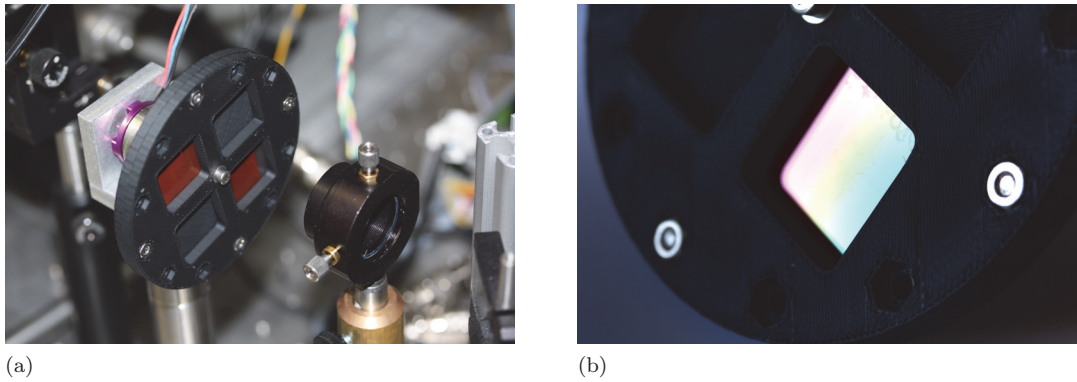(a)   (b)

Figure 6.2: (a) Photograph of the organic laser mounted of axis on a disc together with a dummy laser device substrate on the opposite side in order to balance masses. (b) The geometry of the sample holder diminishes the visible area of the DFB laser sample to $(22 \times 22)\,\mathrm{mm}^2$

pump laser beams excite the DFB laser sample arbitrarily on a circular scan path with a radius of $25\,\mathrm{mm}$.

6.2.2   Time synchronized pump pulse generation

The microcontroller software and the electronic circuit of the motor driver were modified to generate a transistor-transistor logic compatible trigger signal with every revolution of the rotating disc. A variable delay time is needed to address different points on the circular scan path. For this purpose a low-cost electronically delay generator was build based on an 8-bit ATMEGA8 microcontroller and inserted into the trigger line. The delay generator features an LCD display and keypad for direct input but can also be programmed conveniently via a serial interface line. This system enables to excite a discrete position on a circular scan path by simply electronically varying the delay time. Figure 6.4 shows the measured relation between the delay time and the organic laser emission wavelength and the laser spectral linewidth respectively for a rotation frequency value of $75\,\mathrm{Hz}$.

The jitter of the pump laser to the external trigger is less than $0.5\,\mathrm{ns}$ and can be neglected regarding the $2\,\mathrm{\mu s}$ (2 clock cycles) jitter of the delay generator. This jitter is a fifth of the average delay time step size required to change the wavelength by $0.1\,\mathrm{nm}$. The according stable operation of the system is illustrated in figure 6.5. The data was acquired by measuring the emission wavelength and the spectral linewidth over a period of $70\,\mathrm{min}$ with a fixed delay time. To prevent photodegradation the pump beam was blocked between measurements. The measured variations are well inside the range of the resolution achievable with the employed spectrometer.
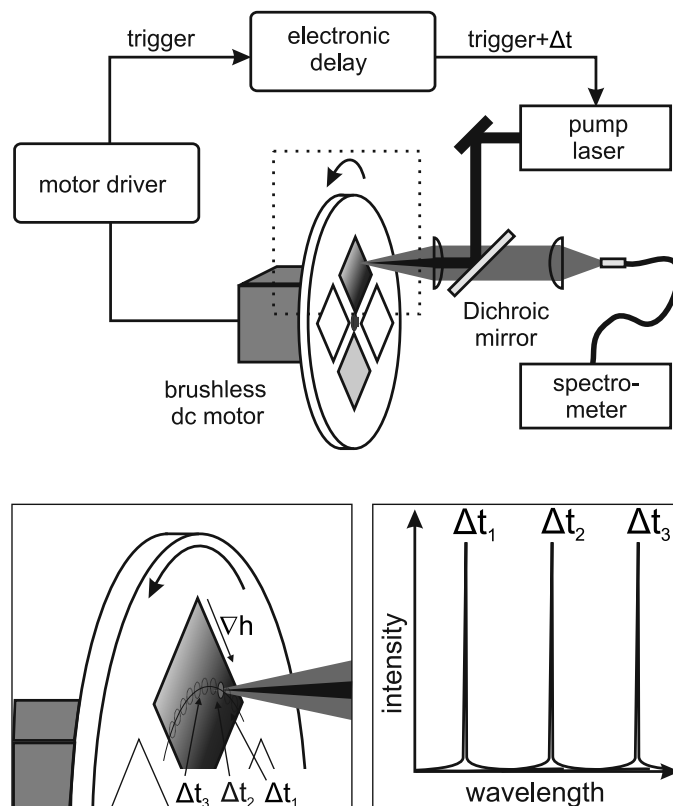
Figure 6.3: Schematic representation of the employed optical setup. With every revolution of the laser disc the motor driver generates a signal. The signal is used to trigger the pump laser after a freely definable delay time. Different delay times cause the pump laser pulse to excite different regions on the DFB laser sample. As these regions are oriented along the thickness gradient $\vec{\nabla}h$ of the active material layer thickness the sample emits at different wavelengths. (T. Woggon et al. [200])
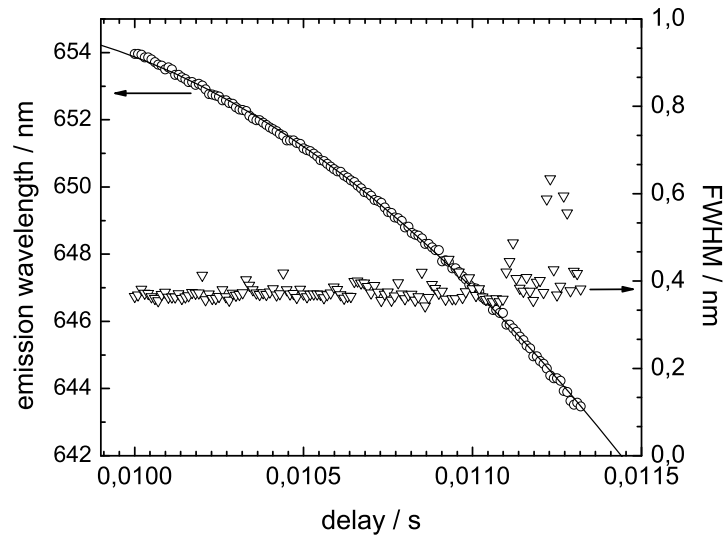
Figure 6.4: Tuning of the laser emission wavelength by increasing the delay time in 10 µs steps. (T. Woggon et al. [200])
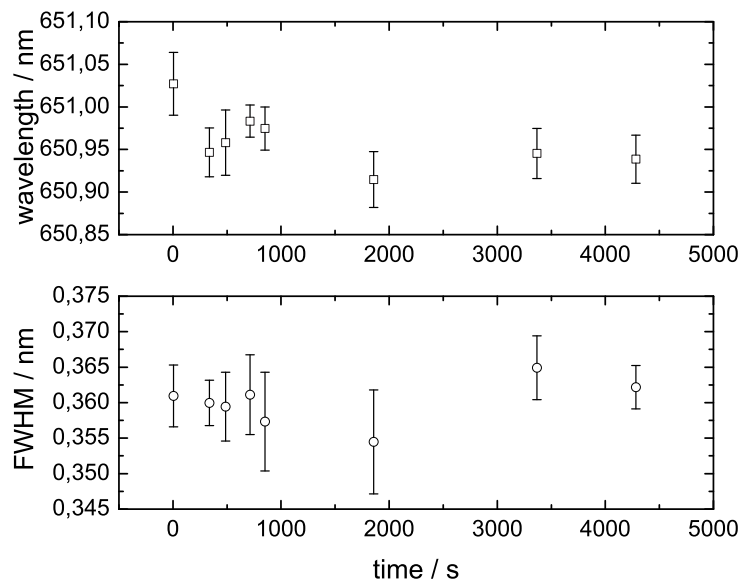
Figure 6.5: Accuracy and long time stability of the electronic setup. The data points and error bars have been determined by binning and averaging over 15 measurements. (T. Woggon et al. [200])

6.3   Multi-wavelength sequence scanning

Beside the fast accessing of a single wavelength the presented tuning approach allows to also rapidly scan a sample with multiple discrete wavelengths in a pre-defined pattern, e.g. to test if it contains specific substances. Instead of running a full high resolution scan and comparing features in the absorption spectrum to reference data one would do only a reduced set of measurements at the wavelengths where the assumed substances exhibit a strong absorbance.

Such a scanning function was implemented as an extension in the microcontroller code of the delay generator by dividing the available delay time parameter window into equal time slots. An 8-bit binary masking of the time slots results in a scanning function providing selectable binary coded sets of multiple laser wavelengths which are emitted in a subsequent order. The corresponding flow-chart for the microcontroller program is depicted in figure 6.6. The trigger signal from the motor driver is captured with a hardware interrupt of the microcontroller. The input capture interrupt service routine (ISR) then starts a timer. When the timer value matches a defined (initial) delay value it induces a timer compare-match ISR. In this ISR the output for triggering the pump laser pulse is switched depending on the state of the current bit in the main program defined bit field. The pointer to the current bit is then incremented and the delay for invoking the next timer compare-match interrupt is set with the value desired between pulses. When the last bit in the bit field is reached, the pointer and the delay variables are reset to their initial values. A selection of such wavelength sets is plotted in figure 6.7. Using the American Standard Code for Information Interchange (ASCII) this scanning method also enables a basic information transfer, admittedly a very slow one.
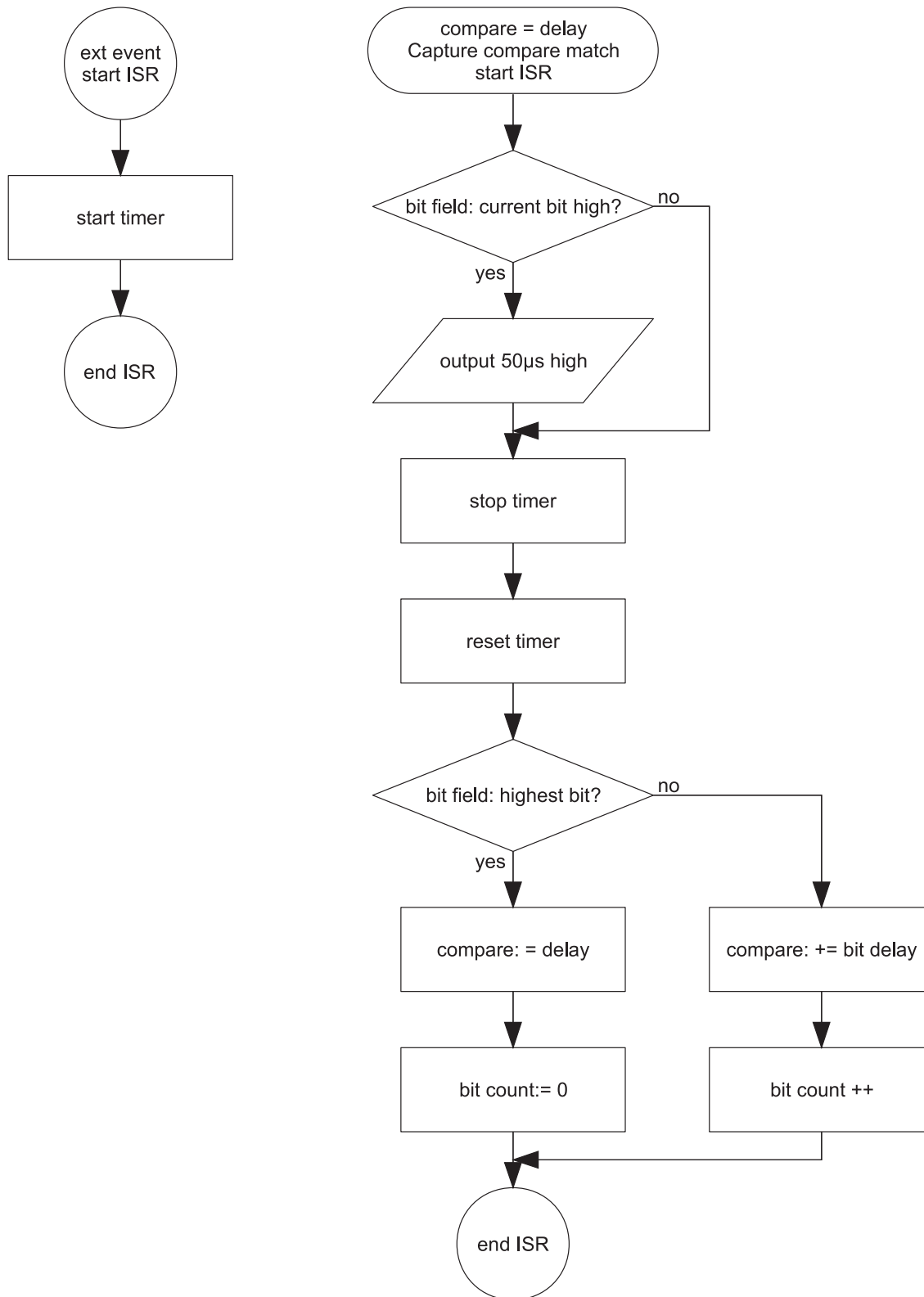
Figure 6.6: Flow-chart of the microcontroller program for generating pulse patterns that can be masked with an 8-bit binary code.
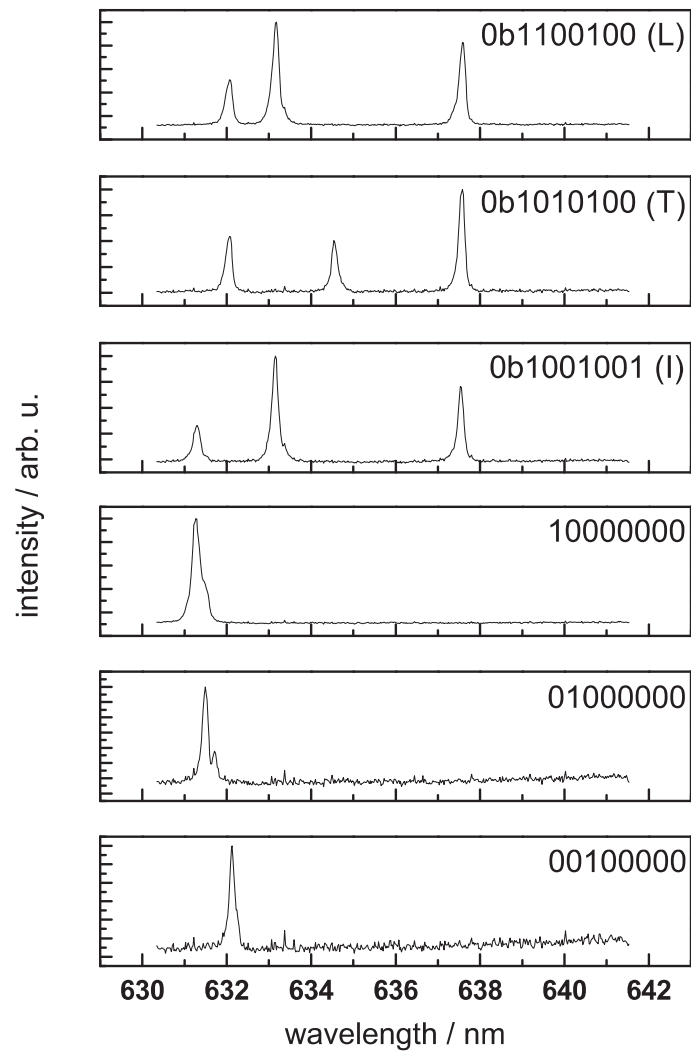
Figure 6.7: Rapid scanning with predefined wavelength sets: Changing the 8-bit binary value results in different wavelength sequences.

6.4   Emission wavelength gradient orientation

The use of equally spaced time slots turned out to be problematic when the circular scan path is not optimally aligned to the waveguide thickness gradient as it is the case here. The vector of the pump spot motion rotates with respect to the gradient $d\lambda/dt$ due to the geometrical alignment of the sample as it is depicted in figure 6.8a. As expected figure 6.9 shows that this misalignment causes higher bits to

(a)   (b)
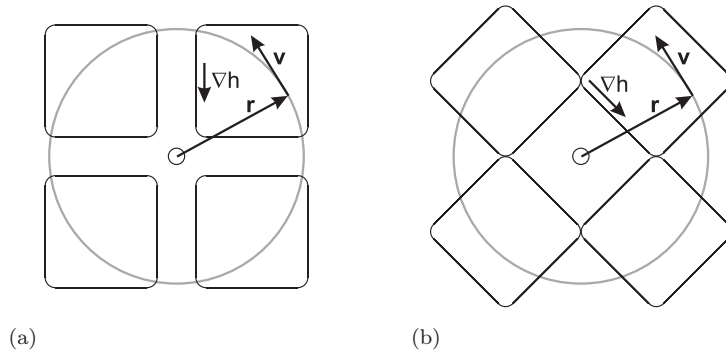
Figure 6.8: Effect of gradient orientation for high-speed wavelength switching with a spin-
ning disc: (a) Schematic representation of the gradient orientation used in the
experiment. The vector of the pump spot motion rotates with respect to the
gradient $d\lambda/dt$ due to the geometrical alignment of the sample. (b) A differ-
ent mounting of the samples would have increased the disk diameter and thus
the proneness to vibrations caused by imbalanced masses.

smear over when going towards shorter pauses between pulses. This issue can be addressed by a different mounting of the samples (see figure 6.8b) or by aligning the gradient diagonally on the square laser sample. The latter is to be preferred as it minimizes the disk diameter and thus yields less proneness to vibrations caused by imbalanced masses.
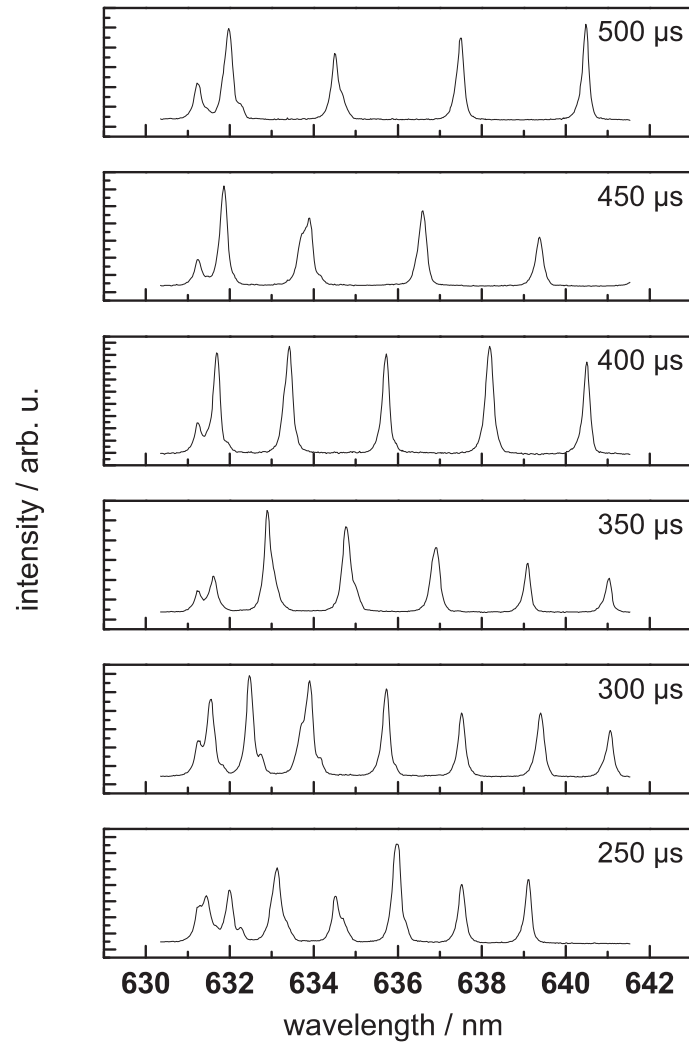
Figure 6.9: Compensation of the annular scan path: Due to the not optimal aligned substrate a constant interval between the time slots leads to smearing of the higher bits. A solution to this problem would be a variable, constantly increasing interval.

6.5   Conclusion

The nonlinear method for tuning a position dependent organic laser elucidated in the preceding sections allows emission wavelength changes in less than 10 ms independently of the tuning bandwidth. This was achieved by mounting the laser device on a constantly spinning disk and exciting it with time-synchronized pump pulses that can be electronically delayed.

It was demonstrated, that the proposed tuning method can be sophistically realized with a low cost hardware solution. The employed closed loop control of the samples rotation and the resetting of the delay counter with each revolution result in a very stable wavelength setting. The flexibility of the electronic delay allows to rapidly measure "fingerprints" of known substances with predefined sets of probe wavelengths. The employed tuning approach can be improved further by employing multiple identical sectors on the rotating disk. The wavelength access time decreases linearly with the number of such sectors.

Chapter 7

The tunable organic laser – a technology with market potential?

Abstract

Some of the employed solutions for tunable light sources are as old as the application of light for sensing purposes. They are commercially available, application proven and were steadily optimized since they entered the market. The most prominent features of organic lasers, however, are often still either in the potential advantages *category or have been demonstrated only as singular results in a loose context. Additionally, the organic laser community, like any other research community, sometimes tends to blind optimism in their judgment. Giving an appraisal of the potential of organic lasers for sensing applications is thus worthless without comparing their overall performance with light sources which are currently employed in this area. This chapter gives a review on currently employed solutions for tunable narrow-bandwidth light sources for spectroscopic applications. For the sake of simplicity, the following considers only solutions which emit visible, continuously tunable light in a spectral domain of at least 10 nm and a spectral bandwidth of no more than 4 nm. Putting them in a direct competition with the laboratory stage organic laser systems presented in the previous chapters would be inappropriate. In order to make them comparable, a prototype bench top tunable organic laser system was designed and set up.*

7.1 Light sources for spectroscopic applications

7.1.1 Lamp based monochromator light sources

Already Sir Isaac Newton[1] studied the separation of light into its spectral components with diffractive and dispersive elements [210]. Today, monochromator systems with incandescent and gas discharge lamp illuminated diffraction gratings form the backbone of optical spectroscopy with 10th of thousands installed systems worldwide. The main reasons for this are, compared with competing technologies, low costs and convenient operation of these systems.

The main drawback, however, is the low conversion efficiency due to their basic working principle: generating spectrally narrow light by filtering a small part out of the broadband emission spectrum of a light source. Additionally, the high divergence of the light source requires complex optical systems with large apertures in order to minimize the systems throughput losses (see 2.1.3 p. 13). The resulting low conversion efficiency is clarified with an exemplary calculation of the output of a typical commercial 1/8 m monochromator light source. It was taken from the Newport product training literature *Oriel product training: Spectral Irradiance* [211]. Reducing the initial broadband output of a 50 W quartz-tungsten halogen lamp (QTH)) to a bandwidth of 10 nm using a monochromator, leaves a optical output power of only about 0.5 mW with a beam divergence of 13.6°. Reducing the bandwidth under the postulated 4 nm would mean to at least halve the entrance slit area and thus to diminish the efficiency further.

Of course, the output power can always be increased by means of using incandescent lamps with higher wattage and longer focal length, however, this also results in bulkier systems and shorter lamp lifetime[2]. Using mercury short arc lamps can yields a much higher efficiency compared to QTH lamps albeit the lower spectral energy density in the visible spectral region (see Fig. 7.1). This originates in the lack of a filament in these lamps which allows the use of a back reflector to collect more light. The drawback of mercury short arc lamps are the strong lines in the UV and the high sensitivity of the bulb to airflow around it. Monochromator system output powers in the µW-region seem sufficient, especially with the single photon sensitivity of modern photodetectors. The high divergence, however, requires quite complex optical setups for spectroscopic applications as it can be seen in the line drawing in Fig. 7.2 showing the optical system of an industry standard photospectrometer (Varian Cary). Another downside of the low output powers of continuous-wave incandescent lamps based systems are the slow obtainable data acquisition rates. With a low irradiance power, acceptable signal-to-noise ratios require long integration times. This means for chopper wheel based systems typically that only data collection rates within (10 to 30) Hz can be obtained. This can be compensated using either high power flash lamps at the cost of drastically decreased lamp life or highly sensitive detectors. Both approaches, however, directly imply increased cost and system complexity.

---

[1] ⋆January 4th, 1643, †March 31th, 1727
[2] the 50 W QTH lamp used for example has a specified lamp life of 50 hours
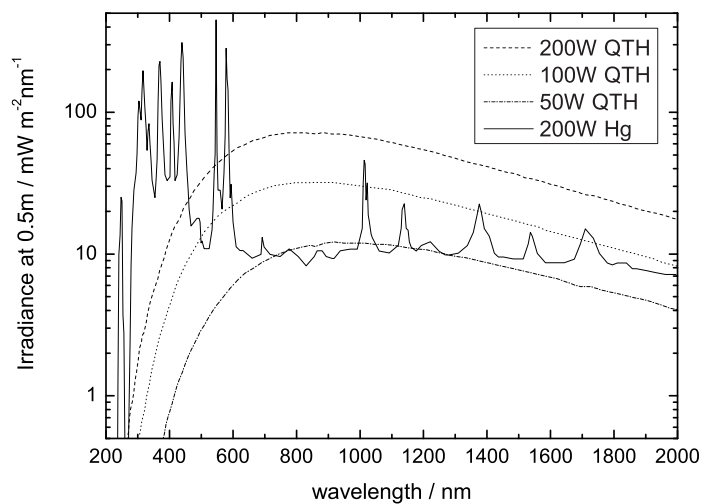
Figure 7.1: Spectral irradiance data for quartz tungsten halogen incandescent lamp and a DC short arc mercury lamp (data from LOT Oriel [211]).
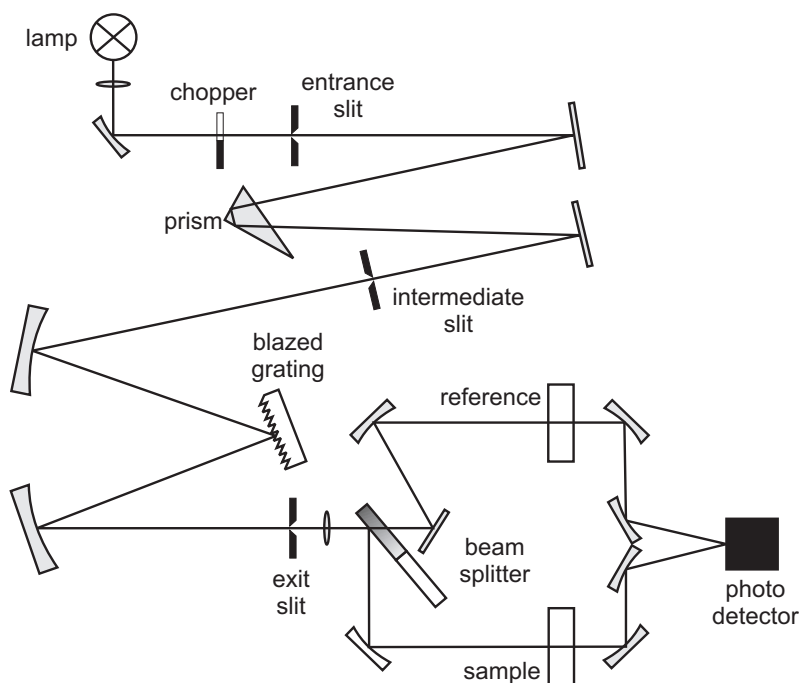

Figure 7.2: Scheme of the optical path of a commercial photospectrometer. The highly divergent emission and the low spectral output power density requires a complex optical system with parabolic mirrors. Stable operation also demands a steady measurement of a reference light beam.

7.1.2   Liquid dye lasers

Sorokin and Lankard [212] and Schäfer et. al [213] presented the first liquid dye lasers in 1966. Laser action from dyes has also been demonstrated independently by Spaet and Bordfield, and by Stepanov et. al [214, 215]. At that time, hundreds of laser active materials were already known. The dye laser, however, was the first solution meeting the experimenters need for an easily wavelength tunable laser source. In 1967 Soffer and McFarland demonstrated a continuously tunable dye solution laser with a bandwidth of 0.06 nm. It employed an optical grating instead of one of the dielectric cavity mirrors [216] and thus fulfilled "an experimenter's pipe dream that was as old as the laser itself: To have a laser that is easily tunable over a wide range of frequencies or wavelengths" (Schäfer, 1977 [51]). This stated the beginning of an era with steady reports of improved dye laser designs. In 1972, Hänsch was able to reduce the line width to less than 0.4 pm by expanding the intra-cavity beam and using a Littrow configuration for the reflection grating [217]. Littman and Metcalf presented a more compact configuration with two gratings instead of a beam expander in 1978 [218]. Their laser achieved a peak output power of 10 kW with a spectral bandwidth of 1.5 pm at 600 nm. Starting from then the dye laser had an extraordinary impact in scientific research. This expresses itself in over 16 000 published papers on the topic *dye laser* in more then 100 subject areas listed today in the *ISI Web of Knowledge*[SM] database. The most remarkable example in this regard is the field of laser spectroscopy which underwent a radical change due to the ability to generate tunable narrow line width coherent emission in the visible spectral region.
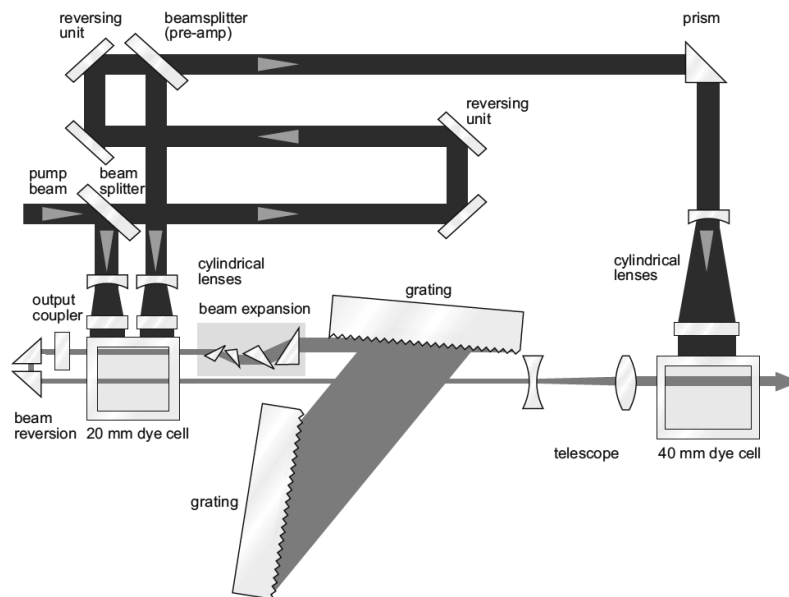

Figure 7.3: Schematic of the optical setup of the PrecisionScan pulsed dye laser from Sirah Laser und Plasmatechnik (Source: Sirah Laser und Plasmatechnik GmbH)

Today, albeit their former successes, dye lasers are rarely used anymore and have been replaced with alternative technologies wherever possible. Although these alternatives often fail to match the performance of dye lasers, the reasons for using

them are the typically lower costs and easier handling compared to dye lasers.

The broad spectral gain of the laser dye requires a complex optical system for the resonator to ensure a narrow bandwidth and a good quality beam. In order to obtain high output power levels, the dye has to be constantly replenished using a circulatory pump system to prevent the accumulation of excited triplet states. As pressure variations have to be avoided, this liquid handling system requires sophisticated mechanics.

With typical dye cell lengths of (10 to 40) mm the temperature of the dye solution becomes the most critical factor for the wavelength stability due to the resulting change in the optical path. The physical properties of the dye solution are hereby mostly defined by the solvent [219] as the laser dye itself is typically dissolved with concentrations between $(10^{-2}$ to $10^{-5})\,\mathrm{mol\,dm^{-3}}$. As listed in table 7.1 the thermo-optical coefficients $\mathrm{d}\,n/\,\mathrm{d}\,T$ of common dye solvents are in the order of $10^{-4}\,\mathrm{K^{-1}}$ [220, 221]. The dye solution temperature thus significantly influences the optical thickness of the dye cell. Hence, highly stable systems control the bulk dye temperature to $10^{-3}\,^\circ\mathrm{C}$ at $16\,^\circ\mathrm{C}$ [222]. The biggest disadvantage of liquid dye laser systems is,

Solvent	Chlorobenzene	DMFM	DMSO	Glycerin	Isobutanol
$(\mathrm{d}\,n/\,\mathrm{d}\,T)10^{-5}\,\mathrm{K^{-1}}$	57.5 ± 0.5	47.5 ± 1.4	44.6 ± 2.0	25.3 ± 1.5	44.3 ± 0.5

Table 7.1: Thermal coefficients of refractive indexes of dye solvents at $632.8\,\mathrm{nm}$ [221]

however, the complicated handling. As a laser dye is usually more durable in the dried state it has to be dissolved prior to use. The resulting laser dye solution usually contains only very small quantities of dye. As stated above the physical properties and thus the potential hazards are defined mainly by the dye solvent. The commonly used solvents are highly inflammable and toxic. Some can also penetrate the skin carrying the also often toxic dyes with them. As the optimal solvent differs from dye to dye, a large variety of solvents is needed which have to be kept in stock. For a wavelength change which requires a different dye solution the dye cell and the circulator have to be flushed with clean solvent.

These mandatory procedures for operating a liquid dye laser hence require extensive additional laboratory infrastructure and specially trained personnel thus driving up operational costs. This, combined all aforementioned restrictions, inspired a huge activity in the field of solid state lasers which led to alternative tunable laser sources such as optical parametric oscillators or super continuum sources.

7.1.3 Optical parametric oscillators

To circumvent the restriction of the laser wavelength to the energy band structure of laser materials, Kroll (in 1962) and Akhmanov and Khokhlov (in 1963) proposed the use of nonlinear optical frequency conversion processes in an optical parametric oscillator (OPO) [223, 224]. The first experimental demonstration of such a device was given by Giordmaine in 1965 [225].

These early tunable OPOs were difficult to operate and often prone to damage, largely because of the operation threshold approaching the damage threshold of nonlinear materials like lithium niobate ($LiNbO_3$).

In the late 1980s interest in OPOs was revived with Fan et. al demonstrating the first wavelength tunable OPO based on the highly nonlinear (NL) crystal beta-barium borate [226] (β-BaB$_2$O$_4$ or BBO) [227]. This aroused a huge interest in developing new, highly efficient NL optical media. Besides conventional grown BBO and potassium titanyl phosphate (KTP) crystals the most recent impetus came from quasi-phasematched NL media like periodically poled lithium niobate (PPLN) [228]. This progress together with the availability of high power Nd:YAG solid state pump lasers led to a wide use of OPOs in narrowband spectroscopy [229].

An OPO system uses a nonlinear optical scattering process [230] in which an input light wave propagating in a nonlinear optical crystal is converted into two output light waves with each having a lower frequency. With OPO systems the obtainable efficiency of this photon conversion process can be several tens of percents. The downside are the high threshold pump power levels between tens of milliwatts to several watts needed for the nonlinear processes. The threshold depends on resonator losses, the frequencies of the interacting light, the power density inside the NL material, and its degree of nonlinearity. An OPO system can be operated in a continuous-wave or pulsed emission mode. With the suited pump source, however, due to the high threshold energies and the short crystal required for high conversion efficiencies [231], most OPO systems operate in a pulsed regime with actively cooled crystals in order to prevent thermally induced damage of the NL media. Also, due to the nature of optical parametric processes, OPOs are very sensitive to noise generated by the pump source.

OPO systems allow to tune the output frequencies by either changing the pump frequency or the phase matching properties of the NL crystal by altering its temperature or orientation or quasi-phase matching period. Additional fine-tuning can be done by varying the optical path length of the resonator [231]. For a wide tuning range and narrow-linewidth emission typically more than one of these parameters have to be altered. Besides the elaborated crystal growth efforts this also requires active control of the optical elements to ensure stable operation. Accordingly, this increases the OPO system complexity and cost.

7.1.4 White light super continuum fiber lasers

The term *white laser light* is usually used for radiation with a broad, continuous spectrum comparable to the spectrum emitted by an incandescent light bulb. In contrast to light bulb radiation, however, the white laser light features a high degree of spatial coherence i.e. a very low divergence angle. Super continuum (SC) generation describes a process where laser light is converted to light with a very broad spectral bandwidth, usually accomplished by sending short laser pulses through a highly nonlinear device, e.g. an optical fiber.

Although there were some earlier results reported on spectral broadening in liquids as well as solids, the first widely accredited report of *super continuum generation* was given by Alfano and Shapiro in 1970 [232]. Their *white light* source yielded a spectral coverage from (400 to 700) nm in a borosilicate glass sample pumped by gigawatt picosecond pulses from a frequency doubled Nd:glass laser.

Whereas early reports on SC generation in optical fibers required pump power

values of several 10th of kW [233–235] the thresholds were soon decreased by an order of magnitude by pumping in the anomalous dispersion region [236] and employing picosecond pump pulses [237]. The publication of a comprehensive model for the formation of SCs in the anomalous dispersion region of fibers using femtosecond pulses by Gross et. al in 1992 [238] and the boom of the telecommunications industry triggered further improvements leading to the first applications of SCs [239, 240] and the first fiber laser pumped SC in a fiber [241].

The breakthrough for SC source was initiated with the invention of photonic crystal fibers (PCF) in 1996 by Knight et. al [242]. These fibers form an excellent medium for SC generation as they offer a high nonlinearity and a customizable zero dispersion wavelength. The physical processes behind SC generation in fibers can be very different, depending on various parameters. As an in-depth discussion of these processes would go beyond the focus of this chapter, the reader is kindly referred to the comprehensive review article by Dudley et al. [243].

When femtosecond pulses are used, the underlying processes of the SC generation differ from each other whether the pumping is done at normal and anomalous dispersion wavelengths. In the normal group velocity regime the spectral broadening is mainly due to self phase modulation. In the anomalous dispersion regime the SC characteristics are a result of a combination of self-phase modulation and dispersion which causes soliton fission.

Although SC generation in fibers has been shown for picosecond [244], nanosecond [245] and even continuous wave schemes [246], most modern sources use femtosecond pump pulses as their kW peak power permits efficient SC generation with only centimeter lengths of fiber. The pump wavelengths are also mainly in the anomalous dispersion region as this yields a much more efficient SC generation. The downside of pumping in the anomalous region is a high sensitivity of the process to the slightest fluctuations (including quantum noise) e.g. in the input pulses causing a strong pulse-to-pulse variation of the properties of the spectrally broadened pulses.

Whereas the applicability of SC sources is evident for novel measurement schemes which benefit from broadband, temporally low coherent light, e.g. optical coherence tomography (OCT) [247], they are not yet able to completely replace conventional light sources in spectroscopy due to their limited spectral power density [248] and their considerable noise level.

With *Fianium*, *Leukos*, *NKT Photonics A/S* and *Toptica Photonics AG*, there are currently four manufacturers of commercial SC sources on the market. In the following the two most popular products, the *SuperK™ White Light Laser* from *NKT Photonics A/S* and the *iChrome* from *Toptica Photonics AG* along with their different concepts will be described exemplarily.

SuperK™ White Light Laser

The SuperK™ family of white light lasers has been launched in 2003 by the start-up venture Koheras which in 2009 merged with Crystal Fibre A/S into the new NKT Photonics A/S. The SuperK™ lasers are often referred to as the industrial standard for broadband white light lasers. Indeed, they proved their applicability not only for OCT [247] but also for research applications like fluorescence microscopy [249]

or flow cytometry [250]. The life science focused journal *The Scientist* honored the SuperK sources by listing it in the top 10 innovations in 2008 [251].

The SpektraK™ family is advertised with total output power values ranging from (1 to 4.5) W, however, most of the power density is distributed in the infrared (see Fig. 7.4). For narrow bandwidth operation the SC output can be filtered with an optional offered acusto-optic tunable filter (AOTF) to a FWHM of (0.5 to 2) nm [252]. Although the filter efficiency is greater than 85% this leaves in case of the entry level system SuperK™ Versa [253] a usable output power of only about (85 to 150) µW in a 0.5 nm broad line. With the repetition rate of 80 MHz and 5 ps long pulses this corresponds to pulse energies of merely (1 to 2) pJ. Fluorescence excitation based applications like flow cytometry therefore require costly high power versions and the use of optical bandpass filters with (10 to 30) nm transmission ranges instead of AOTFs to produce a total emission of (10 to 50) mW. This corresponds to pulse energy values of (0.3 to 0.6) nJ [250].
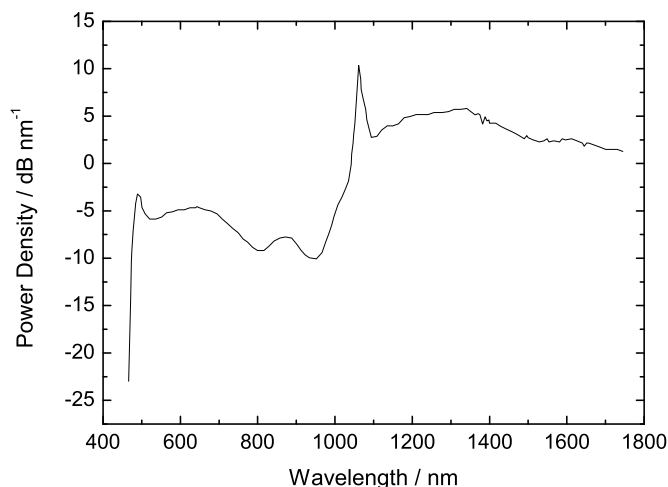
Figure 7.4: Spectral output power density of a SuperK™ white light SC source. Most of the output power is distributed in the infrared. [253]

Toptica Photonics iChrome

Instead of directly generating a white light SC it can also be generated indirectly with an intermediate infrared SC and subsequent nonlinear frequency conversion. The infrared SC can be efficiently created by pumping nonlinear fibers with high power mode locked rare earth element doped fiber lasers and amplifiers which are widely used for telecommunication applications. Such a continuum exhibits a spectral peak in the short wavelength region whose central wavelength can be continuously tuned with an adjustable dispersion control [254]. This tunable peak can be as broad as 100 nm which allows compressing it to a femtosecond pulse and thus efficient frequency doubling in PPLN crystals [255]. Due to a special tunable quasi phasematching design additional sum frequency generation processes are exploited

to further reduce the spectral linewidth along with the second harmonic generation [254].

The Toptica Photonics AG offers this technology as an option for their *Ultra Fast Fiber Lasers* and as a complete *hands-free* OEM system named *iChrome*. According to the product datasheet [256] the *iChrome* from Toptica Photonics AG provides tunable laser emission in the spectral range from 488 nm to 640 nm with an average output power of more than 1.5 mW. The spectral bandwidth (FWHM) is less then 3 nm and the laser operates at a repetition rate of 40 MHz with 3.5 ps short pulses. Although, with 38 pJ, the system provides high pulse energies compared to other SC solutions, the rather complex design (see Fig. 7.5) with the multiple use of nonlinear frequency conversion makes the system very susceptible for noise.
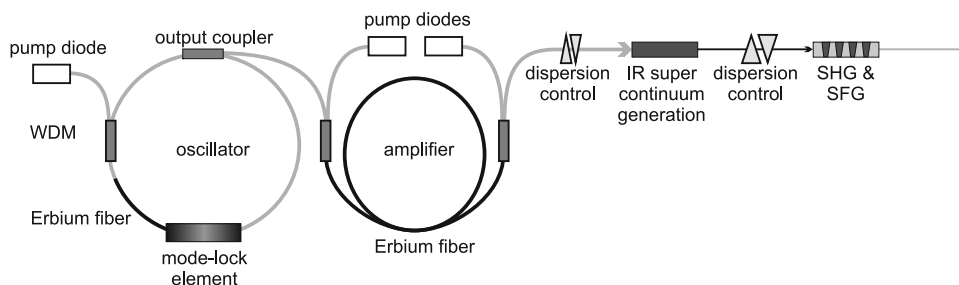
Figure 7.5: Optical system of a tunable laser source based on an intermediate SC. The pump laser pulse from a mode-locked Erbium doped fiber laser is amplified and coupled into a highly nonlinear optical fiber. Prior adaption of the dispersion control parameters allows to continuously tune the central wavelength of a short wavelength peak in the so generated SC. By compressing the pulse this peak is efficiently frequency doubled using a PPLN crystal. With a special quasi-phasematching design the SC peak is spectrally narrowed by sum frequency generation processes.

7.1.5 Tunable external cavity diode laser

External cavity diode laser (ECDL) provide narrowband laser light with unmatched conversion efficiency due to the direct electrical injection. They are composed of a low-cost laser diode combined with a frequency selective optical feedback mechanism. The feedback is typically realized via diffraction gratings in various configurations [257–259]. Using MEMS (micro electromechanical system) processing technology, ECDLs can be realized with extremely small form factors [260]. Diode lifetimes around 10 000 h and only few moving parts permit very durable systems.

These features combined with the ease of turn-key operation made ECDLs quite popular for optical spectroscopy applications [261]. The downsides of ECDLs, however, are certainly the very limited attainable tuning bandwidths in the visible spectrum and the lack of full spectral coverage. Table 7.2 lists commercially available laser diodes with visible emission wavelengths. At first sight, it seems to be a remarkable wavelength range attainable from semiconductor laser diodes. However, there are some gaps in the spectrum with the most evident being in the yellow wavelength region. Until recently this gap was even larger with extending down to the

semiconductor type	spectral coverage	available tuning range [262]
GaN	(395 to 410) nm	(1 to 2) nm
InGaN/GaN	(410 to 524) nm	(2 to 5) nm
InGaP/AlGaInP	(630 to 690) nm	(4 to 10) nm
GaAsP/AlGaAs	(730 to 860) nm	(10 to 18) nm

Table 7.2: Approximate visible wavelength ranges covered by semiconductor laser diodes

blue-green around 490 nm. There have been reports on green laser diodes based on zink-selenide compounds [263–265] but these devices could be operated only a couple of hours at room temperature before they degraded. The epitaxial growth processes for the InGaN material system, which enabled high power green LEDs, lacked the necessary crystal quality for laserdiodes up to 2009 [64, 266, 267]. Thanks to the huge demand for green laser diodes which are powerful enough for laser projection a tremendous optimization on epitaxial growth processes [64] was made since then. Today, InGaN based direct green laser diodes are widely commercially available from multiple manufacturers.

The broad spectral coverage listed in table 7.2 is only achieved by variing the ratios of the semiconductor materials during epitaxial growth. It can not be covered in a single laser diode. The band gap energy and the optical gain of semiconductors depends on the temperature. This allows for tuning semiconductor laser diodes via temperature control. For InGaAs based ECDL broadband tuning over 90 nm in the NIR has been reported [268]. But, as the spectral gain bandwidth of semiconductors depends on the band gap energy [269], the available tuning ranges in the visible spectral region diminish when going towards shorter wavelengths. Thus, a blue GaN ECDL for example allows only for tuning over 4 nm [270].

7.2   A tunable organic laser – a technology demonstration

Putting the aforementioned, application proven, spectroscopy light sources in a direct competition with laboratory stage, organic lasers would be inappropriate. For concluding this work and to provide a sharper picture of the *potential* organic lasers exhibit for spectroscopy applications, it was therefore required to demonstrate the capabilities of organic lasers beyond laboratory conditions.

For this purpose a prototype bench top laser system was designed, which, as the photograph of the optical setup in figure 7.6a illustrates, employs only few OEM opto-mechanical components. Additionally to the compact and rigid design, the system consumes less than 20 W of electrical power and features an automated,computer controlled tuning of the emission wavelength. Apart from the fiber port for the laser output, the power inlet and an USB interface for remote control of the laser output wavelength and power the system requires no further interfaces. The laser system hosts interchangeable cartridges with encapsulated organic DFB laser chips pumped with a DPSS microchip laser.
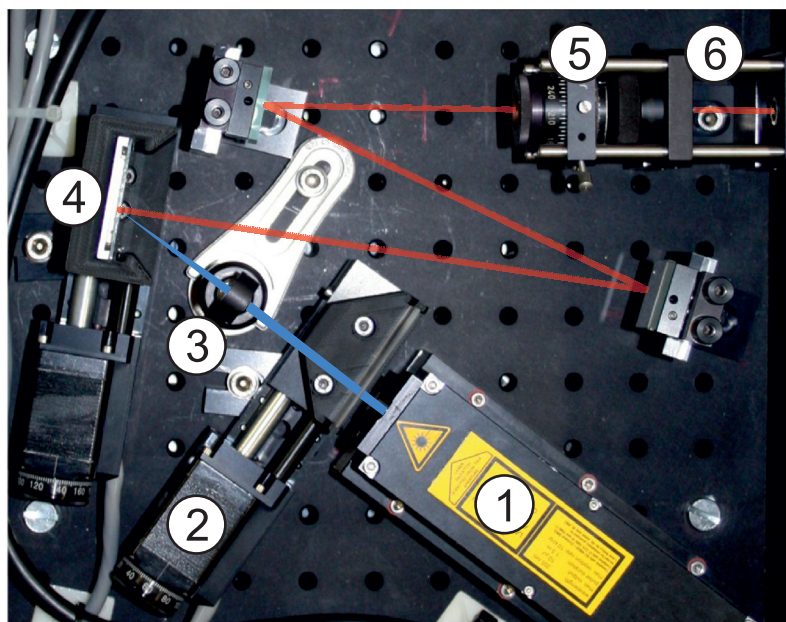
(a)
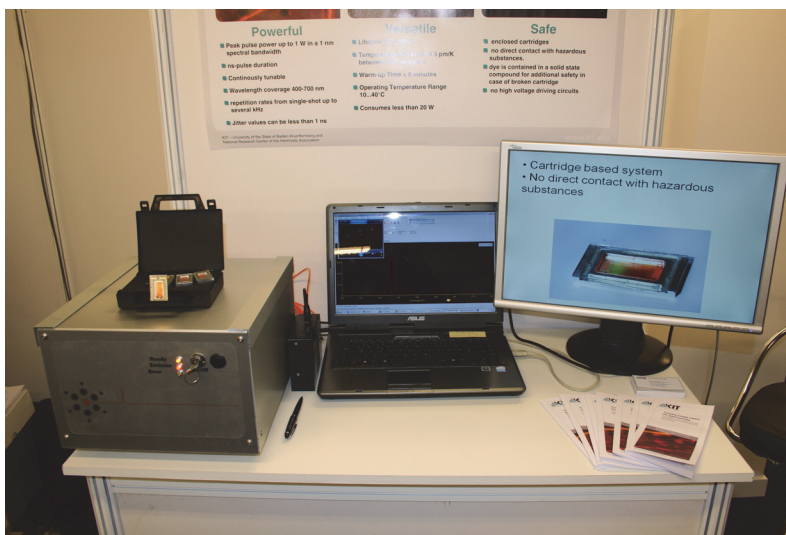
(b)

Figure 7.6: (a) Photograph of the prototype optical setup. The compact laser system comprises a 355 nm DPSS microchip laser ① for pumping the interchangeable organic laser chip cartridges ④. A motorized neutral density filter ②, focusing lens ③, polarizer ⑤ and a fiber coupling with a long pass filter ⑥ complete the opto-mechanical system. (b) Technology demonstration of a tunable organic laser system at the SPIE Photonics Europe 2010 in Brussels.

To get an unbiased appraisal of the performance of this system it was presented to a professional audience by participating at the *Innovation Village* contest at the *SPIE Photonics Europe 2010* conference in Brussels. During the three days of the contest the continuous tuning from 610 nm to 650 nm using encapsulated tunable DFB laserchips[3] could be demonstrated. The laser chips allow output pulse energies up to 1 nJ with a pulsewidth of one nanosecond. The prototype system was honored by the international jury with the first prize in the *Best Innovation* category [271]. Based on this technology demonstration device it is possible to estimate the
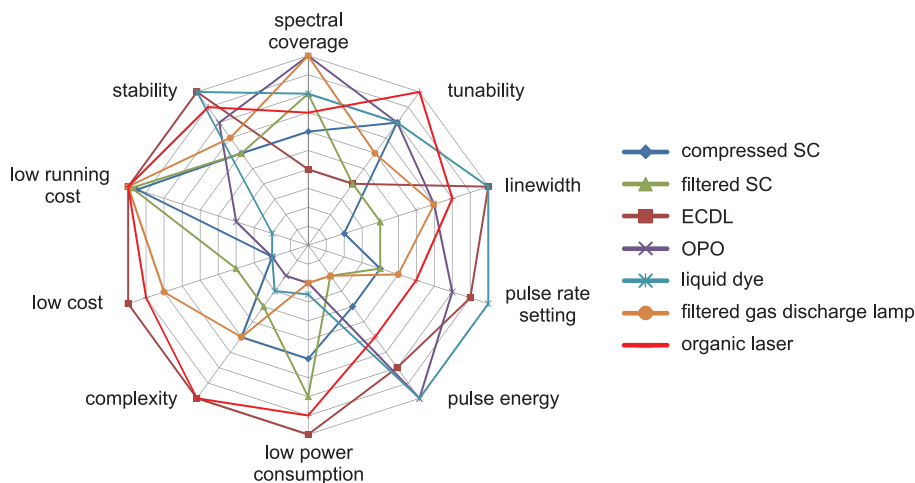
Figure 7.7: Radar chart for comparing the applicability of different spectroscopy light sources. The chart reflects the physical performance as well as economically and application relevant parameters.

applicability of a tunable organic laser for sensing applications compared with the in the previous sections introduced spectroscopy light sources. Figure shows 7.7 a radar chart were the different light sources are benchmarked for selected parameters. The chart reflects not only the physical performance and costs, it includes also "soft" values as power consumption and complexity which play a major role in judging the applicability. The chart shows that organic laser sources cannot compete with dye lasers and OPOs in terms of physical performance. They have, however, a high potential to be an appealing alternative for applications which do not require a high power, narrow linewidth or continuous wave emission but cannot be done with a gas discharge lamp monochromator source. This consolidates the high potential of organic DFB lasers to be a real alternative for conventional spectroscopy light sources.

---

[3]The laser chips have been kindly fabricated and encapsulated by Sönke Klinkhammer, LTI

Chapter 8

Conclusions and Outlook

Organic lasers are promising light sources for sensing applications due to their broad wavelength coverage in the visible spectrum. The possibility to fabricate organic DFB lasers with tailored wavelength at low costs and the simple integration of them into chip based sensing devices may enable the development of the next stage in the evolution of analysis, the lab-on-a-chip for point-of-care deployment.

In this thesis, solutions for rapidly prototyping DFB resonators with sub-micron feature sizes were presented. The developed processing strategies and optimizations for the two-photon-absorption 3D direct laser writing technology render it to a powerful tool for the development of future advanced organic laser resonators with rotational-symmetric geometries, photonic crystal resonators or optical gratings with intentionally introduced variations of the grating period. Moreover the demonstrated capability to pattern extended microoptical systems proves the applicability of 3D-DLW for patterning at all scales from micro- to nanostructures.

The considerations made in this work on substrate materials, excitation geometries, temperature stability and operating lifetime of tunable organic lasers allowed the demonstration of the first applications of organic lasers for optical transmission measurements and fluorescence excitation. The proposed encapsulation approach enabled operational lifetimes which can easily compete with current high repetition rate flash lamps. The illustrated spectroscopy applications employed standardized laboratory optics and opto-mechanics. Using more sophisticated detection methods as avalanche photodetectors and lock-in amplifiers may allow highly sensitive absorbance measurements.

The proposed tuning of a position dependent organic laser by mounting it on a spinning disc and exciting it with time-synchronized pump pulses allows emission wavelength changes in less than 10 ms independently of the tuning bandwidth. It was demonstrated, that the proposed tuning method can be sophistically realized with a low-cost hardware solution. The flexibility of the electronic delay can be used for advanced detection schemes as monitoring the kinetics of multiple color reactions in a quasi-simultaneously manner.

Finally, in this work a benchtop tunable organic laser system was presented as a technology demonstration. It served as the basis for evaluating the commercial potential of tunable organic laser sources compared to established tunable spectroscopy light sources. Valid arguments have been presented, that organic laser based devices

can be an appealing solution for filling the gap between high-end monochromator gas discharge lamp sources and liquid dye lasers or OPOs.

In summary, the presented solutions in this thesis allow the rapid prototyping of organic laser resonators and the convenient development of sensing applications which benefit most from the broad wavelength coverage of organic gain materials. This opens up prospects for commercial applications of organic lasers in the near future.

Bibliography

[1] I. D. W. Samuel and G. A. Turnbull, "Organic semiconductor lasers," *Chem. Rev.*, vol. 107, no. 4, pp. 1272–1295, 2007.

[2] S. Forrest, "The path to ubiquitous and low-cost organic electronic appliances on plastic," *Nature*, vol. 428, pp. 911–918, 2001.

[3] D. Pisignano, L. Persano, P. Visconti, R. Cingolani, G. Gigli, G. Barbarella, and L. Favaretto, "Oligomer-based organic distributed feedback lasers by room-temperature nanoimprint lithography," *Appl. Phys. Lett.*, vol. 83, p. 2545, 2003.

[4] M. Stroisch, **T. Woggon**, U. Lemmer, G. Bastian, G. Violakis, and S. Pissadakis, "Organic semiconductor distributed feedback laser fabricated by direct laser interference ablation," *Opt. Express*, vol. 15, no. 7, pp. 3968–3973, 2007.

[5] V. G. Kozlov, V. Bulovic, P. E. Burrows, M. Baldo, V. B. Khalfin, G. Parthasarathy, S. R. Forrest, Y. You, and M. E. Thompson, "Study of lasing action based on förster energy transfer in optically pumped organic semiconductor thin films," *J. of Appl. Phys.*, vol. 84, no. 8, pp. 4096–4108, 1998.

[6] U. Scherf, S. Riechel, U. Lemmer, and R. Mahrt, "Conjugated polymers: lasing and stimulated emission," *Curr. Opin. Solid State Mater. Sci.*, vol. 5, pp. 143–154, 2001.

[7] D. Schneider, T. Rabe, T. Riedl, T. Dobbertin, M. Kröger, E. Becker, H.-H. Johannes, W. Kowalsky, T. Weimann, J. Wang, and P. Hinze, "Laser threshold reduction in an all-spiro guest-host system," *Appl. Phys. Lett.*, vol. 85, no. 10, pp. 1659–1661, 2004.

[8] G. Heliotis, R. Xia, D. D. C. Bradley, G. A. Turnbull, I. D. W. Samuel, P. Andrew, and W. L. Barnes, "Two-dimensional distributed feedback lasers using a broadband, red polyfluorene gain medium," *J. of Appl. Phys.*, vol. 96, no. 12, pp. 6959–6965, 2004.

[9] R. Xia, G. Heliotis, P. N. Stavrinou, and D. D. C. Bradley, "Polyfluorene distributed feedback lasers operating in the green-yellow spectral region," *Appl. Phys. Lett.*, vol. 87, no. 3, p. 031104, 2005.

[10] T. Spehr, A. Siebert, T. Fuhrmann-Lieker, J. Salbeck, T. Rabe, T. Riedl, H. H. Johannes, W. Kowalsky, J. Wang, T. Weimann, and P. Hinze, "Organic solid-state ultraviolet-laser based on spiro-terphenyl," *Appl. Phys. Lett.*, vol. 87, no. 16, p. 161103, 2005.

[11] T. Kobayashi, J.-B. Savatier, G. Jordan, W. J. Blau, Y. Suzuki, and T. Kaino, "Near-infrared laser emission from luminescent plastic waveguides," *Appl. Phys. Lett.*, vol. 85, no. 2, pp. 185–187, 2004.

[12] M. Stroisch, "Organische Halbleiterlaser auf Basis Photonischer Kristalle," Doctoral dissertation, Universität Karlsruhe (TH), 2007.

[13] S. Klinkhammer, **T. Woggon**, U. Geyer, C. Vannahme, S. Dehm, T. Mappes, and U. Lemmer, "A continuously tunable low-threshold organic semiconductor distributed feedback laser fabricated by rotating shadow mask evaporation," *Appl. Phys. B*, vol. 97, no. 4, pp. 787–791, 2009.

[14] M. Stroisch, **T. Woggon**, C. Teiwes-Morin, S. Klinkhammer, K. Forberich, A. Gombert, M. Gerken, and U. Lemmer, "Intermediate high index layer for laser mode tuning in organic semiconductor lasers," *Opt. Express*, vol. 18, no. 6, pp. 5890–5895, 2010.

[15] M. Gaal, C. Gadermaier, H. Plank, E. Moderegger, A. Pogantsch, G. Leising, and E. List, "Imprinted conjugated polymer laser," *Advanced Materials*, vol. 15, no. 14, pp. 1165–1167, 2003.

[16] M. Ichikawa, Y. Tanaka, N. Suganuma, T. Koyama, and Y. Taniguchi, "Low-threshold photopumped distributed feedback plastic laser made by replica molding," *Japanese Journal of Applied Physics*, vol. 42, no. Part 1, No. 9A, pp. 5590–5593, 2003.

[17] M. Punke, S. Mozer, M. Stroisch, M. P. Heinrich, U. Lemmer, P. Henzi, and D. G. Rabus, "Coupling of organic semiconductor amplified spontaneous emission into polymeric single-mode waveguides patterned by deep-UV irradiation," *IEEE Photonics Technol. Lett.*, vol. 19, no. 2, pp. 61–63, 2007.

[18] M. Punke, **T. Woggon**, M. Stroisch, B. Ebenhoch, U. Geyer, C. Karnutsch, M. Gerken, U. Lemmer, M. Bruendel, J. Wang, and T. Weimann, "Organic semiconductor lasers as integrated light sources for optical sensor systems," *Proc. SPIE*, vol. 6659, 2007.

[19] M. Christiansen, M. Schøler, and A. Kristensen, "Integration of active and passive polymer optics," *Opt. Exp.*, vol. 15, no. 7, pp. 3931–3939, 2007.

[20] A. L. Washburn and R. C. Bailey, "Photonics-on-a-chip: recent advances in integrated waveguides as enabling detection elements for real-world, lab-on-a-chip biosensing applications," *Analyst*, vol. 136, pp. 227–236, 2011.

[21] C. Karnutsch, M. Stroisch, M. Punke, U. Lemmer, J. Wang, and T. Weimann, "Laser diode-pumped organic semiconductor lasers utilizing two-dimensional photonic crystal resonators," *IEEE Photonics Technol. Lett.*, vol. 19, no. 10, pp. 741–743, 2007.

[22] T. Riedl, T. Rabe, H. Johannes, W. Kowalsky, J. Wang, T. Weimann, P. Hinze, B. Nehls, T. Farrell, and U. Scherf, "Tunable organic thin-film laser pumped by an inorganic violet diode laser," *Appl. Phys. Lett.*, vol. 88, p. 241116, 2006.

[23] Y. Yang, G. A. Turnbull, and I. D. W. Samuel, "Hybrid optoelectronics: A polymer laser pumped by a nitride light-emitting diode," *Appl. Phys. Lett.*, vol. 92, no. 20, p. 163306, 2008.

[24] P. Yager, T. Edwards, E. Fu, K. Helton, K. Nelson, M. R. Tam, and B. H. Weigl, "Microfluidic diagnostic technologies for global public health," *Nature*, vol. 442, no. 7101, pp. 412–418, 2006.

[25] S. Tisa, A. Tosi, and F. Zappa, "Fully-integrated cmos single photon counter," *Opt. Express*, vol. 15, no. 6, pp. 2873–2887, Mar 2007.

[26] D. Schneider, U. Lemmer, T. Riedl, and W. Kowalsky, "Low threshold organic semiconductor lasers," in *Organic Light Emitting Devices*, K. Müllen and U. Scherf, Eds. Wiley-VCH, Weinheim, 2006.

[27] C. Karnutsch, C. Pflumm, G. Heliotis, J. deMello, D. Bradley, J. Wang, T. Weimann, V. Haug, C. Gärtner, and L. U., "Improved organic semiconductor lasers based on a mixed-order distributed feedback resonator design," *Appl. Phys. Lett.*, vol. 90, p. 131104, 2007.

[28] M. Meier, A. Dodabalapur, J. A. Rogers, R. E. Slusher, A. Mekis, and A. Timko, "Emission characteristics of two-dimensional organic photonic crystal lasers fabricated by replica molding," *J. Appl. Phys.*, vol. 86, no. 7, pp. 3502–3507, 1999.

[29] A. Jebali, R. F. Mahrt, N. Moll, D. Erni, C. Bauer, G.-L. Bona, and W. Bächtold, "Lasing in organic circular grating structures," *J. Appl. Phys.*, vol. 96, no. 6, pp. 3043–3049, 2004.

[30] D. Labilloy, H. Benisty, C. Weisbuch, T. F. Krauss, C. J. M. Smith, R. Houdré, and U. Oesterle, "High-finesse disk microcavity based on a circular Bragg reflector," *Appl. Phys. Lett.*, vol. 73, no. 10, pp. 1314–1316, 1998.

[31] R. G. Hunsperger, "Integrated optics: theory and technology," ser. Optical Sciences. Springer Verlag, 1984, ch. 2.

[32] E. Marcatili, "Dielectric rectangular waveguide and directional coupler for integrated optics," *Bell Syst. Tech. J.*, vol. 48, pp. 2071–2088, 1969.

[33] T. Ito and S. Okazaki, "Pushing the limits of lithography," *Nature*, vol. 406, no. 6799, pp. 1027–1031, 2000.

[34] G. B. Airy, "On the diffraction of an object-glass with circular aperture," *Trans. Cambridge Philos. Soc.*, vol. 5, pp. 283–291, 1835.

[35] E. Wolf, "Electromagnetic diffraction in optical systems I – An integral representation of the image field," *Proc. R. Soc. London, Ser. A*, vol. 253, no. 1274, pp. 349–357, 1959.

[36] B. Richards and E. Wolf, "Electromagnetic diffraction in optical systems II – Structure of the image field in an aplanatic system," *Proc. R. Soc. London, Ser. A*, vol. 253, no. 1274, pp. 358–379, 1959.

[37] A. E. Siegman, "Lasers." University Science Books, Mill Valley, Calif., 1986, ch. 1, pp. 1–49.

[38] K. Thom, "Nuclear pumped gas laser research," in *2nd NASA Conf. on Laser Energy Conversion*, 1976, pp. 127–132.

[39] H. Kogelnik and T. Li, "Laser beams and resonators," *Appl. Opt.*, vol. 5, no. 10, pp. 1550–1567, 1966.

[40] A. J. Schwab and F. W. Hollinger, "Compact high-power N_2 laser: Circuit theory and design," *IEEE J. Quantum Electron.*, vol. QE-12, no. 3, 1976.

[41] H. Kogelnik and C. V. Shank, "Coupled-wave theory of distributed feedback lasers," *J. of Appl. Phys.*, vol. 43, no. 5, pp. 2327–2335, 1972.

[42] H. Kogelnik and C. V. Shank, "Stimulated emission in a periodic structure," *Appl. Phys. Lett.*, vol. 18, pp. 152–154, 1971.

[43] C. V. Shank, J. E. Bjorkholm, and H. Kogelnik, "Tunable distributed-feedback dye laser," *Appl. Phys. Lett.*, vol. 18, no. 9, pp. 395–396, 1971.

[44] T. Kavc, G. Langer, W. Kern, G. Kranzelbinder, E. Toussaere, G. A. Turnbull, I. D. W. Samuel, K. F. Iskra, T. Neger, and A. Pogantsch, "Index and relief gratings in polymer films for organic distributed feedback lasers," *Chem. Mater.*, vol. 14, no. 10, pp. 4178–4185, 2002.

[45] J. R. Lawrence, P. Andrew, W. L. Barnes, M. Buck, G. A. Turnbull, and I. D. W. Samuel, "Optical properties of a light-emitting polymer directly patterned by soft lithography," *Applied Physics Letters*, vol. 81, no. 11, pp. 1955–1957, 2002.

[46] T. Zhai, X. Zhang, Z. Pang, and F. Dou, "Direct writing of polymer lasers using interference ablation," *Advanced Materials*, pp. n/a–n/a, 2011.

[47] **T. Woggon**, M. Punke, M. Stroisch, M. Bruendel, M. Schelb, C. Vannahme, T. Mappes, J. Mohr, and U. Lemmer, "Semiconductor lasers as integrated light sources for optical sensors," in *Organic Electronics in Sensors and Biotechnology*, ser. Biophotonics, R. Shinar and J. Shinar, Eds. Mcgraw-Hill, 2009, chapter 7, pp. 265–298.

[48] S. Wang and S. Sheem, "Two-dimensional distributed-feedback lasers and their applications," *Appl. Phys. Lett.*, vol. 22, no. 9, 1973.

[49] H. Haken and H. C. Wolf, "Molecular physics and elements of quantum chemistry." Springer, 2004.

[50] C. Adachi, M. A. Baldo, M. E. Thompson, and S. R. Forrest, "Nearly 100% internal phosphorescence efficiency in an organic light-emitting device," *Journal of Applied Physics*, vol. 90, no. 10, pp. 5048–5051, 2001.

[51] F. P. Schaefer, "Dye lasers," in *Topics in Applied Physics*, 2nd ed., F. P. Schaefer, Ed. Springer Verlag, 1977, vol. 1.

[52] T. Förster, "Zwischenmolekulare Energiewanderung und Fluoreszenz," *Annalen der Physik*, vol. 2, no. 6, pp. 55–75, 1948.

[53] S. Riechel, "Organic semiconductor lasers with two-dimensional distributed feedback," Doctoral dissertation, Ludwig-Maximilians-Universität München, 2002.

[54] N. Tessler, G. Denton, and R. Friend, "Lasing from conjugated-polymer microcavities," *Nature*, vol. 382, no. 6593, pp. 695–697, 1996.

[55] F. Hide, M. A. Diaz-Garcia, B. J. Schwartz, M. R. Andersson, Q. Pei, and A. J. Heeger, "Semiconducting polymers: A new class of solid-state laser materials," *Science*, vol. 273, no. 5823, pp. 1833–1836, 1996.

[56] C. Gärtner, "Organic laser diodes: Modelling and simulation," Doctoral dissertation, Universität Karlsruhe (TH), 2008, Universitätsverlag Karlsruhe, ISBN 978-3-86644-204-7.

[57] I. D. W. Samuel, E. B. Namdas, and G. A. Turnbull, "How to recognize lasing," *Nat. Photon.*, vol. 3, pp. 546–549, Oct. 2009.

[58] D. Schneider, "Organische Halbleiterlaser," Doctoral dissertation, Technische Universität Carolo-Wilhelmina zu Braunschweig, 2005, Papierflieger, ISBN 978-3-89720-804-9.

[59] D. Wright, E. Brasselet, J. Zyss, G. Langer, and W. Kern, "Dye-doped organic distributed-feedback lasers with index and surface gratings: the role of pump polarization and molecular orientation," *J. Opt. Soc. Am. B: Opt. Phys.*, vol. 21, pp. 944–950, 2004.

[60] S. Riechel, U. Lemmer, J. Feldmann, S. Berleb, A. Mückl, W. Brütting, A. Gombert, and V. Wittwer, "Very compact tunable solid-state laser utilizing a thin-film organic semiconductor," *Opt. Lett.*, vol. 26, pp. 593–595, 2001.

[61] G. A. Turnbull, P. Andrew, W. L. Barnes, and I. D. W. Samuel, "Operating characteristics of a semiconducting polymer laser pumped by a microchip laser," *Appl. Phys. Lett.*, vol. 82, no. 3, pp. 313–315, 2003.

[62] A. Vasdekis, G. Tsiminis, J. Ribierre, L. O'Faolain, T. Krauss, G. Turnbull, and I. Samuel, "Diode pumped distributed Bragg reflector lasers based on a dye-to-polymer energy transfer blend," *Opt. Express*, vol. 14, no. 20, pp. 9211–9216, 2006.

[63] C. Karnutsch, V. Haug, C. Gärtner, U. Lemmer, T. Farrell, B. Nehls, U. Scherf, J. Wang, T. Weimann, G. Heliotis, C. Pflumm, J. deMello, and D. Bradley, "Low threshold blue conjugated polymer DFB lasers," in *Proc. CLEO/QUELS*, 2006, pp. 1–2.

[64] A. Avramescu, T. Lermer, J. Müller, C. Eichler, G. Bruederl, M. Sabathil, S. Lutgen, and U. Strauss, "True green laser diodes at 524 nm with 50 mw continuous wave output power on *c*-plane GaN," *Applied Physics Express*, vol. 3, no. 6, p. 061003, 2010.

[65] **T. Woggon**, "Lasertätigkeit in organischen Photonischen Kristallen mit Defektmoden," diploma thesis, Universität Karlsruhe (TH), 2007.

[66] D. Schneider, T. Rabe, T. Riedl, T. Dobbertin, M. Kröger, E. Becker, H.-H. Johannes, W. Kowalsky, T. Weimann, J. Wang, and P. Hinze, "Ultrawide tuning range in doped organic solid-state lasers," *Appl. Phys. Lett.*, vol. 85, no. 11, pp. 1886–1888, 2004.

[67] N. Tsutsumi and A. Fujihara, "Tunable distributed feedback lasing with narrowed emission using holographic dynamic gratings in a polymeric waveguide," *Appl. Phys. Lett.*, vol. 86, no. 6, p. 061101, 2005.

[68] R. Ozaki, T. Shinpo, K. Yoshino, M. Ozaki, and H. Moritake, "Tunable liquid crystal laser using distributed feedback cavity fabricated by nanoimprint lithography," *Appl. Phys. Express*, vol. 1, no. 1, p. 012003, 2008.

[69] M. H. Song, B. Wenger, and R. H. Friend, "Tuning the wavelength of lasing emission in organic semiconducting laser by the orientation of liquid crystalline conjugated polymer," *J. Appl. Phys.*, vol. 104, no. 3, p. 033107, 2008.

[70] M. R. Weinberger, G. Langer, A. Pogantsch, A. Haase, E. Zojer, and W. Kern, "Continuously color-tunable rubber laser," *Adv. Mater.*, vol. 16, no. 2, pp. 130–133, 2004.

[71] B. Schütte, H. Gothe, S. I. Hintschich, M. Sudzius, H. Fröb, V. G. Lyssenko, and K. Leo, "Continuously tunable laser emission from a wedge-shaped organic microcavity," *Appl. Phys. Lett.*, vol. 92, no. 16, p. 163309, 2008.

[72] D. Schneider, S. Hartmann, T. Benstem, T. Dobbertin, D. Heithecker, D. Metzdorf, E. Becker, T. Riedl, H.-H. Johannes, W. Kowalsky, T. Weimann, J. Wang, and P. Hinze, "Wavelength-tunable organic solid-state distributed-feedback laser," *Appl. Phys. B*, vol. 77, no. 4, pp. 399–402, 2003.

[73] F. Träger, "Springer handbook of lasers and optics." New York: Springer Science+Business Media, 2007.

[74] S. Goods, R. Watson, and M. Yi, "Thermal expansion and hydration behavior of pmma molding materials for LIGA applications," *SAND REPORT*, vol. 2003, no. 8000, p. 55, 2003.

[75] *Ormocomp – technical datasheet*, Microresist, 2003.

[76] *Optical glass*, data sheets ed., Schott, 2011.

[77] D. Nilsson, "Polymer based miniaturized dye lasers for lab-on-a-chip systems," PhD thesis, Technical University of Denmark (DTU), Department of Micro and Nanotechnology, 2005.

[78] F. Chollet, "SU-8: Thick photo-resist for MEMS. online-ressource - 2007," http://memscyclopedia.org/su8.html.

[79] *SU-8 2000 Permanent Epoxy Negative Photoresist*, Processing guidelines for: Su-8 2025, su-8 2035, su-8 2050 and su-8 2075 ed., Microchem, 2006.

[80] R. Buestrich, F. Kahlenberg, M. Popall, P. Dannberg, R. Müller-Fiedler, and O. Rösch, "Ormocer® s for optical interconnection technology," *J. Sol-Gel Sci. Technol.*, vol. 20, no. 2, pp. 181–186, 2001.

[81] S. L. Evans, "Fatigue of pmma bone cement," in *Fracture of Nano and Engineering Materials and Structures*, E. E. Gdoutos, Ed. Springer Netherlands, 2006, pp. 271–272.

[82] A. Welle and E. Gottwald, "UV-based patterning of polymeric substrates for cell culture applications," *Biomed. Microdevices*, vol. 4, pp. 33–41, 2002, 10.1023/A:1014267712144.

[83] D. Rabus, M. Bruendel, Y. Ichihashi, A. Welle, R. Seger, and M. Isaacson, "A bio–fluidic–photonic platform based on deep UV modification of polymers," *IEEE J. Sel. Top. Quantum Electron.*, vol. 13, no. 2, pp. 214–222, 2007.

[84] C. Janiak and P. G. Lassahn, "The vinyl homopolymerization of norbornene," *Macromol. Rapid Commun.*, vol. 22, no. 7, pp. 479–493, 2001.

[85] W. Kaminsky and A. Bark, "Copolymerization of ethene and dimethanooctahydronaphthalene with aluminoxane containing catalysts," *Polym. Int.*, vol. 28, no. 3, pp. 251–253, 1992.

[86] T. Sasaki, T. Ebara, and H. Johoji, "New materials from new catalysts," *Polym. Adv. Technol.*, vol. 4, no. 7, pp. 406–414, 1993.

[87] H. Cherdron, M.-J. Brekner, and F. Osan, "Cycloolefin-copolymere: Eine neue Klasse transparenter Thermoplaste," *Die Angew. Makromol. Chem.*, vol. 223, no. 1, pp. 121–133, 1994.

[88] M. Arnold, J. Knorr, F. Köller, and S. Bornemann, "Modified polypropenes via metallocene catalysis," *J. Macromol. Sci. Part A Pure Appl. Chem.*, vol. 36, no. 11, pp. 1655–1681, 1999.

[89] F. Garbassi and R. Po, "Engineering thermoplastics." John Wiley & Sons, Inc., 2000.

[90] T. Rische, A. J. Waddon, L. C. Dickinson, and W. J. MacKnight, "Microstructure and morphology of cycloolefin copolymers," *Macromolecules*, vol. 31, no. 6, pp. 1871–1874, 1998.

[91] M. Punke, "Organische Halbleiterbauelemente für mikrooptische Systeme," Doctoral dissertation, Universität Karlsruhe (TH), 2007.

[92] *TOPAS®- Cycloolefin Copolymer (COC)*, Topas Advanced Polymers GmbH, 2006.

[93] J. D. Gelorme, R. J. Cox, and S. A. R. Gutierrez, "Photoresist composition and printed circuit boards ans packages made therewith," Patent US 4,882,245, 1989.

[94] M. Deubel, "Three-dimensional photonic crystals via direct laser writing: Fabrication and characterization." Shaker Verlag, 2006.

[95] B. Bilenberg, S. Jacobsen, M. Schmidt, L. Skjolding, P. Shi, P. Bøggild, J. Tegenfeldt, and A. Kristensen, "High resolution 100 kV electron beam lithography in SU-8," *Microelectron. Eng.*, vol. 83, no. 4-9, pp. 1609–1612, 2006, micro- and Nano-Engineering MNE 2005.

[96] H. Lorenz, M. Despont, N. Fahrni, N. LaBianca, P. Renaud, and P. Vettiger, "SU-8: a low-cost negative resist for MEMS," *J. Micromech. Microeng.*, vol. 7, no. 3, p. 121, 1997.

[97] H. Lorenz, M. Laudon, and P. Renaud, "Mechanical characterization of a new high-aspect-ratio near UV-photoresist," *Microelectron. Eng.*, vol. 41-42, pp. 371–374, 1998.

[98] G. Witzgall, R. Vrijen, E. Yablonovitch, V. Doan, and B. J. Schwartz, "Single-shot two-photon exposure of commercial photoresist for the production of three-dimensional structures," *Opt. Lett.*, vol. 23, no. 22, pp. 1745–1747, Nov 1998.

[99] Y.-J. Chen and Y.-C. Chen, "High-aspect-ratio sub-diffraction-limit objects fabricated with two-photon-absorption photopolymerisation," in *Conf. on Lasers & Electro-Optics (CLEO)*. Optical Society of America, 2002.

[100] H. Schmidt, "New type of non-crystalline solids between inorganic and organic materials," *J. Non-Cryst. Solids*, vol. 73, no. 1-3, pp. 681 – 691, 1985, glass Science and Technology Problems and Prospects for 2004.

[101] K.-H. Haas and H. Wolter, "Synthesis, properties and applications of inorganic-organic copolymers (ORMOCER®s)," *Curr. Opin. Solid State Mater. Sci.*, vol. 4, no. 6, pp. 571–580, 1999.

[102] R. Buestrich, F. Kahlenberg, M. Popall, A. Martin, and O. Rösch, "Ormocer® s for optical interconnection technology," *Mater. Res. Soc. Symp. Proc.*, vol. 628, pp. CC9.8.1–CC9.8.6, 2000.

[103] A. Ovsianikov, A. Doraiswamy, R. Narayan, and B. N. Chichkov, "Two-photon polymerization for fabrication of biomedical devices," *Proc. SPIE*, vol. 6465, 2007.

[104] R. Houbertz, G. Domann, J. Schulz, B. Olsowski, L. Fröhlich, and W.-S. Kim, "Impact of photoinitiators on the photopolymerization and the optical properties of inorganic–organic hybrid polymers," *Appl. Phys. Lett.*, vol. 84, no. 7, pp. 1105–1107, 2004.

[105] V. Schmidt, L. Kuna, V. Satzinger, R. Houbertz, G. Jakopic, and G. Leising, "Application of two-photon 3D lithography for the fabrication of embedded ormocer waveguides," *Proc. SPIE*, vol. 6476, 2007.

[106] R. Houbertz, J. Schulz, L. Fröhlich, G. Domann, M. Popall, J. Serbin, and B. Chichkov, "Inorganic-organic hybrid materials for real 3-D sub-µm lithography," *Mater. Res. Soc. Symp. Proc.*, vol. 780, pp. Y4.12.1–Y4.12.6, 2003.

[107] P. R. Hammond, "Laser dye DCM, its spectral properties, synthesis and comparison with other dyes in the red," *Opt. Commun.*, vol. 29, no. 3, pp. 331–333, 1979.

[108] S. Sinzinger and J. Jahns, "Microoptics." WILEY-VCH, 1999.

[109] M. J. Madou, "Fundamentals of microfabrication: The science of miniaturization." CRC Press, 2002.

[110] A. Gombert, B. Bläsi, C. Bühler, P. Nitz, J. Mick, W. Hoßfeld, and M. Niggemann, "Some application cases and related manufacturing techniques for optically functional microstructures on large areas," *Opt. Eng.*, vol. 43, pp. 2525–2533, 2004.

[111] K. Forberich, "Organische Photonische-Kristall-Laser," Doctoral dissertaion, Albert-Ludwigs-Universität Freiburg, 2005.

[112] C. Rensch and S. Hell, "Laser scanner for direct writing lithography," *Appl. Opt.*, vol. 28, no. 17, pp. 3754–3758, 1989.

[113] S. Maruo and K. Ikuta, "Three-dimensional microfabrication by use of single-photon-absorbed polymerization," *Appl. Phys. Lett.*, vol. 76, no. 19, pp. 2656–2658, 2000.

[114] A. C. Sullivan and M. W. Grabowski, "Three-dimensional direct-write lithography into photopolymer," *Appl. Opt.*, vol. 46, no. 3, pp. 295–301, 2007.

[115] Z. Bayindir, Y. Sun, M. J. Naughton, C. N. LaFratta, T. Baldacchini, J. T. Fourkas, J. Stewart, B. E. A. Saleh, and M. C. Teich, "Polymer microcantilevers fabricated via multiphoton absorption polymerization," *Appl. Phys. Lett.*, vol. 86, no. 6, p. 064105, 2005.

[116] H.-B. Sun, K. Takada, and S. Kawata, "Elastic force analysis of functional polymer submicron oscillators," *Appl. Phys. Lett.*, vol. 79, no. 19, pp. 3173–3175, 2001.

[117] M. Thiel, G. von Freymann, and M. Wegener, "Layer-by-layer three-dimensional chiral photonic crystals," *Opt. Lett.*, vol. 32, no. 17, pp. 2547–2549, 2007.

[118] H. Sun, T. Kawakami, Y. Xu, J.-Y. Ye, S. Matuso, H. Misawa, M. Miwa, and R. Kaneko, "Real three-dimensional microstructures fabricated by photopolymerization of resins through two-photon absorption," *Opt. Lett.*, vol. 25, no. 5, pp. 1110–1112, 2000.

[119] H. Sun and S. Kawata, "Two-photon laser precision microfabrication and its applications to micro-nano devices and systems," *J. Lightwave Techn.*, vol. 21, no. 3, p. 819, 2003.

[120] M. Deubel, G. von Freymann, M. Wegener, S. Pereira, K. Busch, and C. Soukoulis, "Direct laser writing of three-dimensional photonic-crystal templates for telecommunications," *Nat. Mater.*, vol. 3, no. 7, pp. 444–447, 2004.

[121] L. Li and J. Fourkas, "Multiphoton polymerization," *Mater. Today*, vol. 10, no. 6, pp. 30–37, 2007.

[122] Nanoscribe GbR.

[123] *Workstation for Laser Direct-Write Processing*, App. note ed., Newport Corporation, Worldwide Headquarters, 1791 Deere Avenue, Irvine, CA 92606, 2009.

[124] J. Serbin, A. Egbert, A. Ostendorf, B. N. Chichkov, R. Houbertz, G. Domann, J. Schulz, C. Cronauer, L. Fröhlich, and M. Popall, "Femtosecond laser-induced two-photon polymerization of inorganic organic hybrid materials for applications in photonics," *Opt. Lett.*, vol. 28, no. 5, pp. 301–303, 2003.

[125] H. Sun, M. Maeda, K. Takada, J. Chon, M. Gu, and S. Kawata, "Experimental investigation of single voxels for laser nanofabrication via two-photon photopolymerization," *Appl. Phys. Lett.*, vol. 83, p. 819, 2003.

[126] S. Maruo, O. Nakamura, and S. Kawata, "Three-dimensional microfabrication with two-photon-absorbed photopolymerization," *Opt. Lett.*, vol. 22, no. 2, pp. 132–134, 1997.

[127] H. B. Sun, S. Matsuo, and H. Misawa, "Three-dimensional photonic crystal structures achieved with two-photon-absorption photopolymerization of resin," *Appl. Phys. Lett.*, vol. 74, no. 6, pp. 786–788, 1999.

[128] R. H. Friend, R. W. Gymer, A. B. Holmes, J. H. Burroughes, R. N. Marks, C. Taliani, D. D. C. Bradley, D. A. Dos Santos, J. L. Brédas, M. Lögdlund, and W. R. Salaneck, "Electroluminescence in conjugated polymers," *Nature*, vol. 397, no. 6715, pp. 121–128, 1999.

[129] V. G. Kozlov, V. Bulovic, P. E. Burrows, and S. R. Forrest, "Laser action in organic semiconductor waveguide and double-heterostructure devices," *Nature*, vol. 389, no. 6649, pp. 362–364, 1997.

[130] G. Duplain, P. G. Verly, J. A. Dobrowolski, A. Waldorf, and S. Bussiére, "Graded-reflectance mirrors for beam quality control in laser resonators," *Appl. Opt.*, vol. 32, no. 7, pp. 1145–1153, Mar 1993.

[131] S. Y. Chou, P. R. Krauss, and P. J. Renstrom, "Imprint of sub-25 nm vias and trenches in polymers," *Appl. Phys. Lett.*, vol. 67, no. 21, pp. 3114–3116, 1995.

[132] T. Hanemann, M. Heckele, and V. Piotter, "Current status of micromolding technology," *Polym. News*, vol. 25, pp. 224–229, 2000.

[133] E. Becker, W. Ehrfeld, P. Hagmann, A. Maner, and D. Münchmeyer, "Fabrication of microstructureswith high aspect ratios and great structural heights by synchrotron radiation lithography, galvanoforming and plastic molding (LIGA process)," *Microelectron. Eng.*, vol. 4, pp. 35–56, 1986.

[134] W. Bacher, W. Menz, and J. Mohr, "The LIGA technique and its potential for microsystems–a survey," *IEEE Trans. Ind. Electron.*, vol. 42, no. 5, pp. 431–441, 1995.

[135] M. Gale, "Replication techniques for diffractive optical elements," *Microelectron. Eng.*, vol. 34, no. 3, pp. 321–339, 1997.

[136] I. Kim and P. Mentone, "Electroformed nickel stamper for light guide panel in lcd back light unit," *Electrochim. Acta*, vol. 52, pp. 1805–1809, 2006.

[137] M. Berggren, A. Dodalapur, and R. Slusher, "Organic solid-state lasers with imprinted gratings on plastic substrates," *Appl. Phys. Lett.*, vol. 72, no. 4, pp. 410–411, 1998.

[138] S. H. Ahn and L. J. Guo, "High-speed roll-to-roll nanoimprint lithography on flexible plastic substrates," *Adv. Mater.*, vol. 20, p. 2044Ű2049, 2008.

[139] J. Rogers, M. Meier, and A. Dodabalapur, "Using printing and molding techniques to produce distributed feedback and bragg reflector resonators for plastic lasers," *Appl. Phys. Lett.*, vol. 73, no. 13, pp. 1766–1768, 1998.

[140] J. Rogers, M. Meier, A. Dodabalapur, E. Laskowski, and M. Cappuzzo, "Distributed feedback ridge waveguide lasers fabricated by nanoscale printing and molding on nonplanar substrates," *Appl. Phys. Lett.*, vol. 74, no. 22, pp. 3257–3259, 1999.

[141] S. Nolte, M. Will, J. Burghoff, and A. Tuennermann, "Femtosecond waveguide writing: a new avenue to three-dimensional integrated optics," *Appl. Phys. A*, vol. 77, pp. 109–111, 2003.

[142] M. Farasi and B. Chichkov, "Materials processing: Two-photon fabrication," *Nat. Photon.*, vol. 3, no. 8, pp. 450–452, 2009.

[143] R. Guo, S. Xiao, X. Zhai, J. Li, A. Xia, and W. Huang, "Micro lens fabrication by means of femtosecond two photon polymerization," *Opt. Express*, vol. 14, pp. 810–816, 2006.

[144] **T. Woggon**, T. Kleiner, M. Punke, and U. Lemmer, "Nanostructuring of organic-inorganic hybrid materials for distributed feedback laser resonators by two photon polymerization," *Opt. Express*, vol. 17, no. 4, pp. 2005–2507, 2009.

[145] B. H. Cumpston, S. P. Ananthavel, S. Barlow, D. L. Dyer, J. E. Ehrlich, L. L. Erskine, A. A. Heikal, S. M. Kuebler, I. Lee, and D. McCord-Maughon, "Two-photon polymerization initiators for threedimensional optical data storage and microfabrication," *Nature*, vol. 398, pp. 51–54, 1999.

[146] M. Miwa, S. Juodkazis, T. Kawakami, S. Matsuo, and H. Misawa, "Femtosecond two-photon stereo-lithography," *Appl. Phys. A*, vol. 5, pp. 561–566, 2001.

[147] X. Yin, N. Fang, X. Zhang, I. B. Martini, and B. J. Schwartz, "Near-field two-photon nanolithography using an apertureless optical probe," *Appl. Phys. Lett.*, vol. 81, pp. 3663–3665, 2002.

[148] W. H. Teh, U. Dürig, G. Salis, R. Harbers, U. Drechsler, R. F. Mahrt, C. G. Smith, and H.-J. Güntherodt, "SU-8 for real three-dimensional subdiffraction-limit two-photon microfabrication," *Appl. Phys. Lett.*, vol. 84, no. 20, pp. 4095–4097, 2004.

[149] W. Haske, V. W. Chen, J. M. Hales, W. Dong, S. Barlow, S. R. Marder, and J. W. Perry, "65 nm feature sizes using visible wavelength 3-D multiphoton lithography," *Opt. Express*, vol. 15, no. 6, pp. 3426–3436, 2007.

[150] C. Eschenbaum, **T. Woggon**, and U. Lemmer, "High speed fabrication of toroidal micro-ring resonators by two photon direct laser writing," in *Nonlinear Photonics*. Optical Society of America, 2010, p. NThB8.

[151] F. Fay, K. Fujiwara, D. D. Rees, and K. E. Fogarty, "Distribution of α-actinin in single isolated smooth muscle cells," *J. Cell. Biol.*, vol. 96, pp. 783–795, 1983.

[152] R. Shack, R. Baker, R. Buchroeder, D. Hillman, R. Shoemaker, and P. H. Bartels, "Ultrafast laser scanner microscope," *J. of Histochem. Cytochem.*, vol. 27, no. 1, pp. 153–159, 1979.

[153] D. K. Cohen, W. H. Gee, M. Ludeke, and J. Lewkowicz, "Automatic focus control: the astigmatic lens approach," *Appl. Opt.*, vol. 23, no. 4, pp. 565–570, 1984.

[154] H. Becker, R. Caspary, C. Toepfer, M. V. Schickfus, and S. Hunklinger, "Low-cost direct writing lithography system for the sub-micron range," *J. Mod. Opt.*, vol. 44, pp. 1715–1723, 1997.

[155] L. L. Deck and S. H. Chakmakjian, "Method and apparatus for automatically and simultaneously determining best focus and orientation of objects to be measured by broad-band interferometric means," Patent US 5,784,164, 1998.

[156] E. H. Hellen and D. Axelrod, "An automatic focus/hold system for optical microscopes," *Rev. Sci. Instrument.*, vol. 61, no. 12, pp. 3722–3725, 1990.

[157] J. Hesse, A. Sonnleitner, G. Freudenthaler, J. Jacak, O. Hoglinger, H. Schindler, and G. J. Schutz, "Single molecule reader for high-throughput bioanalysis," *Anal. Chem.*, vol. 76, pp. 5960–5964, 2004.

[158] P. Westphal, D. Bublitz, and R. Mitzkus, "Autofokuseinrichtung für die Mikroskopie," Patent DE 10 2006 027 836 A1, 2006, Offenlegungsschrift.

[159] M. Farsari, M. Vamvakaki, and B. N. Chichkov, "Multiphoton polymerization of hybrid materials," *J. Opt.*, vol. 12, no. 12, p. 124001, 2010.

[160] G. Kumi, C. O. Yanez, K. D. Belfield, and J. T. Fourkas, "High-speed multiphoton absorption polymerization: fabrication of microfluidic channels with arbitrary cross-sections and high aspect ratios," *Lab Chip*, 2010.

[161] I. Sakellari, A. Gaidukeviciute, A. Giakoumaki, D. Gray, C. Fotakis, M. Farsari, M. Vamvakaki, C. Reinhardt, A. Ovsianikov, and B. Chichkov, "Two-photon polymerization of titanium-containing sol-gel composites for three-dimensional structure fabrication," *Appl. Phys. A*, vol. 100, pp. 359–364, 2010.

[162] J. Fischer, G. von Freymann, and M. Wegener, "The materials challenge in diffraction-unlimited direct-laser-writing optical lithography," *Adv. Mater.*, vol. 22, no. 32, pp. 3578–3582, 2010.

[163] H.-B. Sun, K. Takada, M.-S. Kim, K.-S. Lee, and S. Kawata, "Scaling laws of voxels in two-photon photopolymerization nanofabrication," *Appl. Phys. Lett.*, vol. 83, no. 6, pp. 1104–1106, 2003.

[164] S. Yokoyama, T. Nakahama, H. Miki, and S. Mashiko, "Two-photon-induced polymerization in a laser gain medium for optical microstructure," *Appl. Phys. Lett.*, vol. 82, no. 19, pp. 3221–3223, 2003.

[165] S. Klein, A. Barsella, V. Stortz, A. Fort, and K. D. Dorkenoo, "Colloid-based photonic crystal for organic lasers and two-photon induced polymerization for tunable DFB lasers," in *Conf. on Lasers & Electro-Optics (CLEO)*, vol. 1-3. Optical Society of America, 2005, pp. 311–313.

[166] D.-Y. Yang, S. H. Park, T. W. Lim, H.-J. Kong, S. W. Yi, H. K. Yang, and K.-S. Lee, "Ultraprecise microreproduction of a three-dimensional artistic sculpture by multipath scanning method in two-photon photopolymerization," *Appl. Phys. Lett.*, vol. 90, no. 1, p. 013113, 2007.

[167] micro resist technology GmbH.

[168] W. Plass, R. Maestle, K. Wittig, A. Voss, and A. Giesen, "High-resolution knife-edge laser beam profiling," *Opt. Commun.*, vol. 134, no. 1–6, pp. 21–24, 1997.

[169] *Die Welt der Mikrooptik*, www.boehringer-ingelheim.de, 2005, online document.

[170] *Alles Mikro, Presseinformation 6 / 2003*, www.fzk.de, 2003, online document.

[171] F. Vollmer and S. Arnold, "Whispering-gallery-mode biosensing: labelfree detection down to single molecules," *Nat. Methods*, vol. 5, pp. 591–596, 2008.

[172] S. Peters, Y. Sui, F. Glöckler, U. Lemmer, and M. Gerken, "Organic photo detectors for an integrated thin-film spectrometer," *Proc. SPIE*, vol. 6765, pp. 676 503–1, 2007.

[173] M. Kuwata-Gonokami, R. H. Jordan, A. Dodabalapur, H. E. Katz, M. L. Schilling, R. E. Slusher, and S. Ozawa, "Polymer microdisk and microring lasers," *Opt. Lett.*, vol. 20, no. 20, pp. 2093–2095, Oct 1995.

[174] A. Tulek, D. Akbulut, and M. Bayindir, "Ultralow threshold laser action from toroidal polymer microcavity," *Appl. Phys. Lett.*, vol. 94, no. 20, p. 203302, 2009.

[175] D. K. Armani, T. J. Kippenberg, S. M. Spillane, and K. J. Vahala, "Ultra-high-Q toroid microcavity on a chip," *Nature*, vol. 421, pp. 925–928, 2003.

[176] T. Grossmann, M. Hauser, T. Beck, C. Gohn-Kreuz, M. Karl, H. Kalt, C. Vannahme, and T. Mappes, "High-Q conical polymeric microcavities," *Appl. Phys. Lett.*, vol. 96, p. 013303, 2010.

[177] M. Hossein-Zadeh and K. J. Vahala, "Free ultra-high-Q microtoroid: a tool for designing photonic devices," *Opt. Express*, vol. 15, pp. 166–175, 2006.

[178] M. Koechlin, "High-resolution laser lithography system based on two-dimensional acousto-optic deflection," *Rev. of Sci. Inst.*, vol. 80, p. 085105, 2009.

[179] M. Bruendel, "Herstellung photonischer Komponenten durch Heißprägen und UV-induzierte Brechzahlmodifikation von PMMA." Universitätsverlag Karlsruhe, 2008.

[180] *Standard Classification System for Poly(Methyl Methacrylate) (PMMA) Molding and Extrusion Compounds*, Astm standard ed., ASTM International, 2004.

[181] T. Soma, J. Satoh, and H. Matsuo, "Thermal expansion coefficient of GaAs and InP," *Solid State Commun.*, vol. 42, no. 12, pp. 889 – 892, 1982.

[182] G. Hernandez, "Fabry-perot interferometers." Cambridge University Press, 1988.

[183] G. Town, A. Vasdekis, G. Turnbull, and I. Samuel, "Temperature tuning of a semiconducting-polymer DFB laser," in *The 18th Annual Meeting of the IEEE*, oct. 2005, pp. 778–779.

[184] X. L. Zhu, L. Shi, J. Chan, J. Wang, C. Ye, and D. Lo, "Optical properties of zirconia-titania-ORMOSIL films for temperature tuning distributed feedback waveguide lasers," *Opt. Commun.*, vol. 251, no. 4-6, pp. 322 – 327, 2005.

[185] U. Geyer, J. Hauss, B. Riedel, S. Gleiss, U. Lemmer, and M. Gerken, "Large-scale patterning of indium tin oxide electrodes for guided mode extraction from organic light-emitting diodes," *J. Appl. Phys.*, vol. 104, no. 9, p. 093111, 2008.

[186] A. Diaspro, G. Chirico, C. Usai, P. Ramoino, and J. Dobrucki, "Photobleaching," in *Handbook of Biological Confocal Microscopy*, J. B. Pawley, Ed. Springer US, 2006, pp. 690–702.

[187] F. Papadimitrakopoulos and X.-M. Zhang, "Environmental stability of aluminum tris(8-hydroxyquinoline) (Alq$_3$) and its implications in light emitting devices," *Synth. Met.*, vol. 85, no. 1-3, pp. 1221 – 1224, 1997.

[188] G. Graff, P. Burrows, R. Williford, and R. Praino, "Barrier layer technology for flexible displays," in *Flexible Flat Panel Displays*, G. Crawford, Ed. New York, USA: John Wiley & Sons, Ltd., 2005, ch. 4, pp. 57–78.

[189] J. Lewis and M. Weaver, "Thin-film permeation-barrier technology for flexible organic light-emitting devices," *IEEE J. Sel. Top. Quantum Electron.*, vol. 10, no. 1, pp. 45 – 57, jan. 2004.

[190] P. E. Burrows, G. L. Graff, M. E. Gross, P. M. Martin, M. Hall, E. Mast, C. C. Bonham, W. D. Bennett, L. A. Michalski, M. S. Weaver, J. J. Brown, D. Fogarty, and L. S. Sapochak, "Gas permeation and lifetime tests on polymer-based barrier coatings," *Proc. SPIE*, vol. 4105, pp. 75–83, 2001.

[191] S. Stagira, M. Zavelani-Rossi, M. Nisoli, S. DeSilvestri, G. Lanzani, C. Zenz, P. Mataloni, and G. Leising, "Single-mode picosecond blue laser emission from a solid conjugated polymer," *Appl. Phys. Lett.*, vol. 73, no. 20, pp. 2860–2862, 1998.

[192] S. Richardson, O. P. M. Gaudin, G. A. Turnbull, and I. D. W. Samuel, "Improved operational lifetime of semiconducting polymer lasers by encapsulation," *Appl. Phys. Lett.*, vol. 91, no. 26, p. 261104, 2007.

[193] *Super-Quite Xenon Flash Lamps*, Specifications ed., Hamamatsu Photonics K.K., Electron Tube Division, 314-5, Shimokanzo, Iwata City, Shizuoka Pref., 438-0193, Japan.

[194] M. Amati and F. Lelj, "Monomolecular isomerization processes of aluminum tris(8-hydroxyquinolinate) (alq3): a dft study of gas-phase reaction paths," *Chem. Phys. Lett.*, vol. 363, no. 5-6, pp. 451 – 457, 2002.

[195] M. Cölle and W. Brütting, "Thermal, structural and photophysical properties of the organic semiconductor alq3," *Phys. Status Solidi A*, vol. 201, no. 6, pp. 1095–1115, 2004.

[196] C.-K. Tai, Y.-M. Chou, and B.-C. Wang, "Investigation of photophysical properties of mer-tris(8-hydroxyquinolinato) aluminum (III) and its derivatives: DFT and TD-DFT calculations," *J. Lumin.*, vol. 131, no. 2, pp. 169 – 176, 2011.

[197] M. Meyer, J. C. Mialocq, and B. Perly, "Photoinduced intramolecular charge transfer and trans-cis isomerization of the DCM styrene dye: picosecond and nanosecond laser spectroscopy, high-performance liquid chromatography, and nuclear magnetic resonance studies," *J. Phys. Chem.*, vol. 94, no. 1, pp. 98–104, 1990.

[198] M. Levichkova, "Influence of the matrix environment on the optical properties of incorporated dye molecules," Doctoral dissertaion, Technische Universität Dresden, 2007.

[199] K. Yagi, S. Shibata, T. Yano, A. Yasumori, M. Yamane, and B. Dunn, "Photostability of the laser dye DCM in various inorganic-organic host matrices," *J. Sol-Gel Sci. Technol.*, vol. 4, pp. 67–73, 1995, 10.1007/BF00486704.

[200] **T. Woggon**, S. Klinkhammer, and U. Lemmer, "Compact spectroscopy system based on tunable organic semiconductor lasers," *Appl. Phys. B*, vol. 99, pp. 47–51, 2010, 10.1007/s00340-010-3953-6.

[201] D. Anderson and M. Archard, "Measuring optical filters," *UV Instruments at work*, vol. UV–54, 1992.

[202] R. Y. Tsien, L. Ernst, and A. Waggoner, "Handbook of biological confocal microscopy," in *Fluorophores for confocal microscopy*, 3rd ed., J. B. Pawley, Ed. Springer Science+Business Media, LCC, New York, 2006, pp. 338–352.

[203] A. S. Waggoner, "Fluorescent probes for cytometry," in *Flow Cytometry and Sorting*, M. R. Melamed, T. Lindmo, and M. L. Mendelsohn, Eds. New York, USA: Wiley-Liss, New York, 1990, ch. 4, pp. 57–78.

[204] L. A. Ernst, R. K. Gupta, R. B. Mujumdar, and A. S. Waggoner, "Cyanine dye labeling reagents for sulfhydryl groups," *Cytometry*, vol. 10, no. 1, pp. 3–10, 1989.

[205] S. Jordan, "Nanopositioning: Long-travel piezomotors 'reboot' the motion-control toolbox," *Laser Focus World*, vol. 44, no. 9, 2008.

[206] Y. Li, "Laser beam scanning by rotary mirrors. II. conic-section scan patterns," *Appl. Opt.*, vol. 34, no. 28, pp. 6417–6430, 1995.

[207] Y. Li and J. Katz, "Laser beam scanning by rotary mirrors. I. modeling mirror-scanning devices," *Appl. Opt.*, vol. 34, no. 28, pp. 6403–6416, 1995.

[208] *ATMega8*, Datasheet ed., Atmel Corporation, 2325 Orchard Parkway, San Jose, CA 95131, USA.

[209] K. Iizuka, H. Uzuhashi, M. Kano, T. Endo, and K. Mohri, "Microcomputer control for sensorless brushless motor," *IEEE Trans. Ind. Appl.*, vol. IA-21, no. 4, pp. 595–601, 1985.

[210] S. I. Newton, "Optik, 2. und 3. Buch," in *Ostwald's Klassiker der Exakten Wissenschaften*, W. Abendroth, Ed.   Verlag von Wilhelm Engelmann, Leipzig, 1898, vol. 97.

[211] *Spectral Irradiance*, Oriel product training ed., Newport, 150 Long Beach Blvd, Stratford, CT 06615 USA, 2007.

[212] P. P. Sorokin and L. J. R., "Stimulated emission observed from an organic dye, chloro-aluminum phthalocyanine," *IBM J. Res. Develop.*, vol. 10, pp. 162–3, 1966.

[213] F. P. Schäfer, W. Schmidt, and J. Volze, "Organic dye solution laser," *Appl. Phys. Lett.*, vol. 9, no. 8, pp. 306–309, 1966.

[214] M. L. Spaeth and D. P. Bortfeld, "Stimulated emission from polymethine dyes," *Appl. Phys. Lett.*, vol. 9, no. 5, pp. 179–181, 1966.

[215] B. I. Stepanov, A. N. Rubinov, and V. A. Mostovnikov, "Optic generation in solutions of complex molecules," *JETP Lett.*, vol. 5, pp. 117–119, 1967.

[216] B. H. Soffer and B. B. McFarland, "Continously tunable, narrow-band organic dye lasers," *Appl. Phys. Lett.*, vol. 10, no. 10, pp. 266–267, 1967.

[217] T. W. Hänsch, "Repetitively pulsed tunable dye laser for high resolution spectroscopy," *Appl. Opt.*, vol. 11, no. 4, pp. 895–898, 1978.

[218] M. G. Littman and H. J. Metcalf, "Spectrally narrow pulsed dye laser without beam expander," *Appl. Opt.*, vol. 17, no. 14, pp. 2224–2227, 1978.

[219] U. Brackman, "Lambdachrome® laser dyes."   D-37079 Göttingen, Germany: Lambda Physik AG, 2000.

[220] R. Ghazy, "Thermo-optical properties of some common laser-dye solvents," *J. Photochem. Photobiol., A*, vol. 119, pp. 61–66, 1998.

[221] H. El-Kashef, "The necessary requirements imposed on polar dielectric laser dye solvents–II," *Physica B*, vol. 311, pp. 376–379, 2002.

[222] G. M. Gale, "A single mode flashlamp-pumped dye laser," *Opt. Commun.*, vol. 7, no. 1, pp. 86–88, 1972.

[223] N. M. Kroll, "Parametric amplification in spatially extended media and application to the design of tuneable oscillators at optical frequencies," *Phys. Rev.*, vol. 127, no. 4, pp. 1207–1211, Aug 1962.

[224] S. A. Akhmanov and R. V. Khokhlov, "Concerning one possibility of amplification of light waves," *Sov. J. Exp. Theor. Phys.*, vol. 16, p. 252, 1963.

[225] J. A. Giordmaine and R. C. Miller, "Tunable coherent parametric oscillation in LiNbO3 at optical frequencies," *Phys. Rev. Lett.*, vol. 14, no. 24, pp. 973–976, Jun 1965.

[226] *BBO Crystal*, Datasheet ed., Laser Components, LASER COMPONENTS GmbH, Werner von Siemens Str. 15, 82140 Olching, Germany.

[227] Y. X. Fan, R. C. Eckardt, R. L. Byer, C. Chen, and A. D. Jiang, "Barium borate optical parametric oscillator," *IEEE J. of Quantum Electron.*, vol. 25, no. 6, pp. 1196–1199, 1989.

[228] L. E. Myers, R. C. Eckardt, M. M. Fejer, R. L. Byer, and W. R. Bosenberg, "Multigrating quasi-phase-matched optical parametric oscillator in periodically poled LiNbO3," *Opt. Lett.*, vol. 21, no. 8, pp. 591–593, 1996.

[229] B. J. Orr, Y. He, and R. T. White, "Spectroscopic applications of tunable optical parametric oscillators," in *Tunable Laser Applications*, F. J. Duarte, Ed. New York, USA: CRC, 2009, ch. 2, pp. 15–96.

[230] W. H. Louisell, "Coupled mode and parametric electronics." John Wiley & Sons, 1960.

[231] A. Borsutzky, "Frequency control of pulsed optical parametric oscillators," *J. Eur. Opt. Soc. Part B*, vol. 9, no. 2, p. 191, 1997.

[232] R. R. Alfano and S. L. Shapiro, "Emission in the region 4000 to 7000 å via four-photon coupling in glass," *Phys. Rev. Lett.*, vol. 24, no. 11, pp. 584–587, Mar 1970.

[233] C. Lin and R. H. Stolen, "New nanosecond continuum for excited-state spectroscopy," *Appl. Phys. Lett.*, vol. 28, no. 4, pp. 216–218, 1976.

[234] C. Lin, V. Nguyen, and W. French, "Wideband near-i.r. continuum (0.7–2.1 µm) generated in low-loss optical fibres," *Electron. Lett.*, vol. 14, no. 25, pp. 822–823, 1978.

[235] Y. Fujii, B. S. Kawasaki, K. O. Hill, and D. C. Johnson, "Sum-frequency light generation in optical fibers," *Opt. Lett.*, vol. 5, no. 2, pp. 48–50, 1980.

[236] K. Washio, K. Inoue, and T. Tanigawa, "Efficient generation of near-i.r. stimulated light scattering in optical fibres pumped in low-dispersion region at 1.3 µm," *Electron. Lett.*, vol. 16, no. 9, pp. 331–333, 1980.

[237] A. Gomes, V. D. Silva, J. Taylor, B. Ainslie, and S. Craig, "Picosecond stimulated raman scattering in P2O5-SiO2 based single mode optical fibre," *Opt. Commun.*, vol. 64, no. 4, pp. 373 – 378, 1987.

[238] B. Gross and J. T. Manassah, "Supercontinuum in the anomalous group-velocity dispersion region," *J. Opt. Soc. Am. B*, vol. 9, no. 10, pp. 1813–1818, 1992.

[239] T. Morioka, K. Mori, and M. Saruwatari, "More than 100-wavelength-channel picosecond optical pulse generation from single laser source using supercontinuum in optical fibres," *Electron. Lett.*, vol. 29, no. 10, pp. 862 –864, 12 1993.

[240] T. Morioka, H. Takara, S. Kawanishi, O. Kamatani, K. Takiguchi, K. Uchiyama, M. Saruwatari, H. Takahashi, M. Yamada, T. Kanamori, and H. Ono, "1 Tbit/s (100 Gbit/s times;10 channel) OTDM/WDM transmission using a single super-continuum WDM source," *Electron. Lett.*, vol. 32, no. 10, pp. 906 –907, 9 1996.

[241] S. V. Chernikov, Y. Zhu, J. R. Taylor, and V. P. Gapontsev, "Supercontinuum self-Q-switched ytterbium fiber laser," *Opt. Lett.*, vol. 22, no. 5, pp. 298–300, 1997.

[242] J. C. Knight, T. A. Birks, P. S. J. Russell, and D. M. Atkin, "All-silica single-mode optical fiber with photonic crystal cladding," *Opt. Lett.*, vol. 21, no. 19, pp. 1547–1549, 1996.

[243] J. M. Dudley, G. Genty, and S. Coen, "Supercontinuum generation in photonic crystal fiber," *Rev. Mod. Phys.*, vol. 78, no. 4, pp. 1135–1184, Oct 2006.

[244] T. Schreiber, J. Limpert, H. Zellmer, A. Tünnermann, and K. P. Hansen, "High average power supercontinuum generation in photonic crystal fibers," *Opt. Commun.*, vol. 228, no. 1-3, pp. 71 – 78, 2003.

[245] L. Provino, J. Dudley, H. Maillotte, N. Grossard, R. Windeler, and B. Eggleton, "Compact broadband continuum source based on microchip laser pumped microstructured fibre," *Electron. Lett.*, vol. 37, no. 9, pp. 558–560, 26 2001.

[246] A. V. Avdokhin∗, S. V. Popov, and J. R. Taylor, "Continuous-wave, high-power, raman continuum generation in holey fibers," *Opt. Lett.*, vol. 28, no. 15, pp. 1353–1355, 2003.

[247] P. Cimalla, J. Walther, M. Mehner, M. Cuevas, and E. Koch, "Simultaneous dual-band optical coherence tomography in the spectral domain for high resolution in vivo imaging," *Opt. Express*, vol. 17, no. 22, pp. 19 486–19 500, 2009.

[248] V. Kapoor, F. V. Subach, V. G. Kozlov, A. Grudinin, V. V. Verkhusha, and W. G. Telford, "New lasers for flow cytometry: filling the gaps," *Nat. Methods*, vol. 4, no. 9, pp. 678–679, 2007.

[249] B. Agnarsson, S. Ingthorsson, T. Gudjonsson, and K. Leosson, "Evanescent-wave fluorescence microscopy using symmetric planar waveguides," *Opt. Express*, vol. 17, no. 7, pp. 5075–5082, 2009.

[250] W. G. Telford and H. Imam, "More flexibility for flow cytometry," *BioPhotonics*, vol. 15, no. 8, 2008.

[251] A. McCook, "The scientist top innovations of 2008," *The Scientist*, vol. 12, pp. 45–52, 2008.

[252] *SuperK™Dual*, product datasheet ed., NKT Photonics A/S (Headquarters), Blokken 84, 3460 Birkerod, Denmark, 2010.

[253] *SuperK™White Light Lasers*, product datasheet ed., NKT Photonics A/S (Headquarters), Blokken 84, 3460 Birkerod, Denmark, 2010.

[254] J. Posthumus, F. Tauser, T. Renner, and W. Kaenders, "Nonlinear frequency conversion with mode-locked Erbium fiber lasers," *Proc. SPIE*, vol. 6453, no. 7, p. 64531Q, 2007.

[255] K. Moutzouris, F. Sotier, F. Adler, and A. Leitenstorfer, "Highly efficient second, third and fourth harmonic generation from a two-branch femtosecond erbium fiber source," *Opt. Express*, vol. 14, no. 5, pp. 1905–1912, 2006.

[256] *iChrome - All-color Ultrafast Flexible Fiber Laser*, product datasheet ed., TOPTICA Photonics AG, Lochhamer Schlag 19, 82166 Graefelfing, Germany, 2010.

[257] R. P. Salathé, "Diode lasers coupled to external resonators," *Appl. Phys. A*, vol. 20, no. 1, pp. 1–18, 1979.

[258] A. S. Arnold, J. S. Wilson, and M. G. Boshier, "A simple extended-cavity diode laser," *Rev. Sci. Instrum.*, vol. 69, no. 3, pp. 1236–1239, 1998.

[259] A. C. Tropper, H. D. Foreman, A. Garnache, K. G. Wilcox, and S. H. Hoogland, "Vertical-external-cavity semiconductor lasers," *J. Phys. D: Appl. Phys.*, vol. 37, pp. R75–R85, 2004.

[260] A. Q. Liu and X. M. Zhang, "A review of MEMS external-cavity tunable lasers," *J. Micromech. Microeng.*, vol. 17, pp. R1–R13, 2007.

[261] C. E. Wieman and L. Hollberg, "Using diode lasers for atomic physics," *Rev. Sci. Instrum.*, vol. 62, no. 1, pp. 1–20, 1991.

[262] *Fabry-Perot Laser Diodes - Stock list*, Stock list ed., TOPTICA Photonics AG, Lochhamer Schlag 19, 82166 Graefelfing (Munich), Germany, 2011.

[263] J. M. Gaines, R. R. Drenten, K. W. Haberern, T. Marshall, P. Mensz, and J. Petruzzello, "Blue-green injection lasers containing pseudomorphic $Zn_{1-x}Mg_xS_ySe_{1-y}$ cladding layers and operating up to 394 K," *Appl. Phys. Lett.*, vol. 62, no. 20, pp. 2462–2464, 1993.

[264] M. A. Haase, P. F. Baude, M. S. Hagedorn, J. Qiu, J. M. DePuydt, H. Cheng, S. Guha, G. E. Höfler, and B. J. Wu, "Low-threshold buried-ridge II-VI laser diodes," *Appl. Phys. Lett.*, vol. 63, no. 17, pp. 2315–2317, 1993.

[265] K. Katayama, H. Yao, F. Nakanishi, H. Doi, A. Saegusa, N. Okuda, T. Yamada, H. Matsubara, M. Irikura, T. Matsuoka, T. Takebe, S. Nishine, and T. Shirakawa, "Lasing characteristics of low threshold ZnSe-based blue/green laser diodes grown on conductive ZnSe substrates," *Appl. Phys. Lett.*, vol. 73, no. 1, pp. 102–104, 1998.

[266] K. Okamoto, J. Kashiwagi, T. Tanaka, and M. Kubota, "Nonpolar m-plane InGaN multiple quantum well laser diodes with a lasing wavelength of 499.8 nm," *Applied Physics Letters*, vol. 94, no. 7, p. 071105, 2009.

[267] T. Miyoshi, S. Masui, T. Okada, T. Yanamoto, T. Kozaki, S. ichi Nagahama, and T. Mukai, "510–515nm InGaN-based green laser diodes on *c*-plane GaN substrate," *Appl. Phys. Express*, vol. 2, no. 6, p. 062201, 2009.

[268] B.-L. Lee and C.-F. Lin, "Wide-range tunable semiconductor lasers using asymmetric dual quantum wells," *IEEE Photonics Technol. Lett.*, vol. 10, no. 3, pp. 322 –324, mar 1998.

[269] K. Ebeling, "Integrierte Optoelektronik." Berlin: Springer-Verlag, 1989.

[270] L. Hildebrandt, R. Knispel, S. Stry, J. R. Sacher, and F. Schael, "Antireflection-coated blue GaN laser diodes in an external cavity and doppler-free indium absorption spectroscopy," *Appl. Opt.*, vol. 42, no. 12, pp. 2110–2118, 2003.

[271] R. Won, "View from... SPIE Photonics Europe 2010: Champion innovations," *Nat. Photon.*, vol. 4, no. 7, pp. 418–420, 2010.

List of Figures

List of Tables

Abbreviations

β	propagational constant of an electromagnetic wave
E	electrical field vector
H	magnetical field vector
r	position vector
ω	circular frequency
c_0	speed of light in a vacuum
3D-DLW	three dimensional direct laser writing
ORMOCER$^®$	trademark for organic modified ceramic
AlGaAs	aluminum gallium arsenide
AlGaInP	aluminum gallium indium phosphide
Alq$_3$	tris-(8-hydroxyquinoline) aluminum
AOTF	acusto-optic tunable filter
ASCII	American Standard Code for Information Interchange
ASE	amplified spontaneous emission
BBO	beta-barium borate, β-BaB_2O_4
COC	cyclic olefin copolymer
DC	direct current
DCM	4-dicyanomethylene-2-methyl-6-(p-dimethylaminostyryl)-4H-pyran
DUV	deep ultra violet
e-beam	electron-beam
ECDL	external cavity diode laser
EMF	electro-magnetical force
g	gravitational constant g=9.81 m s^{-2}
GaAsP	gallium arsenide phosphide
GaAsP	gallium arsenide phosphide
GaN	gallium nitride
InGaAs	indium gallium arsenide
InGaN	indium gallium nitride
InGaP	indium gallium phosphide
ISR	interrupt service routine
KTP	potassium titanyl phosphate
LASER	light amplification by stimulated emission of radiation
LED	light emitting diode
LIA	laser interference ablation
LIGA	'Lithographie, Galvanik und Abformung', german acronym denominating the individual process steps lithography, electroforming, and plastic molding
LIL	laser interference lithography
LiNbO$_3$	lithium niobate
MEMS	micro electro mechanical system
NA	numerical aperture

Nd	neodymium
NIL	nano imprint lithographie
NIR	near infrared
NL	nonlinear
OCT	optical coherence tomography
OEM	original equipment manufacturer
OPO	optical parametric oscillator
OTR	oxygen transmission rate
PCF	photonic crystal fiber
PDMS	polydimethylsiloxane
PL	photoluminescence
PMMA	Poly(Methyl MethAcrylate)
PPLN	periodically poled lithium niobate
PTC	positive thermal coefficient
PWM	pulse width modulation
QTH	quartz tungsten halogen
RISC	reduced instruction set computer
SC	super continuum
SMU	source measurme-unit
TE	transversal electrical mode
TM	transversal magnetic mode
TPA	two photon absorption
TPA	two photon absorption
UV	ultra violet
WVTR	water vapor transmission rate
YAG	yttrium aluminum garnet
YLF	yttrium lithium fluoride
YVO$_4$	yttrium vanadate

Acknowledgments

This thesis would not have been possible without the help of many individuals to whom I wish to express my deep sense of gratitude.

First and foremost, I am deeply indebted to Prof. Uli Lemmer and Prof. Volker Saile for their commitment to examine this thesis. I would also like to thank Prof. Uli Lemmer for his guidance and useful suggestions which helped me to complete this work.

I offer my sincerest gratitude to the Agilent Technologies foundation for funding my work which allowed me to freely explore my own ideas. My mentor Bernd Nawracala and Gerard Rozing, both from Agilent made their support available in a number of ways. The fruitful discussions in Waldbronn spared me from reinventing a couple of wheels.

I am indebted to all my colleagues at the LTI for supporting me throughout my research and for making the institute a pleasant workplace. In particular, I wish to thank Martin Punke and Marc Stroisch for sharing their considerable experience and knowledge. Sacrificing their valuable time spared me hours of trial and error. I also benefited from many discussions on many different topics with Felix Glöckler, Sebastian Valouch and Martin Perner.

I greatly appreciated working with Sönke Klinkhammer and Christoph Vannahme on the subject of organic lasers and sharing our ideas and results. "My" students Thomas Kleiner, Tobias Kappler, Carsten Eschenbaum, Karl Lüll and Johannes Bach deserve many thanks for working hard and contributing to this work.

It is a pleasure to thank Felix Geislhöringer, Astrid Dittrich and Claudia Holeisen for their help in the many administrative issues, and without fail, for providing something much greater: a friendly smile and a hello every time. I also cannot forget to express my appreciation to Mario Sütsch, Hans Vögele and Klaus Ochs from the mechanical workshop, who provided me with custom mechanical parts of consistent high quality and even allowed me to craft parts by myself.

On a special note I would like to extend my thanks to my colleagues and friends from the Institute of Microstructure Technology for the fruitful discussions and inspirations for defining a new challenge for me after completion of my PhD. In particular I would like to mention Johannes Kenntner, Johannes Barth, Laura Zimmermann, Thomas Grund and Markus Simon.

I am also indebted to all, even those far from Karlsruhe, whose friendship supported me in any respect during the completion of this project.

Finally, yet importantly, my infinite gratitude belongs to my family for their endless confidence and support.

Lebenslauf

Thomas Woggon
geboren am 16. Dezember 1980 in Berlin

Ausbildung

1987–1992	Pestalozzi Oberschule Berlin
1992–1993	Integrierte Gesamtschule Kaiserslautern
1993–1996	Pestalozzi Gymnasium Berlin
1996–2000	Goethe Gymnasium Karlsruhe
27.06.2000	Abitur am Goethe Gymnasium Karlsruhe
07/2000–04/2001	Grundwehrdienst, Heeresflieger Regiment 25 Laupheim
04/2001–07/2005	Diplomstudium der Physik an der Universität Karlsruhe (TH)
07/2005–07/2006	Externe Diplomarbeit am Lichttechnischen Institut und am Institut für Theoretische Festkörperphysik der Universität Karlsruhe (TH) *Lasertätigkeit in organischen photonischen Kristallen mit Defektmoden*
10/2006–09/2009	Promotionsstudium am Lichttechnischen Institut der Universität Karlsruhe (TH) als Stipendiat der Agilent Technologies Foundation
seit 10/2009	Wissenschaftlicher Mitarbeiter des Instituts für Mikrostrukturtechnik des Karlsruher Institutes für Technologie (KIT)

Lehrtätigkeiten

2003–2005	Betreuung von Laborpraktika Physik und Programmieren in C++ an der Fakultät für Physik, Universität Karlsruhe (TH)
2006–2007	Assistenz zur Vorlesung *Optische Systeme* am Lichttechnischen Institut, Universität Karlsruhe (TH)
2007–2009	Konzeption und Durchführung von Laborpraktika Optoelektronik für Studenten der Fakultät Elektro- und Informationstechnik und der Karlsruhe School of Optics and Photonics der Universität Karlsruhe (TH).

praktische Tätigkeiten

04/2009–07/2009	Industrieprojektarbeit bei OpSyTec
seit 10/2009	Projektverantwortlicher für den Technologietransfer von organischen Festkörperlasern für Analyseanwendungen
seit 05/2011	Technischer Geschäftsführer der VISOLAS GmbH